Fundamental Limits on Performance for Cooperative Radar-Communications Coexistence

by

Alex R. Chiriyath

A Dissertation Presented in Partial Fulfillment
of the Requirements for the Degree
Doctor of Philosophy

Approved February 2018 by the
Graduate Supervisory Committee:

Daniel W. Bliss, Chair
Douglas Cochran
Oliver Kosut
Christ D. Richmond

ARIZONA STATE UNIVERSITY

May 2018

ABSTRACT

Spectral congestion is quickly becoming a problem for the telecommunications sector. In order to alleviate spectral congestion and achieve electromagnetic radio frequency (RF) convergence, communications and radar systems are increasingly encouraged to share bandwidth. In direct opposition to the traditional spectrum sharing approach between radar and communications systems of complete isolation (temporal, spectral or spatial), both systems can be jointly co-designed from the ground up to maximize their joint performance for mutual benefit. In order to properly characterize and understand cooperative spectrum sharing between radar and communications systems, the fundamental limits on performance of a cooperative radar-communications system are investigated. To facilitate this investigation, performance metrics are chosen in this dissertation that allow radar and communications to be compared on the same scale. To that effect, information is chosen as the performance metric and an information theoretic radar performance metric compatible with the communications data rate, the radar estimation rate, is developed. The estimation rate measures the amount of information learned by illuminating a target. With the development of the estimation rate, standard multi-user communications performance bounds are extended with joint radar-communications users to produce bounds on the performance of a joint radar-communications system. System performance for variations of the standard spectrum sharing problem defined in this dissertation are investigated, and inner bounds on performance are extended to account for the effect of continuous radar waveform optimization, multiple radar targets, clutter, phase noise, and radar detection. A detailed interpretation of the estimation rate and a brief discussion on how to use these performance bounds to select an optimal operating point and achieve RF convergence are provided.

TABLE OF CONTENTS

CHAPTER Page

CHAPTER Page

CHAPTER Page

LIST OF FIGURES

Figure Page

Figure Page

LIST OF TABLES

Chapter 1

INTRODUCTION

Spectral congestion is caused by too many RF communications users concurrently accessing the electromagnetic spectrum. This congestion may degrade communications performance and decrease or even restrict access to spectral resources. With the increase in communications users, spectral congestion has become a major issue for the telecommunications sector. A proposed solution is to share spectral resources that were previously allocated for radar systems. As a result, the problem of spectral congestion is forcing legacy radar band users to investigate methods of cooperation and co-design with a growing number of communications applications [1, 2]. This problem has motivated government entities like The Defense Advanced Research Projects Agency (DARPA) to begin funding and investigating these methods to not only ensure military radar coverage is maintained as spectral allocation is renegotiated, but to potentially improve both military radar and military communications by co-designing the systems from the ground up [3]. However, these issues extend far beyond just commercial communications and military radar, and include a wide variety of applications such as next generation automobiles, medical devices, and 5G wireless backhaul. As a result, researchers have begun investigating not just methods of military radar and communications coexistence, but more fundamentally methods of joint remote sensing and communications.

The two functions of sensing and communications, at their core, tend to be at odds with one another. For example, sensing typically sends a known waveform or stimulus and measures a response from the environment, often referred to as the channel. In the case of the radar system, the sent signal is known and the target channel

is unknown and is desired to be sensed (estimated). However, a communications system typically sends an *unknown* signal with the assumption that the propagation channel is known or previously estimated. We can also consider the near inverse of this situation: passive radar. In this case, we must estimate the data as a nuisance parameter to obtain the information we care about (channel estimation). A non-adaptive communications channel, where the channel is stationary or controlled, is the dual of the traditional radar system. Therefore, when considering the general task of jointly sensing and communicating, it becomes immediately apparent that the solution is non-trivial.

With opposing requirements, sensing and communications systems are often designed in isolation. The only consideration for the other user in legacy systems has been in the form of regulatory constraints, such as those imposed by the FCC in the United States. However, governmental regulation does nothing to incentivize either user to minimize interference beyond the required limits or assist each other to mutual benefit. As future systems vie for spectral resources, RF convergence and cooperation are the solutions to an increasingly crowded wireless domain. We formally define RF convergence as the operating point at which a given bandwidth allocation is used jointly by both remote sensing and communications systems to mutual benefit.

Achieving RF convergence for joint radar-communications coexistence is incredibly complicated. Even for a simple case involving a single radar and communications link, one must consider spatial, spectral, and temporal degrees of freedom. In practice, there are many contributing sources in a given spectrum-space-time, and regulatory restrictions may not adequately protect both users even if isolation is acceptable. An example of the type of complicated scenario that is associated with achieving RF convergence is shown in Figure 1.1. Future users will find it advantageous to consider

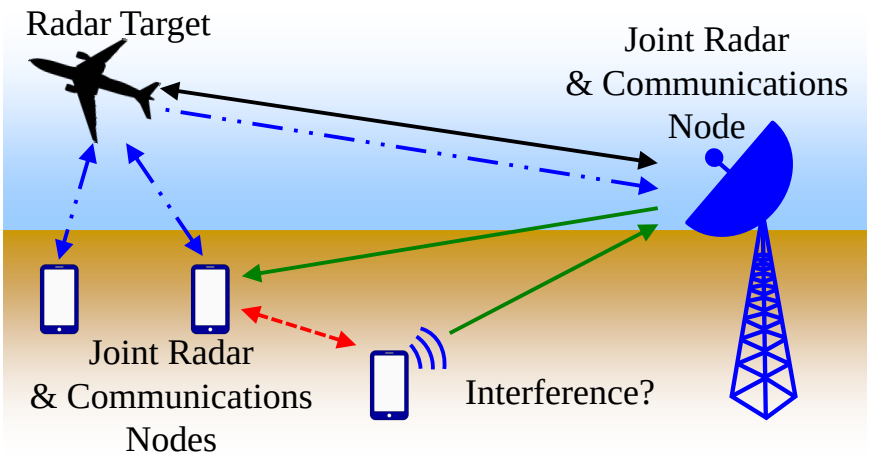

Figure 1.1: An example highlighting the difficulties of achieving RF convergence. As the number of sources of RF energy increase, it becomes increasingly difficult to identify an optimal operating point such that the allocated bandwidth is cooperatively utilized by each user to mutually benefit all involved users. Future systems must be co-designed to not just mitigate interference, but jointly consider each other in their inherent operation.

co-designing systems to handle these complicated RF convergence scenarios.

One approach to solving the RF convergence problem is to present the joint radar-communications problem as a joint information problem. Information is chosen because it forces one to identify uncertainty in the situation and develop plans to reduce it. Estimation theory and signal processing are often presented with traditional metrics such as the Cramér-Rao lower bound (CRLB), minimum mean-squared error (MMSE), or signal-to-noise ratio (SNR). While some of these metrics provide a measure of information gained (especially the CRLB), none of these metrics address information gained from spectral access. When focusing on reducing estimation error variance, if the information about the target of interest gained through estimation is minimal, precious spectrum in a given space-time is being inefficiently utilized. If a target's state is known perfectly, the information content about the target is null, since there is no uncertainty to reduce, regardless of the SNR. Hence, as long as the target's state in known, there is no need to allocate spectrum for radar estimation.

Another reason for using information is that it is already a key metric for communications systems, and it allows radar and other remote sensing systems to be considered in a multiple access channel (MAC).

Viewing the problem in an information context, one can easily see how radar and communications are interrelated. Radar estimation is attempting to reduce uncertainty in the channel, and so all the information content is in the unknown channel. To estimate the unknown channel, a known waveform is transmitted. The radar processor exploits the fact that it knows what was sent to extract the unknown channel delay and Doppler spread. The communications system on the other hand considers channel estimation a nuisance operation, with the goal of sending arbitrary, unknown information. At a signals level, the two waveforms can look identical. By looking for the information content, the true uncertainty is revealed. This view quickly reveals the challenge of joint radar-communications. One may note that communications users periodically send known training sequences to estimate unknown channels before transmitting information. It is not a far stretch to start thinking of joint systems where communications equalization functions are doubly tasked to perform radar operations, making more efficient dual-use of spectrum.

In order to provide a tractable solution to achieving RF convergence, we provide a point of departure in this dissertation by defining and proposing solutions to a simple multiple-access joint radar-communications problem, the 'basic multiple-access scenario.' It is a simple scenario involving a radar and communications user attempting to use the same spectrum-space-time. This scenario is instructional, and can easily be scaled to more complicated scenarios by using it as a building block to construct real world examples. We present a diagram of the 'basic multiple-access scenario' in Figure 2.1.

1.1 Contributions

The estimation rate is the radar information measure used in this dissertation. The concept of estimation information rate (or estimation rate) [4] - an information theoretic measure compatible with the communications channel capacity - was developed to characterize the fundamental limits on performance of a joint sensing and communications system. Conceptually, the estimation rate represents the amount of information learned by illuminating a target. The radar estimation rate was also expanded upon in References [5, 6]. With the development of the estimation rate, standard multi-user communications performance bounds were extended to produce bounds on the performance of a joint sensing and communications system for the standard scenario shown in Figure 2.1 [5]. System performance was investigated for variations of the standard scenario and inner bounds on performance were extended to account for the effect of continuous radar waveform optimization [7], multiple radar targets [8], clutter [9], phase noise [10], and radar detection [11].

The key contributions discussed in this dissertation are as follows

- Develop the estimation rate, a metric analogous to communications data rate.
- Provide an intuitive understanding of radar estimation rate and the implications of altering it
- Develop several cooperative radar and communications signaling schemes for the 'basic multiple-access scenario'
- Introduce and elaborate on the concept of 'Not All Bits are Equal'; bits representing information gained for each system can be weighted differently
- Present two methods for selecting the operating point of a joint radar-communications system

- Develop and study the minimum estimation error variance radar waveform design method that maximizes joint performance
- Extend the joint performance bounds for multiple radar targets, presence of clutter and phase noise, and radar detection

1.2 Background

In this dissertation, we reformulate and extend the performance bounds introduced in [4]. It is worth noting that the majority of our efforts presented here focus radar estimation performance rather than radar detection considered in [12–15]. However, we do extend the bounds presented in [4] to include radar detection performance as well. To be more specific, unless explicitly stated otherwise, our work focuses on the estimation of a target parameter, time delay or target range, from the received target return and the performance of the radar system is measured in terms of the estimation rate.

Information is well known in the field of communications, but less so in radar. Perhaps surprisingly, radars were looked at in the context of information theory soon after Shannon's seminal work [16] by Woodward [13]. The work presented in [12, 13] investigated the application of information theory to improve radar system performance. It was in these classical works that the idea that SNR does not measure information is introduced. Over fifty years ago, at the time these works were published, it was generally assumed that the higher the output SNR, the better the detection performance of a radar system. Hence, most radar systems or waveforms were designed to maximize the output SNR; however, this simple formulation misses a lot of the subtleties. The primary focus of these works is to dispel such a simplistic interpretation by using information theory to formulate a new type of receiver, the

a posteriori radar receiver, that does not try to maximize output SNR but attempts to maximize the amount of information, given by the *a posteriori* distribution of a target parameter.

Interest in radar information resurged many years later with Bell's work on waveform design using information for statistical scattering targets [14]. In [14], waveform optimization for detection and target information extraction are considered. The radar waveform is designed so as to maximize the mutual information between the target parameter of interest and the measurements obtained from the receiver. It is shown that the maximization of mutual information improves the radar system performance measured in terms of target classification ability or average measurement error. However, performance of the optimized waveforms in terms of target parameter estimation is not explicitly discussed. References [17, 18] employ the concept of maximizing the expected information gain and apply it to develop information driven sensor scheduling schemes for target tracking problems. It was shown that such information driven sensor management schemes outperform task based sensor management schemes when considering multiple performance criteria, such as target tracking performance as well as target classification performance. In Reference [19], information theory is utilized to develop a mutual information measure used for waveform and power spectrum design to jointly optimize the performance of radar and communications systems that overlap in frequency. Similarly, the work presented in Reference [15] also uses information theory to develop an expression for radar capacity (for radar systems performing target detection only) which, in combination with traditional communications capacity, can be used to measure the total capacity of a joint radar-communications network.

Recent results have found connections between information theory and estimation theory, equating estimation information and the integrated MMSE [20]. In addi-

tion, cognitive radar architectures have been proposed using information to prioritize physical location access based on uncertainty [21]. These advances make the joint consideration of radar and communications information interesting when considering co-designed solutions.

A new joint radar-communications performance metric is developed in Reference [22] that extends the traditional Neyman-Pearson detection metric for radars to include the communications data rate. This new metric is used to develop performance bounds for uncooperative and fully cooperative reception. Finally, Reference [23] investigates utilizing the energy from communications users to improve a radar user's probability of detection. In this scenario, the radar waveform is optimized to function with the in-band communications system operating as the primary user.

Achieving radar-communications RF convergence is complicated, and so the solution space tends to be greatly varied. Nevertheless, certain methods are gaining more traction than others.

Waveform design has become a dominant research thread in the joint radar-communications phenomenology. Researchers have considered a variety of waveform options including orthogonal frequency-division multiplexing (OFDM) [24–33] or spread spectrum waveforms [34–37].

Most of these results are attempting co-designed systems, where OFDM waveforms are used for bi-static communications, and as a mono-static radar. However, results showed conflicting cyclic prefix requirements, data-dependent ambiguities, and trouble mitigating peak-to-average power ratio (PAPR) for typical radar power requirements. In Reference [31], the radar system along with the communication system uses OFDM waveforms for transmission and algorithms are presented to assign OFDM sub-carriers to each system in such a way so as to optimize channel capacity for the communication system and the target detection performance (Mahalanobis distance

[38]) for the radar system. The first algorithm is a low-complexity algorithm that assigns sub-carriers to each system such that the channel capacity and target detection performance are optimized separately while the second algorithm jointly optimizes the channel capacity and target detection performance. Reference [39] considers a spectrum sharing scheme for radar and communications systems which utilize the same OFDM waveform for transmission (communications) and environment illumination (radar). A communications capacity vs radar detection probability performance bound is also provided.

Similar to OFDM, spread spectrum waveforms have been proposed for their attractive, noise-like autocorrelation properties [35–37]. In Reference [37], a communications system using radar illumination signals like linear frequency modulation (LFM) chirp waveforms as modulation signals to transmit data have been developed. It has been shown in [37] that such a modulation scheme when used with a radar system shows good system performance in terms of bit error rate (BER) (for communications) and false-alarm rate (for radar).

Multiple-input multiple-output (MIMO) radar techniques have also been proposed, given that the independent transmitted waveforms allow more degrees of freedom for joint radar-communications co-design [40–42].

Multiple orthogonal LFM chirps have also been proposed to accomplish both radar detection and communications transmissions in a MIMO system [43].

Researchers have also looked at optimization theory based radar waveform design methods in spectrally dense environments that attempt to maximize some radar performance metrics (detection probability, ambiguity function features etc.) while keeping interference to other in-band systems at a minimum [44–46].

Employing the existing cellular framework has also been proposed as a solution to augment the dwindling radar spectrum [47, 48]. These approaches range from sub-

scribing as cellular users when there is a need for radar illumination, to using cellular protocols to prioritize radar tasks. As such, the radar is conforming to the design of the cellular user, and is subsequently close to cooperation than co-design. Other approaches accept that the existing cellular infrastructures will dominate and aim to design optimal radar waveforms that ensure spectral compatibility and minimize interference to in-band, nearby cellular users and also improve radar performance (such as detection, tracking etc.) using non-convex optimization techniques [49].

Some other techniques such as interference mitigation [50], precoding or spatial separation [51] or waveform shaping [40, 52–56] allow both radar and communications to share the spectrum and coexist. In Reference [54], waveform shaping is done by projecting radar waveforms into the null space of the interference channel matrix, which ensures that there is minimal interference on the communications system from the radar system. The interference channel matrix can be extracted from the complete channel matrix. The channel is assumed to be reciprocal (thus making it easier to estimate the channel matrix) and the radar system is assumed to be a colocated MIMO radar in which each antenna transmit mutually orthogonal waveforms. The channel matrix between the primary and secondary user is estimated by the secondary user and either system can be considered as the primary user. Once the channel matrix is estimated and the null space of the interference channel matrix is calculated, the original radar waveform (any radar waveform) is then projected onto the null space and the resultant waveform is transmitted. It is then shown that such a radar system is able to perform at levels comparable to a case where null space projections on radar signals are not done and the radar system has no interference. In References [52, 53], the theory of matched illumination, the process of optimizing the pulse shape of the radar waveform (finite duration and finite energy) and the impulse response of the receiver, is used to design a target detection system that maximizes the target SNR.

Current research has investigated the benefits of using methods similar to cooperative sensing to solve the problem of radar and communications co-existence [57–62]. Radar nodes that employ some form of cooperative sensing have shown an improvement when compared to traditional nodes that did not employ cooperative sensing. In Reference [57] four regions of coexistence are defined between radar and communication systems which are separated based on whether the two systems interfere with each other and if this interference is detectable by either system. These regions are defined based on a set of interference-to-noise ratio (INR)/SNR thresholds and probability of interference/detection thresholds. The non-detectable/non-interfering region is the worst case region and the system parameters should be chosen in such a way so as to make this region of coexistence as small as possible. Simple algorithms can be developed for the other regions. It is then shown that coexistence between radar and communications is feasible for radar nodes without cooperative sensing only when subject to stringent interference restrictions such as low radar transmit power. However, among radar nodes that utilize cooperative sensing, coexistence is not subject to such stringent constraints. Furthermore radar nodes with cooperative sensing demonstrate an improvement in performance (especially if the nodes are spaced far apart, ensuring that the channel correlation between nodes is low) in terms of probability of detection, detection range etc. Another approach is employed in Reference [58] wherein the surveillance space of the radar system is divided into sectors and priorities are assigned to all radar and communication systems that want to transmit in each sector. The priorities are determined using fuzzy logic. The criteria used to assign these priorities include target separation, SNR, clutter etc. Bandwidth is allocated or 'shared' based on these priorities by performing multi-objective optimization.

Other methods utilize isolation approaches such as polarization for co-designed systems [63]. Space-time dynamic isolation techniques have been proposed, such as

communications devices communicating carefully to avoid spectrum-space-time collisions with rotating radars [64, 65]. These also varied from coexisting to cooperative systems.

There is a long standing trade-off between signal sharing systems utilizing radar waveforms versus signal sharing systems utilizing communications waveforms [66]. Some approaches to shared waveform outside of coding have been investigated, such as a radar system modulating low-rate communications on the waveform sidelobe levels [67, 68]. Some researchers have looked at communications systems that receive radar pulses reflected from targets and re-modulate these pulses on a intrapulse basis into communications signals, enabling a improvement in communications data rate [69]. Reference [70] provides a scheduling and resource management perspective for an ideal shared waveform system.

Advancements in cognitive radios and radar have been proposed as a natural solution to spectrum congestion problems [71–75]. Cognitive radio has been advancing spectral sharing potential in the communications realm [76].

However, RF convergence between radar and communications users is largely an open area of research. These two systems, unlike the cognitive radio user base, have vastly different goals, metrics, and operators. Joint coding techniques, such as robust codes for communications that have desirable radar ambiguity properties, as well as codes that trade data rate and channel estimation error have been investigated as a co-design solution [77, 78].

Many modern applications have transitioned from classical design approaches to co-designed, joint radar-communications systems. A wide range of these applications are categorized in [2]. Emerging applications include automotive radar and vehicle-to-vehicle communications systems [24, 79], automated flight control and collision avoidance [80, 81], and high frequency imaging [82] and gesture recognition [83].

Recent publications consider more advanced topologies, such as simultaneous multi-static synthetic aperture radar with multiple-access communications [84, 85]. Recent publications have also focused on developing experimental platforms with which to test these emerging topologies [86, 87].

Finally, machine learning algorithms have only recently been applied to joint radar-communications problems such as spectral congestion. Machine learning and reinforcement learning, however, have been utilized to solve several problems in communications networks. In Reference [88], reinforcement learning is applied to wireless sensor networks to develop a novel media access control protocol that enables improved network performance (lower power consumption and higher throughput). The media access control protocol layer is formulated as a performance optimization problem (in terms of throughput and power consumption) and a reinforcement learning framework with an underlying Markov decision process is used to solve it, generating a set of node parameters that provides optimal performance. Reference [89] applies reinforcement learning algorithms for routing in cognitive radio networks and investigates the effects of various reinforcement learning parameters on network performance. A new reinforced learning routing scheme is proposed that explores the trade-off between improving the primary user's network performance versus improving the secondary user's network performance. Reference [90] presents an opportunistic spectral access algorithm for a single user in a cognitive radio network that employs a Markov decision process.

Reinforcement learning has also been applied in communications networks to improve routing performance [91–93]. Reference [94] presents a method, based on fuzzy reinforced learning techniques, that enables self-optimization of the capacity and coverage in a communications Long-Term Evolution (LTE) network.

Reinforcement learning also finds utility in the field of communications transmis-

sions. Reference [95] applies reinforcement learning to solve the problem of energy-efficient transmission of delay-sensitive data over a fading channel. A new reinforcement learning algorithm is proposed that finds a policy that is jointly optimal in terms of power-control, adaptive modulation schemes and dynamic power management. In Reference [96], reinforcement learning is applied to a mobile communications transmission problem and is shown to find optimal policies that maximize channel usage and minimize power consumption.

Finally, reinforcement learning has also been employed in cognitive radars. In Reference [97], a novel target tracking algorithm is developed for cognitive radars that utilizes reinforcement learning. Reference [98] presents a cognitive radar network architecture which optimizes radar performance and supports the application of machine learning algorithms. Reinforcement learning is used optimize the survivability of a naval ship by managing the modes of an air surveillance radar.

1.3 The Multiple-Access Communications Performance Bound - Motivation Behind Joint Radar-Communications Performance Bounds

We present the multiple-access communications system performance bound [99, 100] as motivation to develop inner bounds on the performance of a joint radar-communications system [4]. The joint radar-communications performance bounds discussed in this dissertation are derived by extending this multiple-access bound to include radar users. This extension of the multiple-access performance bound is made possible due to development of the radar estimation rate, an information theoretic performance metric for radar systems similar to the communications data rate.

We consider a scenario in which the channel propagation gain for the first communications system is given by a_1 and channel propagation gain for the second communications system is given by a_2. The power of the first communications transmitter

is denoted by P_1 and the power of the second communications transmitter is given by P_2. The scenario under consideration is shown in Figure 1.2.

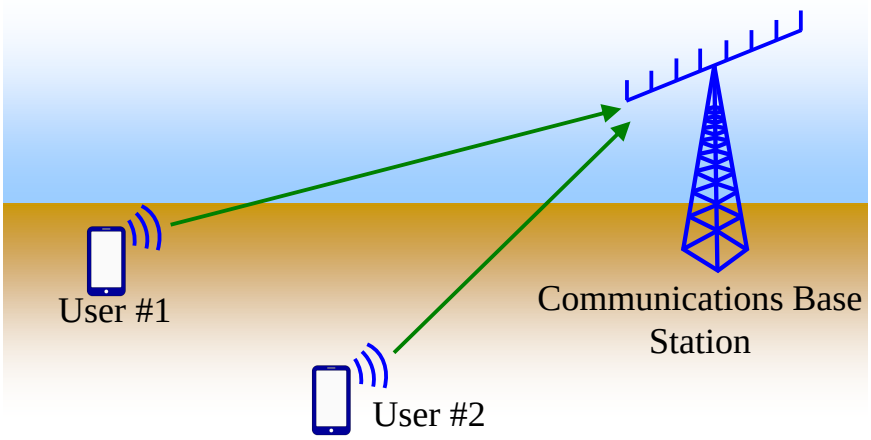

Figure 1.2: Physical multiple-access communications system scenario with 2 users. It is assumed both users are occupying the same bandwidth, and their transmitted signals converge at same time the communications base station. As a result, their communication rates must be considered jointly.

Their corresponding rates are denoted R_1 and R_2. Assuming that the noise variance is given by σ^2_{noise}, the fundamental limits on communications rate are shown in Figure 1.3. Vertices are found by jointly solving the two bounds to get [4, 5],

$$\{R_1,\, R_2\} = \left\{ \log_2\left(1 + \frac{\|a_1\|^2 P_1}{1 + \|a_2\|^2 P_2}\right), \log_2\left(1 + \frac{\|a_2\|^2 P_2}{\sigma^2_{\text{noise}}}\right) \right\}. \tag{1.1}$$

The other vertex can be found by switching the subscripts 1 and 2 in Equation (1.1). The region that satisfies these theoretical bounds is depicted in Figure 1.3. The achievable rate region is obtained by taking the convex hull [101] of the vertices 1-4. Because a radar signal return is not derived from a countable dictionary, the fundamental assumption of a communications signal is violated, and the bounds presented here can not be achieved by a joint radar-communications system [4]. The result presented in this section can be extended for more than two communications systems. For N different communications systems, the resultant achievable rate region will be a N-dimensional polytope [99].

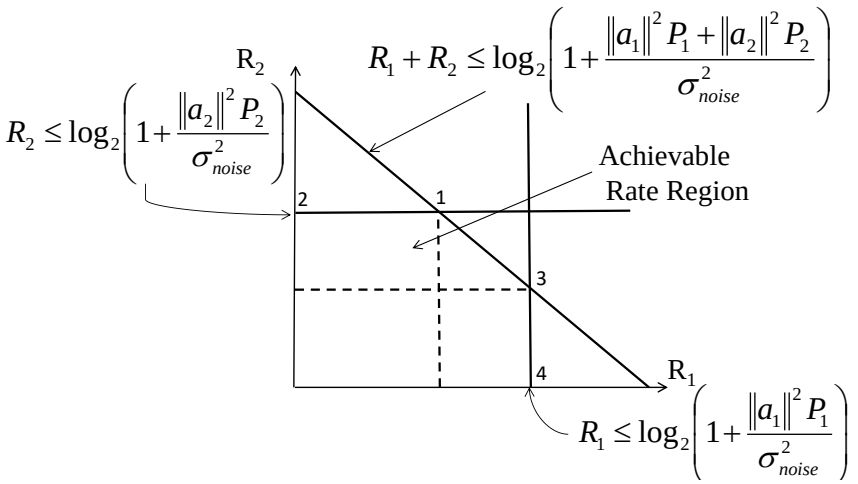

Figure 1.3: Pentagon containing two-user communications multiple-access achievable rate region. Lines 1,2 and 3,4 are the rates achieved considering each communications user in an isolated band. The bisecting diagonal is the joint achievable rate. As a result, the convex hull of the three lines constructs the achievable region of two-user communications within a given shared band.

1.4 Organization

This dissertation is organized as follows. In Chapter 2, we discuss the underlying models used to define a joint radar-communications system. We list the assumptions made for the simulation scenario that is being considered in this dissertation. We also discuss the successive interference cancellation (SIC) mitigation techniques that are employed at the receiver. in Chapter 3, we present a brief exposition of communications capacity theory to lay groundwork for the sections to come. We also derive two specific data rates that are used throughout this dissertation to measure communications performance. In Chapter 4 we introduce the estimation rate, a novel parametrization of radar information that provides a radar performance metric symmetric to the communications data rate. We also discuss the global estimation rate, an extension to the estimation rate that takes into account both local and non-local estimation errors. In Chapter 5, we develop several inner bounds on the performance of the joint radar-communications system by considering various scenarios

and developing estimation and data rates for the radar and communications systems respectively. In Chapter 6, we evaluate the performance bounds derived in Chapter 5 for an example set of parameters. We also introduce and discuss the concept of 'Not All Bits are Equal' and present two methods for selecting an ideal operating point for the joint radar-communications system. In Chapter 7, we present a new radar waveform design method for a joint radar-communications system in which the radar waveform spectrum and communications power spectral distribution are optimized to maximize joint performance. In Chapter 8, we develop several different extensions to the inner bounds on joint radar-communications system performance presented in Chapters 5 and 6. Finally, in Chapter 9, we summarize the work done and results obtained in this dissertation.

Chapter 2

JOINT RADAR-COMMUNICATIONS SYSTEM MODEL

In this chapter, we discuss the underlying models used to define a joint radar-communications system. We define the 'basic multiple-access scenario', a simple multiple-access joint radar-communications problem that is the simulation scenario being considered in this dissertation. Throughout this dissertation, we will derive joint radar-communications performance bounds for several variations of this 'basic multiple-access scenario'. We also state what assumptions are to be made for general simulation scenarios (such as the one shown in Figure 1.1) and what assumptions are to be made for the 'basic multiple-access scenario' considered in this paper only. The latter assumptions would need to be re-evaluated when considering different radar communications sharing schemes or scenarios. We also discuss the SIC mitigation techniques that are employed at the receiver. A table that defines all significant notation employed in this dissertation and their respective definitions is provided as well.

2.1 Notation Used

We present a table of significant notation that will be employed in this paper in Table 2.1.

Table 2.1: Survey of notation used in this dissertation.

Variable	Description
$\langle \cdot \rangle$	Expectation

Continued on next page

Table 2.1 – *Continued from previous page*

Variable	Description
$\|\| \cdot \|\|$	L2-norm or absolute value
$\theta, \boldsymbol{\theta}$	Estimation parameters
$s(\theta; z(t))$	Score function of $z(t)$ with respect to θ
$Q_M(.)$	Marcum Q-function
$\delta(.)$	Dirac-delta function
f	Frequency
t	Time
J	Fisher information
B	Full bandwidth of the system
B_{rms}	root mean square (RMS) radar bandwidth
$x(t)$	Unit-variance transmitted radar signal
$X(f)$	Radar signal frequency response
P_{rad}	Radar power
E_{rad}	Radar energy
τ_m	Time delay to m^{th} target
$\tau_m^{(k)}$	k^{th} observation of delay for m^{th} target
$\tau_{m,\text{pre}}$	Predicted time delay to m^{th} target

Continued on next page

Table 2.1 – *Continued from previous page*

Variable	Description
a_m	Complex combined antenna, cross-section, and propagation gain for m^{th} target
T	Radar pulse duration
N	Number of targets
δ	Radar duty factor
γ	Radar spectral shape parameter
σ^2_{resi}	Clutter residual power
$r(t)$	Unit-variance transmitted communications signal
P_{com}	Total communications power
b	Combined antenna gain and communications propagation loss (amplitude)
$n(t)$	Receiver thermal noise
σ^2_{noise}	Thermal noise power
k_B	Boltzmann constant
T_{temp}	Absolute temperature
$n_{\text{int+n}}(t)$	Interference plus noise for communications receiver
$n_{\text{radresi}}(t)$	Post-SIC radar residual

Continued on next page

Table 2.1 – *Continued from previous page*

Variable	Description
$\sigma^2_{\text{int+n+resi}}$	Interference plus thermal noise plus clutter residual for communications receiver
$\sigma^2_{\tau,\text{proc}}$	Variance of range fluctuation process
σ^2_{CRLB}	CRLB or estimation error variance
B_{com}	Communications only sub-band
B_{rad}	Radar only sub-band
B_{mix}	Mixed radar and communications sub-band
ρ_{RO}	Power spectral density used by radar only sub-band
ρ_{MU}	Power spectral density used by mixed use sub-band
α	Bandwidth fraction ratio for sub-band splitting
β	Power fraction used by communications only sub-band
R_{est}	Radar estimation rate
R_{CO}	Communications rate for communications only sub-band
R_{MU}	Communications rate for mixed use sub-band

Continued on next page

Table 2.1 – *Continued from previous page*

Variable	Description
$p_1, \ldots, p_N$	Phase parameters of polynomial chirp
ISNR	Integrated radar SNR

2.2 Problem Setup

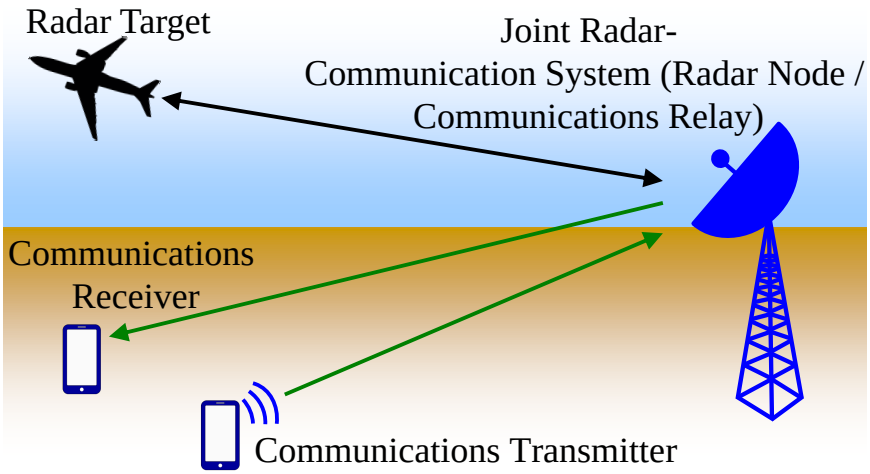

Figure 2.1: The joint radar-communications system 'basic multiple-access scenario.' This is a simplified version of the complicated RF convergence scenario shown in Figure 1.1. However, it provides a point of departure for discussing future work, and enables tractable, intuitive solutions presented here.

Due to the non-trivial nature of achieving RF convergence in a realistic simulation scenario as mentioned in Chapter 1, in this dissertation, we consider what we call the 'basic multiple-access scenario.' It is a simple scenario involving a radar and communications user attempting to use the same spectrum-space-time. This scenario is instructional, and can easily be scaled to more complicated scenarios by using it as a building block to construct real world examples. We present a diagram of

the 'basic multiple-access scenario' in Figure 2.1. In this scenario, the joint radar-communications system consists of an active, mono-static, pulsed radar and a single user communications system. We consider the joint radar-communications receiver to be a radar transmitter/receiver that can act as a communications receiver. The joint receiver can simultaneously estimate the radar target parameters from the radar return and decode a received communications signal. While the node architecture can easily be generalized to function as a communications relay by including a communications transmitter, this is not explicitly discussed in this paper. We refer to the scenario described in Figure 2.1 throughout the rest of this dissertation.

Despite the difficulty in achieving RF convergence in scenarios such as the one seen in Figure 1.1, we do know that some important assumptions have to be made in order to develop a tractable solution. Those key assumptions made in this work are as follows

- Radar and communications operate in the same frequency allocation simultaneously
- Joint radar-communications receiver has the ability to simultaneously decode a communications signal and estimate a target parameter
- Radar detection and track acquisition have already taken place

On top of the assumptions made above, the key assumptions made that apply for the scenario described in Figure 2.1 are as follows

- Radar system is an active, single-input single-output (SISO), mono-static, and pulsed system
- Radar system operates without any maximum unambiguous range
- A single SISO communications transmitter is present

- Only one radar target is present
- Target range or delay is the only parameter of interest
- Target cross-section is well estimated
- Communications signal is received through an antenna sidelobe; Antenna gains are not identical

It should be noted that this last set of assumptions are specific to the 'basic multiple-access scenario' shown in Figure 2.1. These assumptions will need to be re-assessed if different simulation scenarios or radar-communications sharing schemes are being taken into consideration.

2.3 Successive Interference Cancellation Receiver Model

We present the joint radar-communications receiver model that employs the SIC mitigation technique. SIC [4] is an algorithm that takes advantage of the target tracking ability of the joint radar-communications system to ensure that communications signal decoding and radar detection can be done cooperatively.

We assume we have some knowledge of the radar target range (or time-delay), based on prior observations, up to some random fluctuation (also called process noise) which is modeled as a zero-mean random variable $n_{\tau,\text{proc}}(t)$. Using this information, we can generate a predicted radar return signal (or pulse) and subtract it from the joint radar-communications received signal. Since there is some error in the predicted and actual target locations, this predicted radar signal suppression leaves behind a residual contribution, $n_{\text{radresi}}(t)$, to the joint received signal. By lowering the communications rate, the receiver can perfectly decode the communications message from the radar-suppressed joint received signal (which consists of the communications signal, thermal noise and radar residual). The joint radar-communications receiver uses

the decoded communications message to reconstruct and remove the communications waveform from the received signal to obtain a radar return signal free of communications interference. This method of interference cancellation is called SIC. We assume that SIC is employed by the joint radar-communications receiver whenever there is any overlap between the radar and communications signals.

SIC is the same optimal multiuser detection technique used for a two user multiple-access communications channel presented in Section 1.3 [99, 100], except it is now reformulated for a communications and radar user instead of two communications users. The block diagram of the joint radar-communications system considered in this scenario is shown in Figure 2.2.

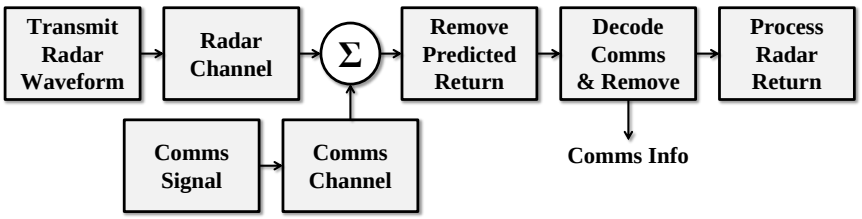

Figure 2.2: Joint radar-communications system block diagram for SIC scenario. The radar and communications signals have two effective channels, but arrive converged at the joint receiver. The radar signal is predicted and removed, allowing a reduced rate communications user to operate. Assuming near perfect decoding of the communications user, the ideal signal can be reconstructed and subtracted from the original waveform, allowing for unimpeded radar access.

As stated earlier, we have some knowledge of the target's range up to some range fluctuation or process noise, $n_{\tau_{\mathrm{m}},\mathrm{proc}}$. We model the process noise, $n_{\tau_{\mathrm{m}},\mathrm{proc}}$ as a random process. During the k^{th} observation, the delay for the m^{th} target is given by,

$$\tau_m^{(k)} = \tau_{m,\mathrm{pre}}^{(k)} + n_{\tau_{\mathrm{m}},\mathrm{proc}} \tag{2.1}$$

$$\tau_{m,\mathrm{pre}}^{(k)} = f(k; T_{\mathrm{pri}}, \boldsymbol{\phi})\,.$$

The function $f(k; T_{\mathrm{pri}}, \boldsymbol{\phi})$ is a prediction function which depends on T_{pri}, the pulse repetition interval (PRI), and a set of nonspecific system and target parameters, $\boldsymbol{\phi}$.

The variance of the range fluctuation process is given by

$$\sigma^2_{\tau_{\mathrm{m}},\mathrm{proc}} = \left\langle \left\| n_{\tau_{\mathrm{m}},\mathrm{proc}} \right\|^2 \right\rangle = \left\langle \left\| \tau_m^{(k)} - f(k; T_{\mathrm{pri}}, \boldsymbol{\phi}) \right\|^2 \right\rangle . \tag{2.2}$$

For N targets, the observed complex baseband [100] radar return $z(t)$ in the presence of a communications signal and noise is given by

$$z(t) = b\sqrt{P_{\mathrm{com}}}\, r(t) + \sqrt{P_{\mathrm{rad}}} \sum_{m=1}^{N} a_m\, x(t-\tau_m) \; + n(t)\,, \tag{2.3}$$

where complex combined antenna, cross-section, and propagation gain for m^{th} target, a_m, is a parameter such that the radar range equation for received power for the m^{th} target can be written as $\|a_m\|^2 P_{\mathrm{rad}}$. The received signal at the communications receiver with the predicted radar return suppressed is given by

$$\begin{aligned} \tilde{z}_{\mathrm{com}}(t) &= b\sqrt{P_{\mathrm{com}}}\, r(t) + n(t) + \sqrt{P_{\mathrm{rad}}} \sum_{m=1}^{N} a_m [x(t-\tau_m) - x(t-\tau_{m,\mathrm{pre}})] \\ &= b\sqrt{P_{\mathrm{com}}}\, r(t) + n(t) + n_{\mathrm{radresi}}(t)\,. \end{aligned} \tag{2.4}$$

Note that we have assumed here that the estimated amplitude is equal to the actual amplitude. This approach is only useful if the error in delay is smaller that $1/B$. For small fluctuations in delay, we can replace the difference between the actual and predicted radar return waveforms with a derivative,

$$x(t-\tau_m) - x(t-\tau_{m,\mathrm{pre}}) \approx \frac{\partial x(t-\tau_m)}{\partial t}\, n_{\tau_{\mathrm{m}},\mathrm{proc}}\,. \tag{2.5}$$

The signal observed by the communications receiver is then given by

$$\tilde{z}_{\mathrm{com}}(t) \approx b\sqrt{P_{\mathrm{com}}}\, r(t) + n(t) + \sqrt{P_{\mathrm{rad}}} \sum_{m=1}^{N} a_m\, \frac{\partial x(t-\tau_m)}{\partial t}\, n_{\tau_{\mathrm{m}},\mathrm{proc}}\,. \tag{2.6}$$

The interference plus noise from the communications system's point of view is given

by

$$
\begin{aligned}
n_{\text{int+n}} &= n(t) + n_{\text{radresi}}(t) \\
&= \sqrt{P_{\text{rad}}} \sum_{m=1}^{N} a_m [x(t-\tau_m) - x(t-\tau_{m,\text{pre}})] + n(t) \\
&\approx \sqrt{P_{\text{rad}}} \left(\sum_{m=1}^{N} a_m \frac{\partial x(t-\tau_m)}{\partial t} n_{\tau_{\text{m}},\text{proc}} \right) + n(t) \,, \qquad (2.7) \\
\sigma^2_{\text{int+n}} &= \left\langle \| n_{\text{int+n}} \|^2 \right\rangle \\
&= P_{\text{rad}} \left(\sum_{m=1}^{N} \| a_m \|^2 (2\pi)^2 B^2_{\text{rms}} \sigma^2_{\tau_{\text{m}},\text{proc}} \right) + \sigma^2_{\text{noise}} \,, \qquad (2.8) \\
B^2_{\text{rms}} &= \frac{\int \mathrm{d}f \, f^2 \, \| X(f) \|^2}{\int \mathrm{d}f \, \| X(f) \|^2} \,, \qquad (2.9)
\end{aligned}
$$

where B_{rms} comes from employing Parseval's theorem to convert $\partial x(t-\tau_m)/\partial t$ into the frequency domain and then using the differentiation property of the Fourier transform [100]. The RMS bandwidth is extracted from bandwidth B as follows

$$\gamma^2 B^2 = (2\pi)^2 B^2_{\text{rms}} \,, \qquad (2.10)$$

where, for a flat spectral shape, $\gamma^2 = (2\pi)^2/12$.

It should be noted that the performance bounds and results presented in this paper are very closely tied to the receiver model that is utilized. In this dissertation, we employ SIC at the receiver. However, employing different mitigation techniques and changing the receiver model will result in a set of performance bounds that are different from the ones presented in this paper. Additionally, we note that further analysis needs to be performed on the optimality of the SIC receiver model.

Chapter 3

THE COMMUNICATIONS DATA RATE

In this section, we present a brief exposition of communications capacity theory to lay groundwork for the chapters to come. The goal is to understand the basic communications phenomenology and to understand dealing with systems in an information theory context. This chapter serves as a useful bridge to discuss radar information theory in the next chapter, and forms the basis of how we consider the joint system. We discuss how to alter the communications data rate and the implications such alterations will have on the communications performance. Finally, we formally define the data rate for a joint radar-communications system after SIC has been applied. We present two methods to model the post-SIC radar residual and their corresponding data rates, the SIC communications data rate and the spectral water-filling (WF) SIC data rate.

3.1 Communications Rate

The communications rate capacity is formally defined as the supremum of achievable communications rates for a given channel model with respect to the input distribution. It tells us how much information as a function of time we can communicate with arbitrarily low BER. This problem was solved by Shannon in his seminal work [16].

3.1.1 Communications Rate Capacity for a Single Link

For our basic multiple-access scenario, we have a single communications user. Here, we present Shannon's results for the capacity of this link, assuming the user

is operating with no interference. We assume we have a single wireless communications link in a continuous memoryless real Gaussian channel with an average power constraint P_{com} and fixed bandwidth B and subject to receiver thermal noise. The additive white Gaussian noise (AWGN) channel is shown in Figure 3.1. The information that we wish to send is X, it is corrupted by the addition of the Gaussian random variable N, and we measure Y at the receiver. The capacity of such a channel was

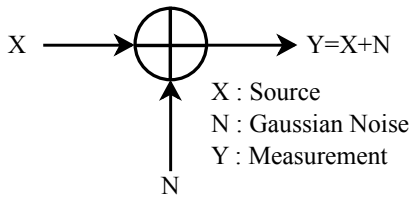

Figure 3.1: An AWGN channel. X contains the information we care about (symbols of arbitrary information), N is the noise added to our channel, and Y is the observation.

shown by Shannon to be [16]

$$R_{\text{com}} \leq \frac{1}{2\,T_s}\,\log_2\!\left[1+\frac{\|b\|^2\,P_{\text{com}}}{k_B\,T_{\text{temp}}\,B}\right] = \frac{1}{2\,T_s}\,\log_2[1+\text{SNR}]\ , \tag{3.1}$$

where $T_s = \frac{1}{2B}$ is the independent sampling rate of the band-limited system.

3.1.2 Altering the Communications Rate

As we have stated previously, the communications rate is simply a measure of the amount of arbitrary information that can be transmitted through the channel given spectrum-space-time access. We can increase the communications rate in a fixed bandwidth by:

Changing Source Entropy

The source entropy is dictated by the source distribution $p(X)$. The more we increase this entropy, the larger the mutual information [99]. While this may appear beneficial,

in doing so, we may exceed the average power constraint, violating the maximizing terms of the capacity problem. Ignoring the mutual information construct, we can attempt to communicate at a faster rate (rate taking into account redundant and non-redundant information [99]). However, exceeding the capacity means an arbitrarily low BER is not achievable. As a result, the spectral efficiency in b/s/Hz goes down when considering a channel with an arbitrarily low BER.

However, if the capacity is not exceeded, we achieve the maximum spectral efficiency given the problem parameters. Thus information must be carefully considered as to the root meaning when trading this parameter, as we see in Section 4.1 when considering radar estimation rate.

Changing Signal-to-Noise Ratio

From Equation (3.1), we see that by increasing the SNR, we get a net gain in information. Sphere packing is a good analogy. In an average power-constrained channel with fixed bandwidth, this amounts to decreasing the noise power. As a result, more "levels" can be transmitted and resolved on average at the receiver, meaning more entropy states and overall more information. Thus by increasing SNR, we can increase the source entropy level at which an arbitrary BER is possible. If less throughput is needed, the bandwidth can be reduced (noting the non-linear mapping), or the communications system can be duty cycled in time. This equates to spectrum-time isolation.

As we see, changing the rate of communication cannot be done arbitrarily, as BERs may preclude proper system operation. Increasing the communications rate through SNR is acceptable, but requires reduction of the thermal noise floor, or a change in the channel constraints. As we see in the next section, increasing the complementary radar estimation rate must also be done with careful consideration to proper system

operation and estimation performance.

3.2 The Successive Interference Cancellation Communications Data Rate

As mentioned in Chapter 2, at the receiver, we employ a process called SIC [4], an algorithm that takes advantage of the target tracking ability of the joint radar-communications system to ensure that communications signal decoding and radar detection can be done cooperatively. In Section 2.3, we assumed that we have some knowledge of the target's range up to some process noise, $n_{\tau_{\mathrm{m}},\mathrm{proc}}(t)$. We now model this process noise, $n_{\tau_{\mathrm{m}},\mathrm{proc}}(t)$ as a Gaussian random variable. As a result, from Equation (2.7), we see that the radar residual, $n_{\mathrm{radresi}}(t)$, is Gaussian as well. Thus, the noise floor from the communications receiver's perspective is higher and given by Equation (2.8). The receiver can perfectly decode the communications message from the joint received signal at a lower communications rate, called the SIC communications rate.

The joint radar-communications receiver uses the decoded communications message to reconstruct and remove the communications waveform from the received signal to obtain a radar return signal free of communications interference. This mitigation technique is called SIC. The block diagram of the joint radar-communications system considered in this scenario is shown in Figure 2.2.

When applying SIC, the interference residual plus noise signal $n_{\mathrm{int+n}}(t)$, from the communications receiver's perspective, is given by Equation (2.7) [4, 5]. The process noise and, as a result, the radar residual are modeled with a Gaussian distribution. Hence, the interference residual plus noise is a zero mean Gaussian random variable with variance, $\sigma^2_{\mathrm{int+n}}$, given by Equation (2.8) [4, 5]. The corresponding communica-

tions rate, known as the SIC data rate, is given by

$$R_{\text{com}} \leq B \log_2\left(1 + \frac{\|b\|^2 P_{\text{com}}}{\sigma^2_{\text{int+n}}}\right). \tag{3.2}$$

It should be noted that the radar residual used to obtain Equation (3.2) is modeled by a Gaussian distribution because Gaussian distributions have a closed form solution to entropy [99], enabling a closed form solution for the SIC communications rate to exist. Employing any other distribution to model the radar residual will result in a different SIC communications rate, as we will see in the next section.

3.3 The Spectral Water-filling Successive Interference Cancellation Data Rate

In this section, we utilize the continuous spectral WF algorithm [99, 102] to determine the optimal communications power distribution over frequency. The continuous spectral WF algorithm optimizes the data rate for a given noise power spectral density [99, 102]. Once the receiver model is known, the communications transmitter can easily determine the noise spectral density at the receiver, $N_{\text{int+n}}(f)$, and apply the continuous spectral WF algorithm to determine the optimal communications transmit power distribution, $P(f)$. This communications power distribution, $P(f)$, maximizes the communications data rate at which the joint radar-communications receiver decodes the communications message. We define this maximized communications rate as the spectral WF SIC data rate. The continuous spectral WF algorithm is a continuous form extension of the WF algorithm employed in References [4, 5]. Figure 3.2 highlights how the continuous spectral WF algorithm selects the optimal power distribution.

As mentioned earlier, since we employ the SIC model at the joint radar-communications receiver, the receiver will decode the communications message after the predicted radar signal has been mitigated from the received signal. As a result, from the com-

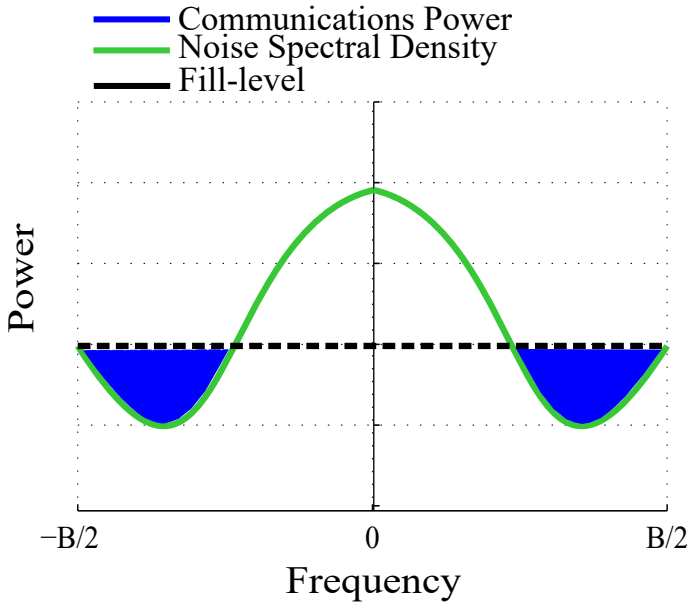

Figure 3.2: An example of the continuous spectral WF algorithm. The black, dashed line indicates the fill level (maximum amount of communications power that can be allocated at any frequency), the green curve represents the noise power spectral density $N_{\text{int+n}}(f)$, and the optimal communications power spectral distribution is shown in blue.

munications receiver's perspective, the channel will be corrupted by noise given by Equation (2.7). In order to find the noise spectral density, $N_{\text{int+n}}(f)$, we first calculate the autocorrelation function of the time- and band-limited noise signal, $n(t)$ (since the received signal is also time- and band-limited),

$$\begin{aligned}
\gamma(\alpha) &= \left\langle n_{\text{int+n}}(t)\, n^*_{\text{int+n}}(t-\alpha)\right\rangle \\
&= \langle n(t)\, n^*(t-\alpha)\rangle + \langle n_{\text{radresi}}(t)\, n_{\text{radresi}}(t-\alpha)\rangle \\
&= k_B\, T_{\text{temp}}\, B\ \text{sinc}(\pi\, B\, \alpha) + \|a\|^2\, P_{\text{rad}}\, \sigma^2_{\tau,\text{proc}}\, \frac{\partial x(t-\tau)}{\partial t}\, \frac{\partial x^*(t-\tau-\alpha)}{\partial t} \\
&= k_B\, T_{\text{temp}}\, B\ \text{sinc}(\pi\, B\, \alpha) + (4\pi^2)\, \|a\|^2\, P_{\text{rad}}\, \sigma^2_{\tau,\text{proc}} \int_{-\infty}^{\infty} df\, f^2 X(f) X^*(f) \mathrm{e}^{i2\pi f\alpha} \\
&= k_B\, T_{\text{temp}}\, B\ \text{sinc}(\pi\, B\, \alpha) + (4\pi^2)\, \|a\|^2\, P_{\text{rad}}\, \sigma^2_{\tau,\text{proc}}\, g(\alpha)\,, \qquad (3.3)
\end{aligned}$$

where Parseval's theorem and the time-shift and time derivative properties of the Fourier transform are used between the second and third steps, $\text{sinc}(x) = \frac{\sin(x)}{x}$, and

$g(\alpha)$ is the inverse Fourier transform with respect to α of $G(f) = \|X(f)\|^2 f^2$. Since the noise power spectral density and autocorrelation are Fourier transform pairs, the noise power spectral density is given by

$$\begin{aligned} N_{\text{int+n}}(f) &= N(f) + N_{\text{radresi}}(f) \\ &= k_B\, T_{\text{temp}}\, B\, \Pi_B(f) + (4\pi^2)\, \|a\|^2\, P_{\text{rad}}\, \sigma^2_{\tau,\text{proc}}\, \|X(f)\|^2\, f^2\,, \end{aligned} \tag{3.4}$$

where $N(f)$ and $N_{\text{radresi}}(f)$ are the Fourier transforms of $n(t)$ and $n_{\text{radresi}}(t)$ respectively, and $\Pi_B(f)$ is a top-hat or rectangular function from $\frac{-B}{2}$ to $\frac{B}{2}$. The optimal communications power spectrum determined by the continuous spectral WF algorithm is given by

$$P(f) = \left(\mu - \frac{N_{\text{int+n}}(f)}{b^2}\right)^+, \tag{3.5}$$

where $(x)^+ = x$ if $x \geq 0$; otherwise $(x)^+ = 0$ and μ is a constant that is determined from the power constraint

$$P_{\text{com}} = \int_{\frac{-B}{2}}^{\frac{B}{2}} df\, P(f) \;= \int_{\frac{-B}{2}}^{\frac{B}{2}} df\; \left(\mu - \frac{N_{\text{int+n}}(f)}{b^2}\right)^+ . \tag{3.6}$$

The spectral WF SIC data rate (the corresponding data rate for the channel with noise spectral density $N_{\text{int+n}}(f)$) is given by [99, 102]

$$R_{\text{com}} = \frac{1}{2} \int_{\frac{-B}{2}}^{\frac{B}{2}} df \log\left(1 \;+\; \frac{b^2\, P(f)}{N_{\text{int+n}}(f)}\right) . \tag{3.7}$$

It should be noted that due to the complexity involved in determining analytical solutions for the integrals shown in Equations (3.6) and (3.7), these integrals are evaluated numerically to determine the optimal value for μ and the communications data rate.

As we see from Equation (3.4), the spectral WF SIC data rate is dependent on the shape of the radar waveform spectrum. Hence, the continuous spectral WF algorithm is ideally suited to be employed in scenarios where the radar waveform spectrum is

not flat such as the one discussed in Chapter 7, where we use optimization theory to shape the radar waveform spectrum to maximize joint radar-communications performance. Furthermore, since we assume that the radar waveform spectrum is flat for a significant part of this dissertation, we argue that the continuous spectral WF algorithm will not provide any significant benefits in terms of communications performance or data rate. This fact coupled with the numerical complexity involved in calculating the spectral WF SIC data rate makes the SIC communications data rate better suited for the other simulation scenarios considered in this dissertation.

Chapter 4

THE RADAR ESTIMATION INFORMATION RATE

In this chapter, we introduce a novel parametrization of radar performance in terms of information, the estimation rate. The estimation rate provides a measure of the amount of information contained in a radar return signal. We present a detailed derivation for the estimation rate for a single radar target and provide an intuitive interpretation of radar information and the estimation rate. We also discuss how to increase or decrease the estimation rate and what such an alteration can imply for radar performance.

Finally, we also extend the estimation rate to account for non-local or low-SNR estimation errors. This extended estimation rate is called the global estimation rate.

4.1 Radar Estimation Rate

The estimation rate is a metric analogous to the communications rate and provides a measure of the information about a target that is gained from radar illumination in radar tracking estimation scenarios. In general, the target has some entropy or information about itself that is not explicitly being communicated to the radar system by the target. Radar illumination can be viewed as the target unwillingly communicating this target entropy or information to the radar receiver. Thus, the radar channel can be characterized as an uncooperative communications channel [5] and the estimation rate can be intuitively thought of as the mutual information between the radar return signal and the target [5].

As stated in previous chapters, we assume that the radar system has some knowledge of the target's range, based on prior observations, up to some range fluctuation.

This range fluctuation, also called process noise, is interpreted as a fluctuation in delay which is modeled by a Gaussian distribution $n_{\tau,\text{proc}}$ with variance given by $\left\langle \|n_{\tau,\text{proc}}\|^2 \right\rangle = \sigma^2_{\tau,\text{proc}}$. By definition, the process noise is the true information that is being transmitted through the radar channel and the estimation rate represents the minimum number of bits needed to encode the process noise. The radar estimation rate can be extended to include estimation of different target parameters as seen in Reference [103], in which the estimation rate is extended to take into account Doppler estimation. It should be noted that modeling the process noise as a Gaussian random variable implies that the radar residual, $n_{\text{radresi}}(t)$, is also modeled by a Gaussian random variable as we see from Equation (2.7).

The estimation rate is formally defined as the quantity that represents the minimum number of bits needed to encode the Kalman residual, which is the statistical deviation from the radar prediction of a target parameter, for a given channel degradation [5]. The estimation rate tells us how much information we stand to gain once we subtract the prediction of the target's parameter, since the predicted target parameter is already known and does not truly convey any information.

Considering the radar channel to act as an uncooperative communications channel, the process noise, $n_{\tau,\text{proc}}$, is the information X being transmitted. This transmitted information X is degraded by the addition of some noise N, which for target parameter estimation is given by the radar estimation error, $n_{\tau,\text{est}}$, and a noisy measurement of X is received at the radar receiver system. The estimation rate for our uncooperative channel is therefore given by [99]

$$R_{\text{est}} = \frac{I\left(X; X+N\right)}{T_{\text{pri}}}, \tag{4.1}$$

where $T_{\text{pri}} = T/\delta$.

Assuming that the radar estimation error, $n_{\tau,\text{est}}$, is Gaussian with variance $\left\langle \|n_{\tau,\text{est}}\|^2 \right\rangle =$

$\sigma^2_{\tau,\text{est}}$, the mutual information can be shown to be [99]

$$R_{\text{est}} \leq \frac{1}{2\,T_{\text{pri}}} \log_2\left(1 + \frac{\sigma^2_{\tau,\text{proc}}}{\sigma^2_{\tau,\text{est}}}\right). \tag{4.2}$$

We leave it as an inequality because typically systems must perform certain non-ideal processing steps, such as quantization. As a result, the data-processing inequality is enforced [99].

It should be noted that a Gaussian distribution is used to model the radar estimation error, $n_{\tau,\text{est}}$, and process noise, $n_{\tau,\text{est}}$, because Gaussian distributions have a closed form solution to entropy, enabling a closed form solution for the estimation rate to exist. In radar estimation problems where a Gaussian distribution is not appropriate and a closed form solution for the estimation rate does not exist, bounds on the radar estimation rate (radar mutual information) exist which can still capture a measure of radar information [104]. We leave the estimation rate as an inequality because typically systems must perform certain non-ideal processing steps, such as quantization. As a result, the data-processing inequality is enforced [99].

Looking at the ratio of variances $\frac{\sigma^2_{\tau,\text{proc}}}{\sigma^2_{\tau,\text{est}}}$, we see that $\sigma^2_{\tau,\text{proc}} = \left\langle \|n_{\tau,\text{proc}}\|^2 \right\rangle$ is the power of the transmitted information, $\left\langle \|X\|^2 \right\rangle$, and that $\sigma^2_{\tau,\text{est}} = \left\langle \|n_{\tau,\text{est}}\|^2 \right\rangle$ is the noise power, $\left\langle \|N\|^2 \right\rangle$. Thus, the ratio of variances $\frac{\sigma^2_{\tau,\text{proc}}}{\sigma^2_{\tau,\text{est}}}$ represents the SNR of the uncooperative communications channel that is used to characterize the radar channel. This is more evident when comparing Equation (4.2) to Equation (3.1). Thus, Equation (4.2) can be written as [4]

$$R_{\text{est}} \leq \frac{1}{2\,T_{\text{pri}}} \log_2(1 + \text{SNR})\ . \tag{4.3}$$

4.1.1 Estimation Rate for Local Estimation Errors

If we assume that we are operating in a high-SNR regime and that the radar estimator achieves the CRLB, the variance of delay estimation, σ^2_{est}, is given by the

CRLB for time delay estimation and Equation (4.2) can be written as

$$\begin{aligned} R_{\text{est}} &\leq \frac{1}{2\,T_{\text{pri}}}\,\log_2\!\left[1+\left(8\pi^2\,\sigma^2_{\tau,\text{proc}}\,B^2_{\text{rms}}\,\text{ISNR}\right)\right]\,, \\ &= \frac{1}{2\,T_{\text{pri}}}\,\log_2\!\left[1+\left(8\pi^2\,\sigma^2_{\tau,\text{proc}}\,\gamma^2\,B^2\,\text{ISNR}\right)\right]\,, \end{aligned} \tag{4.4}$$

where the CRLB for time delay estimation is given by [105]

$$\begin{aligned} \sigma^2_{\text{CRLB}} &= (8\pi^2 B^2_{\text{rms}}\text{ISNR})^{-1} \\ &= (2\,\gamma^2\,B^2\,\text{ISNR})^{-1}\,. \end{aligned} \tag{4.5}$$

It should be noted here that if the delay estimator doesn't achieve the CRLB, the estimation rate will be lowered. Furthermore, since we are bounding the estimation error variance with the CRLB, the estimation rate only takes into account local estimation errors. In practice, the estimation noise depends not only on the CRLB, but also global estimation ambiguity error as well, especially at low SNRs.

4.2 Altering the Estimation Rate

As we have stated before, the estimation rate is simply a measure of the amount of information about the target that can be gained through the radar channel through illumination. Thus, an increase in the estimation rate implies an increased amount of information about the target is gained by the radar system through the channel. As we see, increasing the estimation rate can lead to better target parameter estimation performance and reducing the estimation rate can result in reduced spectral access but a higher estimation rate is not necessarily always favorable. However, the estimation rate is still a metric that can be used to determine how to allocate spectral resources as we will see in Chapters 6 and 7. From Equation (4.2), we see that the estimation rate can be altered by:

4.2.1 Changing Process Noise

Process noise represents the amount of information of the target that is unknown. From Equation (4.2), we see that by increasing the process noise, we increase the estimation rate. Increasing the process noise essentially means that the target behaves in an unexpected manner when compared to how the target was modeled by the radar system. Thus, the amount of information that can be gained about the target through radar illumination increases and this is reflected via an increase in the estimation rate.

However, if the target was modeled accurately, then the information content gained through radar illumination is low because much of the true uncertainty about the target was bought down by accurately modeling the target. This is beneficial since, as seen in [106], by reducing the process noise, the radar system can illuminate less frequently. Thus, by using a more accurate model of the target and reducing process noise, the radar system needs less spectral access which is beneficial for co-operative radar-communications coexistence.

4.2.2 Changing Estimation Performance

From Equation (4.2), we see that by improving the estimation performance or decreasing the mean-squared estimation error σ^2_{est}, we increase the estimation rate. By improving the estimation performance, the radar system is able to extract more information about the target, thus increasing the estimation rate. Increasing the estimation rate in this manner, enhances the target parameter estimation quality of the radar which is always desirable.

As we have seen above, an increase or decrease in the estimation rate is neither strictly good nor bad, rather it is the manner in which the estimation rate was altered that can be beneficial or detrimental to the joint radar-communications system. If

the estimation rate is decreased by lowering the process noise, then the radar system needs less spectral access which results in a less congested spectrum (aids in radar-communications coexistence). However, if the process noise is arbitrarily increased by ignoring prior information (a physical predictive model, for example), then we gain more information through measurement, but the estimation performance is degraded and radar system performance is lowered. However, increasing SNR increases both estimation rate, and estimation parameter performance.

There is a trade-off between reducing radar spectral access and increasing target parameter estimation quality. On one hand reducing estimation rate by reducing process noise frees up more of the spectrum to be used by communications systems, aiding coexistence, whereas increasing the estimation rate by improving target parameter estimation quality increases the radar system performance. Accordingly, attempts should be made to maximize the estimation rate from an SNR perspective, while jointly considering estimation error performance. That is, estimation error should never be increased to increase estimation rate, but steps to maximize the mutual information for a fixed process noise should always been taken.

4.3 Global Estimation Rate

In the previous section, we derived the estimation rate that takes into account local estimation errors only. We use the method of interval errors [107, 108] to calculate the effect of non-local errors on time-delay estimation performance. The method of interval errors is an estimation technique that is used to extend local parameter estimation bounds (such as the CRLB) to include non-local effects (such as confusing the mainlobe with a sidelobe) [107]. For the sake of simplicity, we assume that only the largest sidelobe can be confused for the main lobe. The values and locations of the largest sidelobe peaks are found through simulation. A closed-form solution of the

probability of sidelobe confusion, $P_{s.l.}$ is obtained in terms of the values and locations of the sidelobe peaks, integrated radar SNR, and the Marcum Q-function Q_M [100]. The method of intervals time-delay estimation variance is then given by

$$\sigma^2_{\text{est}} = [1 - P_{s.l.}(\text{ISNR})]\ \sigma^2_{\text{CRLB}}(\text{ISNR}) \ +\ P_{s.l.}(\text{ISNR})\, \phi^2_{s.l.}\,, \tag{4.6}$$

where $\phi_{s.l.}$ is the offset in time (seconds) between the autocorrelation peak sidelobe and main lobe [5]. The probability of sidelobe confusion, $P_{s.l.}$, is given by [100]

$$\begin{aligned} P_{s.l.}(\text{ISNR}) = 1 - Q_M \Bigg(& \sqrt{\frac{\text{ISNR}}{2}\left(1 + \sqrt{1 - \|\rho\|^2}\right)}, \\ & \sqrt{\frac{\text{ISNR}}{2}\left(1 - \sqrt{1 - \|\rho\|^2}\right)} \Bigg) \\ + Q_M \Bigg(& \sqrt{\frac{\text{ISNR}}{2}\left(1 - \sqrt{1 - \|\rho\|^2}\right)}, \\ & \sqrt{\frac{\text{ISNR}}{2}\left(1 + \sqrt{1 - \|\rho\|^2}\right)} \Bigg), \end{aligned} \tag{4.7}$$

where ρ is the ratio of the main lobe to the peak sidelobe of the autocorrelation function. The global estimation rate is calculated by utilizing the method of intervals estimation error variance, given by Equation (4.6), in Equation (4.2).

Chapter 5

LIMITS ON JOINT RADAR-COMMUNICATIONS PERFORMANCE

In this chapter we develop several inner bounds on the performance of the joint radar-communications system by considering various scenarios and developing estimation and data rates for the radar and communications systems respectively.

5.1 Inner Bounds on Joint Radar-Communications Performance

In this section, we derive inner bounds on the performance of the joint radar-communications system. As mentioned earlier, performance is measured in data information rate for the communications system and estimation information rate for the radar system. To find these inner bounds, we hypothesize an idealized receiver and determine the bounding rates. To simplify the discussion, we consider only a single radar target with delay τ and gain-propagation-cross-section product a.

Additionally, for the sake of simplicity, we assume that there is only a single communications link present. The results derived in this section can be extended for more than the single communications channel link. Similar to the multi-access channel case described in Section 1.3, this extension results in an $(N+1)$-dimensional polytope, for N communications users and a single radar case.

5.1.1 Isolated Sub-Band Inner Bound

In this section, we derive an inner bound by considering a scenario in which we partition the total bandwidth into two sub-bands, one for radar only and the other for communications, which is the standard, isolated solution. Each system functions without any interference in their respective sub-band [4, 5]. The bandwidth is split

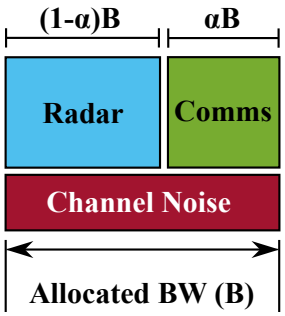

Figure 5.1: isolated sub-band (ISB) bandwidth split. The noise floor is flat across the total bandwidth. The radar user and communications user are then given some complementary fraction of the overall bandwidth B, parameterized by the blending ratio α.

between the two sub-bands according to some blending ratio α such that,

$$B = B_{\text{rad}} + B_{\text{com}}\,,\; B_{\text{com}} = \alpha\, B\,,\; B_{\text{rad}} = (1-\alpha)\, B\,, \tag{5.1}$$

as shown in Figure 5.1. The corresponding communications rate (for the communications only sub-band) is given by

$$R_{\text{com}} \leq B_{\text{com}} \log_2\!\left(1 + \frac{\|b\|^2\, P_{\text{com}}}{k_B\, T_{\text{temp}}\, B_{\text{com}}}\right)\,, \tag{5.2}$$

where b is the combined gain and communications propagation loss product defined in Equation (3.1). The corresponding radar estimation rate is given by

$$R_{\text{est}} \leq \frac{1}{2\, T_{\text{pri}}} \log_2\!\big(1 + \big(2\, \sigma^2_{\tau,\text{proc}}\, \gamma^2\, B^2_{\text{rad}}\, \text{ISNR}\big)\big)\,. \tag{5.3}$$

5.1.2 Successive Interference Cancellation Inner Bound

We discuss the technique of SIC and use it to construct a inner bound on performance. As stated in Section 4.1, we have some knowledge of the radar target parameter (in this case, range or time-delay) up to some range fluctuation (also called process noise). Using this information, we can generate a predicted radar return and subtract it from the joint radar-communications received signal. After suppressing the radar return, the receiver then decodes and removes the communications signal

from the observed waveform to obtain a radar return signal free of communications interference. This method of interference cancellation is called SIC. An achievable inner bound on joint radar-communications system performance can be derived by taking the convex hull of all achievable communications and estimation rate pairs, the SIC inner bound [4, 5]. The block diagram of the joint radar-communications system considered in this scenario is shown in Figure 2.2.

If $R_{\text{est}} \approx 0$ (for example, because of a low power return or well modeled target), it is as if the radar interference is not present and the communications system can operate at a data rate determined by the isolated communications bound,

$$R_{\text{com}} \leq B \log_2\left(1 + \frac{\|b\|^2 P_{\text{com}}}{k_B T_{\text{temp}} B}\right) . \tag{5.4}$$

If the estimation rate is non-trivial, then the residual contributes to the communications system's noise floor. We can mitigate this by reducing R_{com} for a given transmit power. After subtraction of the predicted radar return, the receiver can decode the communications signal. With knowledge of the communications system, forward error correction and spectral shaping can be reapplied, and the radar system can remove the ideal communications signal from the observed waveform, leaving just the radar return. Thus, radar parameter estimation can be done without corruption from any outside interference. This implies that from the communications receiver's perspective, it observes interference plus noise as described by Equation (2.8) [4, 5] and the corresponding communications rate is given by Equation (3.2).

In this regime, the corresponding estimation rate bound R_{est} is given by Equation (4.4). The SIC inner bound is given by connecting points given by Equations (3.2), (4.4) and (5.4). This is equivalent to time sharing between full band SIC operation (normal radar, reduced communications), and communications only (no radar). In [106], it was proposed to modulate radar spectral access based on the

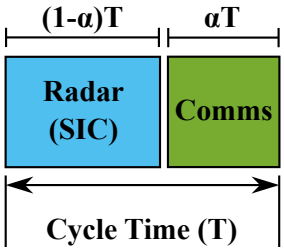

Figure 5.2: The constant information radar (CIR) time-sharing scheme. For a given cycle time T, part of the cycle is allocated to radar operation, where a reduced rate communications user is operating using SIC. For the remainder of the cycle, the communications user is free to operate without any radar emissions. Note that the radar access time can be fixed at the duration for a single spectral access, and then the cycle time can be varied.

estimation rate measure, or more specifically, the radar estimation information. The goal was to delay target revisit until k bits of information about the target would become available. This fixed the information rate locally around radar access, enforcing a spectral efficiency for allowing radar access. During periods when the target was well-modeled, or the SNR was low, insufficient information could be obtained, and so the communications user is allowed to broadcast freely. Figure 5.2 shows this scheme in action. Our blending ratio α now modulates radar time access, in which the communications user is allowed to communicate slower at the SIC node. α is increased when the target is well-modeled, or the SNR is low. In the former case, there is little information gained through measurement, since the target is well predicted [106]. For the SNR, measurement noise dominates the entropy, and very little "good" information is obtained through access of the spectrum. The rates are then given by

$$R_{\text{com}} \leq \alpha B \log_2\left(1 + \frac{\|b\|^2 P_{com}}{\sigma^2_{\text{int+n}}}\right) + (1-\alpha)\, B\, \log_2\left(1 + \frac{\|b\|^2 P_{\text{com}}}{k_B\, T_{\text{temp}}\, B}\right), \tag{5.5}$$

$$R_{\text{est}} \leq (1-\alpha)\, \frac{1}{2\, T_{\text{pri}}} \log_2\big(1 + \big(8\,\pi^2\, \sigma^2_{\tau,\text{proc}}\, B^2_{\text{rms}}\, \text{ISNR}\big)\big)\,. \tag{5.6}$$

5.1.3 *Communications Water-filling Bound*

In this section, we consider a scenario in which the total bandwidth is split into two sub-bands, one sub-band for communications only and the other sub-band for both radar and communications. It is not necessary that the sub-bands be of equal bandwidth. We use WF to distribute the total communications power between the two sub-bands [4, 5]. WF optimizes the power and rate allocation between multiple channels [99, 100]. In this scenario, the bandwidths of the two channels need not be equal. This means that the problem formulation in this scenario is not a standard formulation. Hence, we expect that the shape of the inner-bound derived by employing WF will be non-intuitive. The mixed use channel operates at the SIC rate vertex defined by Equations (3.2) and (4.4). The block diagram of the joint radar-communications system considered in this scenario is shown in Figure 5.3.

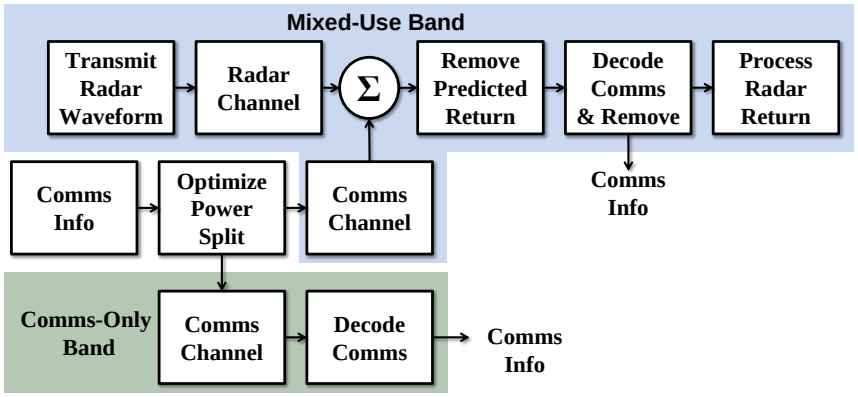

Figure 5.3: Joint radar-communications system block diagram for communications only and mixed use sub-bands. One band is operating only for communications, and is spectrally isolated from the radar operation. The other sub-band is operating using SIC, where the communications and radar RF energy converge at the receiver. The optimal power split is determined using WF.

As in the ISB case, we use the blending ratio α to split the overall bandwidth B into a communications only sub-band, and a mixed sub-band operating at the SIC

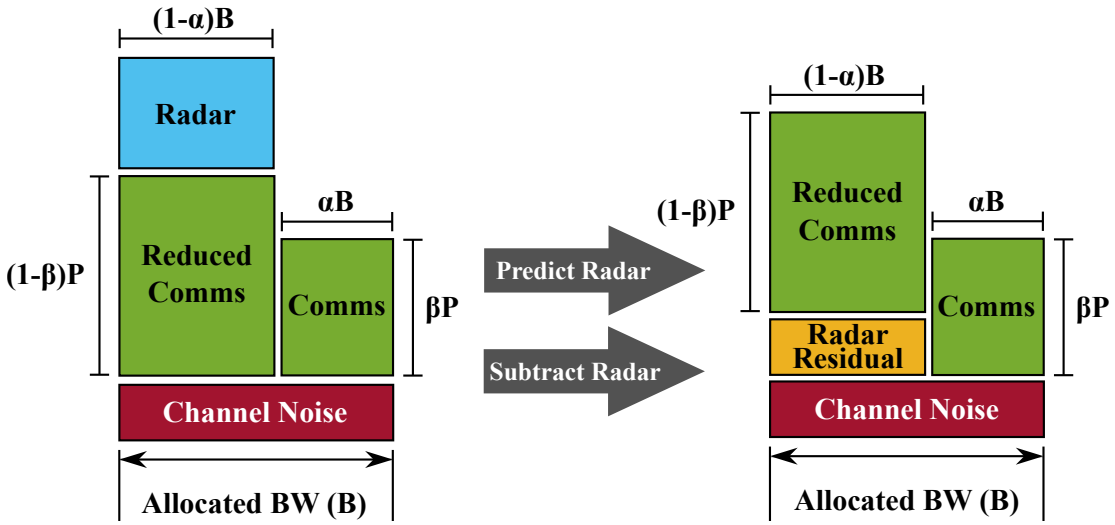

Figure 5.4: WF bandwidth allocation. As in the ISB case, we use our blending ratio α to parameterize the allocation of bandwidth between the communications only user, and the joint radar-communications band operating using SIC. After the radar is predicted and subtracted, the mixed band has a radar residual contributing to the communications noise floor. We then have two channels with differing noise degradations, and the normal WF solution follows.

node:

$$B = B_{\text{com}} + B_{\text{mix}}\,,\; B_{\text{com}} = \alpha\, B\,,\; B_{\text{mix}} = (1-\alpha)\, B\,. \tag{5.7}$$

We then optimize the power utilization, β, between sub-bands,

$$P_{\text{com}} = P_{\text{CO}} + P_{\text{MU}}\,,\; P_{\text{CO}} = \beta\, P_{\text{com}}\,,\; P_{\text{MU}} = (1-\beta)\, P_{\text{com}}\,. \tag{5.8}$$

There are two effective channels

$$\mu_{\text{com}} = \frac{b^2}{k_B\, T_{\text{temp}}\, B_{\text{com}}}\,,\; \mu_{\text{mix}} = \frac{b^2}{\sigma^2_{\text{int+n}}}\,, \tag{5.9}$$

$$\sigma^2_{\text{int+n}} = \|a\|^2\, P_{\text{rad}}\, \gamma^2\, B^2_{\text{mix}}\, \sigma^2_{\tau,\text{proc}} + k_B\, T_{\text{temp}}\, B_{\text{mix}}\,. \tag{5.10}$$

The first for the communications only channel, and the second for the mixed use channel. We apply the WF result derived in [4] and see that the optimal power

distribution (β) between the two sub-channels is given by:

$$\beta = \alpha + \frac{1}{P_{\text{com}}}\left(\frac{\alpha - 1}{\mu_{\text{com}}} + \frac{\alpha}{\mu_{\text{mix}}}\right) ; \quad \text{when } P_{\text{com}} \geq \frac{\alpha}{(1-\alpha)\,\mu_{\text{mix}}} - \frac{1}{\mu_{\text{com}}} . \tag{5.11}$$

The resulting communications rate bound in the communications-only sub-band, $R_{\text{com,CO}}$, is given by

$$R_{\text{com,CO}} \leq B_{\text{com}} \log_2\left(1 + \frac{\beta\, P_{\text{com}}\, b^2}{k_B\, T_{\text{temp}}\, B_{\text{com}}}\right) . \tag{5.12}$$

The mixed use communications rate inner bound, $R_{\text{com,MU}}$, is given by

$$R_{\text{com,MU}} \leq B_{\text{mix}}\, \log_2\left(1 + \frac{b^2\,(1-\beta)\, P_{\text{com}}}{\sigma^2_{\text{int+n}}}\right), \tag{5.13}$$

where $\sigma^2_{\text{int+n}}$ is given by Equation (5.10). The corresponding radar estimation rate inner bound is then given by

$$R_{\text{est}} \leq \frac{1}{2\,T_{\text{pri}}} \log_2\big(1 + \big(2\,\sigma^2_{\tau,\text{proc}}\,\gamma^2\,B^2_{\text{mix}}\,\text{ISNR}\big)\big) . \tag{5.14}$$

5.1.4 Optimal-Fisher-Information Inner Bound

In this section, we construct an inner rate bound by splitting the total bandwidth into two sub-bands and distributing the radar power (or power spectral density) between the two sub-bands in a way that minimizes the CRLB (or maximizes the Fisher information) for time-delay estimation. The block diagram of the joint radar-communications system considered in this scenario is shown in Figure 5.5.

The bandwidth will be split between the two sub-bands according to some α such that,

$$B = B_{\text{rad}} + B_{\text{mix}} \,,\; B_{\text{rad}} = \alpha\, B \,,\; B_{\text{mix}} = (1-\alpha)\, B \,, \tag{5.15}$$

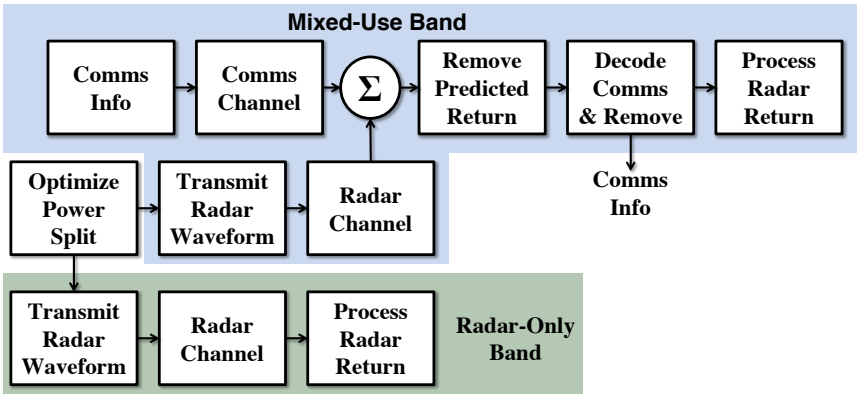

Figure 5.5: Joint radar-communications system block diagram for radar only and mixed use sub-bands. One band is operating only for radar, and is spectrally isolated from the communications operation. The other sub-band is operating using SIC, where the communications and radar RF energy converge at the receiver. We use our blending ratio α to parameterize the allocation of bandwidth between the radar only user, and the joint radar-communications band operating using SIC. We derive the optimal radar power split between both channels that minimizes the estimation error variance.

and we will optimize the power spectral densities, ρ_{RO} and ρ_{MU}, utilized by the radar only and mixed use sub-bands respectively, to maximize the Fisher information, where

$$P_{\text{rad}} = P_{\text{RO}} + P_{\text{MU}} \tag{5.16}$$

$$P_{\text{RO}} = \alpha\, B\, \rho_{\text{RO}}\,,\; P_{\text{MU}} = (1-\alpha) B\, \rho_{\text{MU}}\,. \tag{5.17}$$

We will have the following constraint on radar power in the two sub-bands,

$$P_{\text{rad}} = \alpha\, B\, \rho_{\text{RO}} + (1-\alpha) B\, \rho_{\text{MU}} \tag{5.18}$$

Now, consider a radar signal $x(t)$ with bandwidth B, whose frequency spectrum $X(f)$ is centered around B_O. We assume that $X(f)$ is spectrally flat. We will now partition the frequency spectrum into two spectrally flat portions, $X_{\text{RO}}(f)$ and $X_{\text{MU}}(f)$ with bandwidths $\alpha\, B$ and $(1-\alpha)B$ respectively, thereby creating two new signals, $x_{\text{RO}}(t)$ and $x_{\text{MU}}(t)$ that will be transmitted in the radar only sub-band and mixed use sub-band respectively. Thus, after transmission, the radar receiver will observe

the following return signal

$$\begin{aligned} z(t) &= a\sqrt{P_{\mathrm{RO}}}\, x_{\mathrm{RO}}(t-\tau) + a\sqrt{P_{\mathrm{MU}}}\, x_{\mathrm{MU}}(t-\tau) + b\sqrt{P_{\mathrm{com}}} r(t) + n(t) \\ &= a\, x(t-\tau) + b\, r(t) + n(t)\,, \end{aligned} \tag{5.19}$$

where $x(t-\tau) = \sqrt{P_{\mathrm{RO}}}\, x_{\mathrm{RO}}(t-\tau) + \sqrt{P_{\mathrm{MU}}}\, x_{\mathrm{MU}}(t-\tau)$. Using this return signal, we derive the CRLB on the variance for time-delay estimation. Let $\theta = \tau$ be the parameter to be estimated. From Equation (5.19), we see that $z(t) \sim \mathcal{CN}(a\, x(t-\tau) + b\sqrt{P_{\mathrm{com}}}\, r(t), \sigma^2)$ and has the following probability density function,

$$p(z(t);\theta) = \frac{1}{\pi\sigma^2} \mathrm{e}^{-\frac{\|z(t) - a\, x(t-\tau) - b\sqrt{P_{\mathrm{com}}}\, r(t)\|^2}{\sigma^2}}\,. \tag{5.20}$$

Now, the Fisher information for this estimation problem, J, is given by [109]

$$J = \left\langle \left\| \frac{n^*(t)\, a\, x'(t-\tau)}{\sigma^2} + c.c. \right\|^2 \right\rangle\,.$$

where c.c. stands for complex conjugate term and $x'(t-\tau) = \frac{\partial}{\partial\tau} x(t-\tau)$. On simplification, we see that

$$J = 2\left\langle \frac{\|a\|^2\, n(t) n^*(t) x'(t-\tau)[x'(t-\tau)]^*}{\sigma^4} \right\rangle\,, \tag{5.21}$$

where the cross-terms in the product become 0 due to $\langle n(t)\rangle = 0$ and the independence of $x(t-\tau)$ and $n(t)$. The factor of two comes from the complex conjugate term. Using the fact that $\langle n(t) n^*(t)\rangle = \sigma^2$ and simplifying, we see that

$$J = \frac{2\|a\|^2 \left\langle \left\| \sqrt{P_{\mathrm{RO}}}\, x'_{\mathrm{RO}}(t-\tau) + \sqrt{P_{\mathrm{MU}}}\, x'_{\mathrm{MU}}(t-\tau) \right\|^2 \right\rangle}{\sigma^2}\,. \tag{5.22}$$

By multiplying the terms out, converting to frequency domain and applying Parseval's Theorem, the time-shift and differentiation properties of the Fourier Transform, the orthogonality of $X_{\mathrm{RO}}(f)$ and $X_{\mathrm{MU}}(f)$, Equation (5.17), and finally evaluating the

integrals for spectrally flat $X_{\mathrm{RO}}(f)$ and $X_{\mathrm{MU}}(f)$, we get [109]

$$J = \frac{8\pi^2 \|a\|^2 \alpha\, TB\, \rho_{\mathrm{RO}}}{3k_B T_{\mathrm{temp}} B} \left[\left(B_O - \frac{B}{2} + \alpha B \right)^3 - \left(B_O - \frac{B}{2} \right)^3 \right] + \frac{8\pi^2 \|a\|^2 (1-\alpha)\, TB\, \rho_{\mathrm{MU}}}{3k_B T_{\mathrm{temp}} B} \left[\left(B_O + \frac{B}{2} \right)^3 - \left(B_O - \frac{B}{2} + \alpha B \right)^3 \right] . \quad (5.23)$$

We consider B_O to be a free parameter chosen such that the regular Fisher information for time-delay estimation, given by Equation (5.23), and the reduced Fisher information [100] for time-delay estimation derived from the Fisher information matrix (FIM) of joint amplitude and time-delay estimation are be equal. In general, the reduced Fisher information is given by Equation (B.8). As shown in Chapter B, the resultant value for B_O is given by [109]

$$B_O = \frac{\alpha\, B\, (\alpha - 1)[\rho_{\mathrm{MU}}(\alpha - 1) + \rho_{\mathrm{RO}}\alpha]}{2(\rho_{\mathrm{MU}}(\alpha - 1)^2 + \rho_{\mathrm{RO}}\alpha^2)} . \quad (5.24)$$

From Equation (5.18), we see that,

$$\rho_{\mathrm{RO}} = \frac{P_{\mathrm{rad}} - (1-\alpha) B\, \rho_{\mathrm{MU}}}{\alpha B} , \; \rho_{\mathrm{MU}} = \frac{P_{\mathrm{rad}} - \alpha B\, \rho_{\mathrm{RO}}}{(1-\alpha) B} . \quad (5.25)$$

Applying Equations (5.24) and (5.25) in Equation (5.23) separately and using the first and second derivative tests, we can get the values of ρ_{RO} and ρ_{MU} that maximize the Fisher information [109]. The resultant estimation rate bound for the radar system in both sub-bands is given by

$$R_{\mathrm{est}} \leq \frac{B}{2} \log_2 \left[1 + \sigma^2_{\mathrm{proc}} J \right]^{\frac{\delta}{TB}} , \quad (5.26)$$

where J is given by Equation (5.23) and related to the variance of the time-delay estimation by $\sigma^2_{\mathrm{est}} = J^{-1}$. The corresponding communications rate bound in the

mixed use channel is

$$R_{\mathrm{MU}} \leq (1-\alpha)\, B\, \log_2\left[1 + \frac{b^2\, P_{\mathrm{com}}}{\sigma^2_{\mathrm{int+n}}}\right] \tag{5.27}$$

$$\sigma^2_{\mathrm{int+n}} = \|a\|^2(1-\alpha)B\,\rho_{\mathrm{MU}}\,\gamma^2\,(1-\alpha)^2B^2\sigma^2_{\mathrm{proc}}$$

$$+\,(1-\alpha)k_B\,T_{\mathrm{temp}}B\,.$$

We expect the resulting inner bound to have end points given by Equations (3.2) and (4.4) (SIC vertex) when $\alpha = 0$ and by Equation (4.4) when $\alpha = 1$.

Chapter 6

EXAMPLE SET OF JOINT RADAR-COMMUNICATIONS SYSTEM PERFORMANCE BOUNDS

In this chapter, we present an example of the performance bounds derived in Chapter 5. The example set of performance bounds are generated by evaluating the bounds for a given set of parameters. We also introduce the concept of weighting or prioritizing the amount of information (in bits) gained by each system differently giving rise to the term 'Not All Bits are Equal'. Finally, we present two methods for selecting an ideal operating point for the joint radar-communications system. This selection process is akin to achieving RF convergence for the joint system shown in Figure 2.1. It should be noted that the spectral isolation bound that is plotted in Figures 6.1 to 6.4 is a simple, unachievable outer bound that corresponds to each system utilizing the full bandwidth with out the presence of each other, given by Equations (5.2) and (5.3) with $\alpha = 1$ and 0 respectively.

6.1 Comparison of Joint Radar-Communications Performance Bounds

In Figure 6.1, we display an example of the inner bounds on performance. The parameters used in the example are displayed in Table 6.1. Through out this report, it is assumed that the communications signal is received through an antenna sidelobe, so that the radar and communications receive gain are not identical. In general, the inner bound is produced by the convex hull of all contributing inner bounds. In the example, we see that the WF bound exceeds the SIC bound and ISB. The WF bound is not guaranteed to be greater than the SIC and ISB. The WF bound is not guaranteed to be convex and its shape is non-intuitive. We also see that

the optimal Fisher information bound is always lower than the WF bound and the linearly interpolated SIC bound. The optimal Fisher information bound can either exceed the ISB or be lower than the ISB depending on the value of α used. Finally, we see that the end points of the optimal Fisher bound are as expected. There are some

Table 6.1: Parameters used to generate example performance bounds for the 'basic multiple-access scenario.'

Parameter	Value
Bandwidth (B)	5 MHz
Center Frequency	3 GHz
Effective Temperature (T_{temp})	1000 K
Communications Range	10 km
Communications Power (P_{com})	0.3 W
Communications Antenna Gain	0 dBi
Radar Target Range	200 km
Radar Antenna Gain	30 dBi
Radar Power (P_{rad})	100 kW
Target Cross Section	10 m^2
Target Process Standard Deviation ($\sigma_{\tau,\text{proc}}$)	100 m
Time-Bandwidth Product (TB)	100
Radar Duty Factor (δ)	0.01

important subtleties with this figure. For example, the CIR time sharing scheme shows a linear interpolation between the full bandwidth SIC node, and the radar free operation (communications only). While it shows a linear decrease in estimation rate, for any given radar spectrum-space-time access, the radar is operating over the full bandwidth, unimpeded by the communications user. Contrast that with the

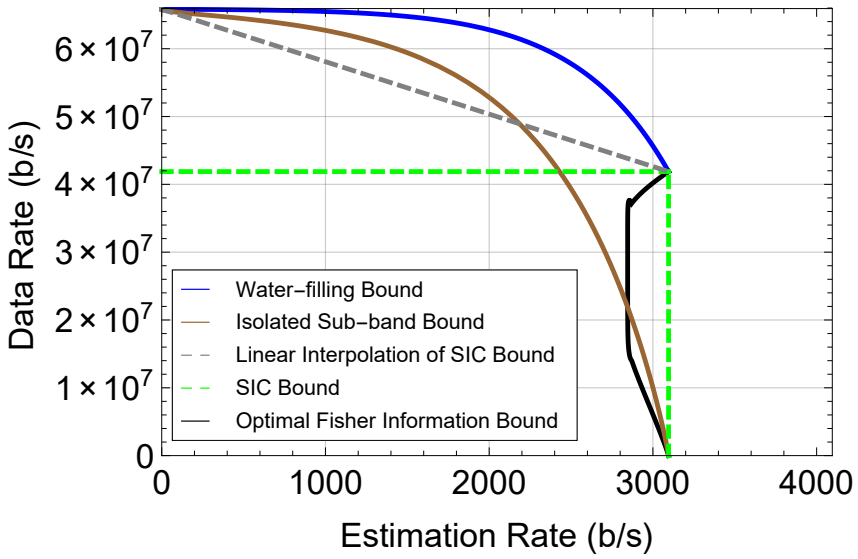

Figure 6.1: Multiple-access bounds for joint radar-communications access. The dashed red lines are created by considering each user independently in the entire bandwidth, without interference. The ISB is given by the brown line, where the blending ratio α is swept from 0 to 1, which allocates the overall bandwidth B proportionally to the radar or communications user. The constant information time share or SIC line is given by dashed green and the linear interpolation between the SIC node and the radar-free communications point is given by dashed gray. Finally, the optimal WF solution is given by the solid blue line and the optimal Fisher information bound is given by the solid black line. The proportion of B allocated to communications only and the mixed-use SIC band is swept with α.

ISB, where traveling along the curve toward the communications only axis implies a reduction in radar bandwidth, which impacts specific radar parameter estimation [110]. The same applies for WF. Finally, it should be stated that the performance bound curves are obtained by sweeping the blending ratio, α from 0 to 1. Changing the blending ratio alters the operating point of a joint radar-communications system along the performance bound curves shown in Figure 6.1.

6.2 Not All Bits are Equal

In this section we present the notion that not all bits are equal; that bits representing information gained for each system can be weighted differently. This allows one to

prioritize the information gained by each system in a appropriate manner. As stated previously, the communications and estimation rates represent the amount of information, in bits, gained through the respective channels through message transmission or radar illumination. However, the bits that are used to represent the amount of information gained for each system can be prioritized differently and the information rate metrics do not clearly highlight this.

For the multiple-access communications system described previously, an increase in performance by 1 bit for the first communications system may not be as critical as an increase in performance by 1 bit for the second communications system and vice versa. For example, in Figure 1.3, if the first communication system with rate R_1 represents a user receiving an emergency broadcast message and the second communication system with rate R_2 represents a local Wi-Fi network connection, an increase in R_1 by 1 bit will be more critical than a similar improvement in R_2.

A similar case exists for joint radar-communications systems as well. As we saw in Section 5.1, we can use the estimation rate to generate achievable rate regions for the joint radar-communications system, such as in Figure 1.3. The bits used by the radar system can have more value or priority than the bits used by the communications system and vice versa.

For example, in Figure 6.1, consider a joint radar-communications system in which the communications system is used to stream a video and the radar system is monitoring air-traffic. An increase in the communications rate by 1 bit will not be as critical as a similar improvement in the estimation rate. As highlighted by the examples provided in this discussion, the importance of bits are application specific. A system engineer can assign priorities to bits for different systems and use the complete profile of achievable rate regions, such as the ones provided by Figures 1.3 and 6.1, to set the appropriate rates for each system.

6.3 Selecting an Operating Point

The concept that not all bits are equal discussed in Section 6.2 can also be used to find the appropriate operating point for a joint radar-communications system from a complete profile of achievable rate regions such as the one shown in Figure 6.1.

As mentioned in Section 6.2, by assigning application specific priorities to bits for different systems, the complete profile of achievable rate regions can be used to select the appropriate rates for each system. Given a set of weights and a complete profile of achievable rate regions, there are two methods to selecting an appropriate operating point, one that selects the highest data and estimation rates or one that selects the highest weighted spectral efficiency.

We first discuss the former method. By assigning suitable weights or priorities to radar and communications bits, plotting this information against the complete profile of achievable rate regions indicates the appropriate operating point for the given joint system. This process is further highlighted in Figure 6.2, where we show two cases, one in which a radar bit is worth 10000 communications bits and another where a radar bit is worth 4000 communications bits. The two lines indicate on each inner bound what the appropriate operating points are for each radar bit weight case. Choosing the furthest of these intersection points (in terms of distance from the origin) will give you the operating point that has the highest data and estimation rates for a given set of weights.

We now discuss the second method that selects an operating point with the highest weighted spectral efficiency. The plots shown in Figures 6.1 and 6.2, while useful, does not give us a notion of how spectrally efficient we are. In Figures 6.3 and 6.4, we attempt to do a more fair comparison by looking at the weighted spectral efficiency of each bound. Here, the weighted spectral efficiency of each performance bound is

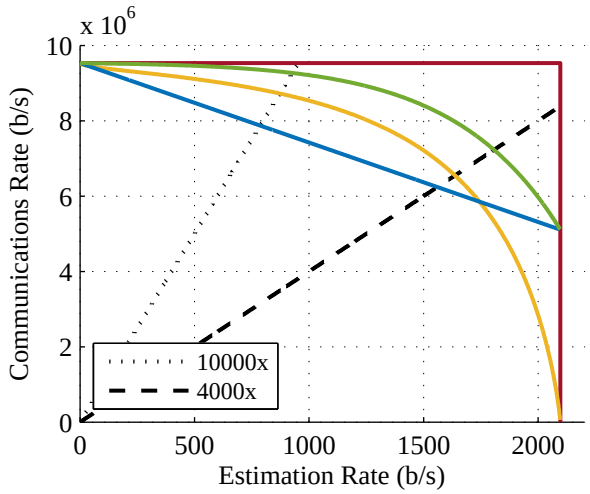

Figure 6.2: Multiple-access bounds for joint radar-communications access describing operating point selection. The dashed and dotted black lines represent two cases where a radar bit is valued against a communication bit. The slopes of the dashed lines indicate how much a radar bit is worth when compared against a communication bit. In the case of the dotted line, a radar bit is worth 10000 communications bits and in the case of the dashed line, a radar bit is worth 4000 communications bits. The solid lines depict the performance bounds shown in Figure 6.1. The intersection of a dashed line against a performance bound indicates the appropriate operating point for a given radar bit weight.

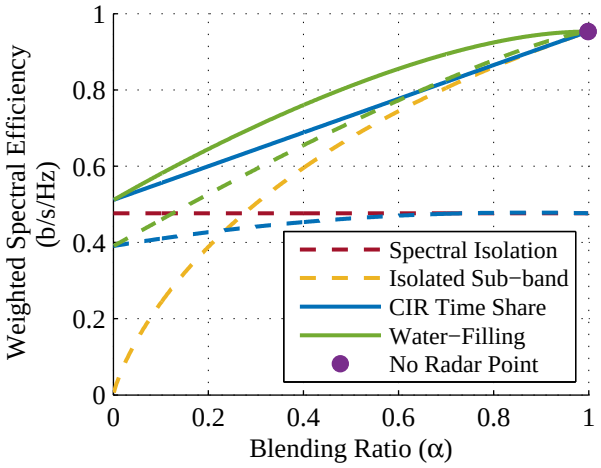

Figure 6.3: Weighted spectral efficiency plots for joint radar-communications access. Note the accompanying colored dashed lines are the equivalent, isolated weighted spectral efficiencies. For example, the dashed blue line is the weighted spectral efficiency obtained if the two systems were operating at the same rate given by the CIR time share scheme in the solid blue line, but isolated in frequency. This means the communications user that is operating after subtraction of the radar would be in its own equivalent band.

given by

$$E_{\text{weighted}} = \frac{w_R\, R_{\text{est}} + w_C\, R_{\text{com}}}{(w_R\, +\, w_C)\, B_{\text{tot}}}, \tag{6.1}$$

where w_R is the radar bit weight, w_C is the communications bit weight, and B_{tot} is the sum of all the bandwidth consumed.

In Figures 6.3 and 6.4, we look at the weighted spectral efficiency of the performance bounds discussed in Chapter 5 for co-designed systems as well as their respective equivalent, isolated systems (spectrally isolated systems operating at the same rates) for a given spectral allocation, B. For these isolated systems, the total consumed bandwidth, B_{tot} is given by

$$B_{\text{tot}} = B\, +\, B_{\text{eff}}\,, \tag{6.2}$$

where B is the bandwidth consumed by an isolated radar system and B_{eff} is the effective bandwidth required by a isolated communications system to achieve the same communications rate as a co-designed system. For the CIR time sharing scheme, we solve for the effective isolated bandwidth by solving

$$B_{\text{eff}} = R_{\text{com}}^{-1}\left(\alpha R_{\text{com,free}} + (1-\alpha)\, R_{\text{com,sic}}\right), \tag{6.3}$$

where $R_{\text{com,free}}$ is the communications rate when there are no other users given by Equation (5.4), and $R_{\text{com,sic}}$ is the reduced communications rate operating at the SIC node, given by Equation (3.2). That is, we solve for B in Equation (5.4), given that the left hand side is equal to the total communications rate for a given point along the CIR time share line. This is the sum of the duty-cycled communications only rate given by Equation (5.4), and the complementary duty-cycled SIC communications rate operating after radar prediction subtraction given by Equation (3.2). We utilize a similar technique for the WF scenario.

For the spectral isolation case, B_{tot} is $2B$ because without coexistence, cooperation, or co-design, the two must occupy separate bandwidths for a given space-time.

The ISB operates in a similar manner, assuming we have split our overall bandwidth into two isolated sub-bands. For the CIR time sharing scheme, we see two blue lines. The solid line is the weighted spectral efficiency gained by cooperation of the two systems. The dashed blue line is the equivalent, isolated weighted spectral efficiency. Here we see a large penalty for the radar bandwidth, especially when the radar bandwidth is not being used.

To emphasize the importance of the concept that not all bits are equal that was discussed in great detail in Section 6.2, we assign both the radar and communications bits a weight of 1 and calculate the weighted spectral efficiency, as shown in Figure 6.3. Here, with solid and dashed lines representing the co-designed system and the equivalent isolated system (systems operating at same rates but isolated in frequency) respectively, we see that cooperation outperforms isolation for this case and that the WF bound is most spectrally efficient. However, on recognizing that the blending ratio α is the x-axis for this plot, it then becomes clear that the peak of this plot is not the optimal operating point, given that $\alpha = 1$ implies no radar use. Since both radar and communications bits are assigned equal priorities of 1 in this scenario, it is evident that not all bits are equal in this optimization process. We can underscore this by setting $w_R = 3000$ and $w_C = 1$ in Equation (6.1), as shown in Figure 6.4. With proper weighting, the maximum in this plot becomes more meaningful when considering spectral allocation. It should be noted that since the radar bits are weighted 3000x what the communications bits are worth, this implies that more power may be required to increase the estimation rate as compared to the communications data rate.

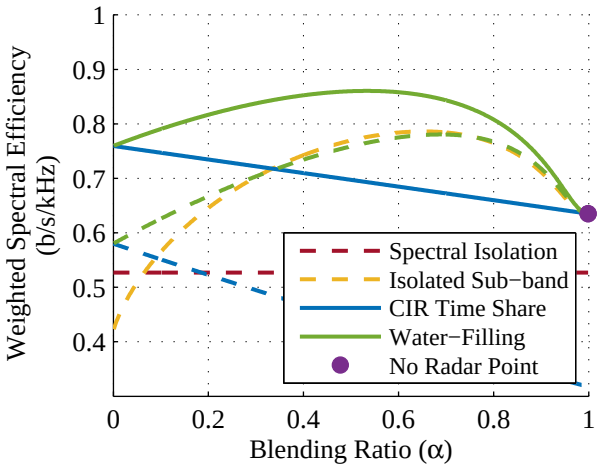

Figure 6.4: Weighted spectral efficiency (measured here in bits per second per kilohertz) plots for joint radar-communications access, weighted for importance. In this example, we weighted the radar bits 3000x what the communications bits are worth. This may be true for certain military radar applications, and the weighting may be scenario dependent. With proper weighting, the maximum point of spectral efficiency has more meaning and utility.

Chapter 7

RESEARCH HIGHLIGHT - RADAR WAVEFORM OPTIMIZATION FOR COOPERATIVE RADAR AND COMMUNICATIONS JOINT RECEIVER

In this chapter, we present a new radar waveform design method for a joint radar-communications system in which the radar waveform spectrum and communications power spectral distribution are optimized to maximize joint performance. The radar waveform spectrum is optimized to maximize radar performance or minimize estimation error variance in the non-local (or low-SNR) regime and by employing the continuous spectral WF algorithm [99], the optimal communications power distribution in frequency is obtained that maximizes communications performance. The global estimation rate, defined in Section 4.3 [111], and spectral WF SIC data rate, defined in Section 3.3, capture radar and communications performance respectively. The results presented in this paper is an extension of the work presented in Reference [111].

In our previous efforts detailed in Chapter 5 [4, 5], the performance bounds of a joint radar-communications system was found to depend on the shape of the radar waveform spectrum (via the radar waveform RMS bandwidth). For a given bandwidth, an impulse-like radar spectral shape (most of the waveform energy is located at frequencies closer to the center of the bandwidth allocation) has a small RMS bandwidth which is more favorable for communications performance, whereas a radar waveform spectrum with more energy at frequencies closer to the edges of the bandwidth allocation has a large RMS bandwidth which is more favorable for estimation performance. However, the latter waveform also has higher autocorrelation sidelobes or ambiguity. When taking into account non-local or low-radar SNR regime estima-

tion errors, these high autocorrelation sidelobes negatively impact estimation performance by increasing the radar threshold SNR at which non-local estimation errors do not occur. Thus, the shape of the radar spectrum poses a trade-off both in terms of radar performance vs. communications performance and in terms of improved estimation performance vs. an increased radar threshold SNR.

In order to place emphasis on the waveform design approaches and their performance, we assume a simple scenario with a single target and no clutter. The problem scenario considered in this paper is given by Figure 7.1. The simulation scenario shown in Figure 7.1 is the same one described in Section 2.2.

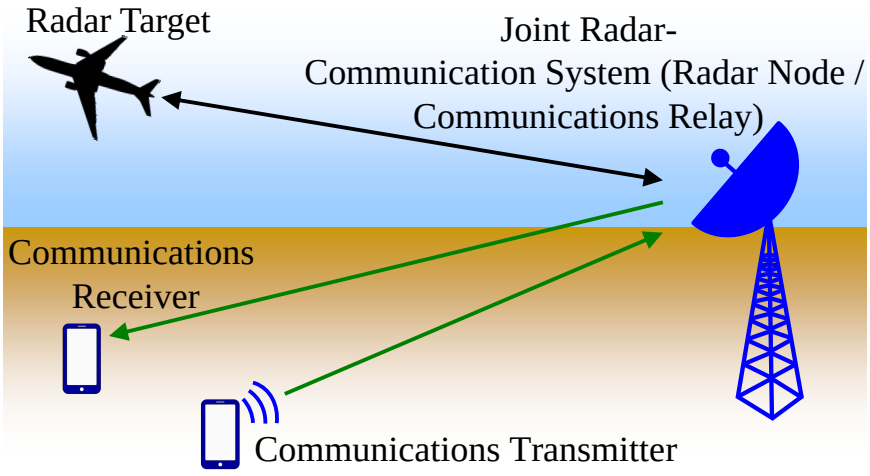

Figure 7.1: The joint radar-communications system simulation scenario for radar waveform design. In this scenario, a radar and communications user attempt to use the same spectrum-space-time. This scenario is instructional, and can easily be scaled to more complicated scenarios by using it as a building block to construct real world examples.

7.1 Non-linear Chirp with Parametric Polynomial Phase

In this section, we briefly introduce the parameterized non-linear chirp that will be used to design the optimal radar waveform in the minimum estimation error variance waveform design method. We also derive an approximate closed-form solution for the spectrum for a special case of this non-linear chirp waveform.

One desirable property for radar waveforms is to have a PAPR as close as possible to 1 (the smallest possible value). Thus, most radar systems now require the signal to be constant modulus or unimodular, which keeps the peak and the average power the same over any time period, granting the signal the smallest possible PAPR of 1. To ensure that the optimized radar waveform is unimodular, we begin by considering the following unimodular non-linear chirp signal with a polynomial phase

$$x(t) = \mathrm{e}^{j\pi(\sum_{i=1}^{N} p_i t^{2i})}, \tag{7.1}$$

where N is a positive integer and $p_i \in \mathbb{R}$, $\forall i$ are phase coefficients. We let the polynomial phase to have only even terms to ensure symmetry in the frequency domain. The shape of the waveform spectrum is determined by the phase coefficients. The minimum estimation error variance method selects the appropriate phase coefficient values so as to optimize the shape of the radar spectrum to maximize joint radar-communications performance.

In the following discussion, we derive an approximate expression for the spectrum of the non-linear chirp waveform shown in Equation (7.1) for the case that $N = 2$.

7.1.1 Spectrum of Non-linear Chirp with Parametric Polynomial Phase

Due to the increased complexity involved in evaluating the spectrum for higher values of N, we consider the simple case of $N = 2$. The spectrum of the band-limited non-linear chirp with bandwidth B and time-duration T is given by

$$\begin{aligned} X(f) &= \int_{\frac{-T}{2}}^{\frac{T}{2}} dt\, \mathrm{e}^{j\pi(p_1 B^2 t^2 + p_2 B^4 t^4)}\, \mathrm{e}^{-j2\pi f t} \\ &= \int_{\frac{-T}{2}}^{\frac{T}{2}} dt\, \mathrm{e}^{j\pi(p_1 B^2 t^2 + p_2 B^4 t^4 - 2 f t)} \\ &= \int_{\frac{-T}{2}}^{\frac{T}{2}} dt\, \mathrm{e}^{j\phi(t,f)}\,. \end{aligned} \tag{7.2}$$

In order to obtain a closed form solution for the above integral, we employ the principle of stationary phase (PSP) [112]. We first find the points in time, t_0, where the phase, $\phi(t, f)$, is stationary i.e. when

$$\begin{aligned} \frac{\partial \phi(t,f)}{\partial t}\Big|_{t=t_0} &= 0 \\ \Rightarrow \pi(2\,p_1\,B^2\,t_0 \,+\, 4\,p_2\,B^4\,t_0^3 \,-\, 2\,f) &= 0 \\ \Rightarrow 2\,p_1\,B^2\,t_0 \,+\, 4\,p_2\,B^4\,t_0^3 \,-\, 2\,f &= 0 \end{aligned} \tag{7.3}$$

Solving for t_0, we get

$$\begin{aligned} t_0 = & \frac{-6^{\frac{2}{3}}\,B^6\,p_1\,p_2}{Q} \\ & + \frac{6^{\frac{1}{3}}\,(9\,B^8\,p_2^2\,f \,+\, \sqrt{3\,B^{16}\,p_2^3\,(2\,B^2\,p_1^3 \,+\, 27\,p_2\,f^2)})^{\frac{2}{3}}}{Q} \end{aligned} \tag{7.4}$$

where

$$Q = 6\,B^4\,p_2\,(9\,B^8\,p_2^2\,f \,+\, \sqrt{3\,B^{16}\,p_2^3\,(2\,B^2\,p_1^3 \,+\, 27\,p_2\,f^2)})^{\frac{1}{3}}\,.$$

Using the PSP, the expression for an approximation of the spectrum is given by [112]

$$\begin{aligned} X(f) &\approx 2\,\sqrt{\frac{-\pi}{2\,\phi''(t_0,f)}}\,\mathrm{e}^{-j\frac{\pi}{4}}\,x(t_0)\,\mathrm{e}^{j\phi(t_0,f)} \\ &= 2\,\sqrt{\frac{-1}{4\,p_1\,B^2 \,+\, 24\,p_2\,B^4\,t_0^2}}\mathrm{e}^{-j\frac{\pi}{4}}\,\mathrm{e}^{j\pi(p_1\,B^2\,t_0^2 + p_2\,B^4\,t_0^4)} \\ &\quad \cdot\,\mathrm{e}^{j\pi(p_1\,B^2\,t_0^2 + p_2\,B^4\,t_0^4 - 2\,f\,t_0)} \end{aligned} \tag{7.5}$$

where $\phi''(t,f) = \frac{\partial^2\phi(t,f)}{\partial t^2} = \pi(2\,p_1\,B^2 + 12\,p_2\,B^4\,t^2)$. Although we do not use the above-discussed expression for the radar spectrum in our numerical study, nevertheless, the above result may be useful in other studies.

7.2 Radar Waveform Design Methods

In this section, we present a novel radar waveform design method, the minimum estimation error variance method.

7.2.1 Minimum Estimation Error Variance Method

The waveform design algorithm that we propose in this section designs an optimal non-linear chirp radar waveform (as modeled in Section 7.1) from a global estimation rate perspective. In other words, we first design the waveform to minimize the global estimation error variance (estimation error variance taking into account both non-local and local estimation errors), given by Equation (4.6). This minimization of the global estimation error variance is accomplished by minimizing the estimation error variance at the radar threshold SNR of the radar estimator. The threshold point of an estimator is the estimator (or radar) SNR value at which the estimator's performance deviates from the CRLB [113] due to error contributions from non-local estimation errors. At SNR values lower than the threshold point, due to autocorrelation mainlobe-sidelobe confusion, non-local estimation errors begin to contribute to estimator's error variance which causes the estimation performance to degrade and deviate from the CRLB [100]. Since the threshold point is the SNR point at which an estimator's performance deviates from the CRLB and also the SNR point at which non-local estimation errors contribute to estimation performance, minimizing the CRLB at the threshold point gives the lowest possible global estimation error variance or highest possible global estimation rate.

For a given SNR, we have to design a radar waveform that has a threshold point at that SNR and has the best (or smallest) estimation error variance. We first eliminate all radar waveforms that have a threshold point higher than the current SNR and then,

from the remaining feasible solution set, we find the radar waveform that minimizes the CRLB given by Equation (4.5). We perform the first elimination step by imposing the following constraint on the ratio of the global estimation error variance (given by Equation (4.6)) and the CRLB (given by Equation (4.5))

$$\frac{\sigma^2_{\text{est}}}{\sigma^2_{\text{CRLB}}} \leq \delta_{\text{constraint}}, \tag{7.6}$$

where $\delta_{\text{constraint}}$ is a parameter whose value determines the size of the feasible solution set. We discuss how to tune this parameter in Section 7.3. By ensuring the above ratio stays below $\delta_{\text{constraint}}$, any radar waveforms with higher threshold points (SNR values) are eliminated. Figure 7.2 depicts how this constraint works on eliminating radar waveforms with higher threshold points.

We also introduce an additional constraint on spectral leakage (constraint $\boldsymbol{C_2}$) to the waveform optimization problem in order to obtain optimal radar waveforms that not only ensure optimal joint radar-communications performance, but also satisfy additional real-world properties that a traditional radar waveform would. Since the system can only receive signals whose spectrum lies within the system's bandwidth, any RF energy that leaks outside of the bandwidth will be lost. To minimize this loss of RF energy, we introduce a constraint on the amount of energy present in the radar spectrum at frequencies out of the system bandwidth range. We enforce this spectral leakage constraint by having the radar spectrum be below a thresholding spectral mask such as the one seen in Figure 7.3.

We consider the non-linear chirp waveform given by Equation (7.1). The spectral shape of the waveform is determined by the parameters $p_i, i = 1, \ldots, N$. In order to design the radar waveform spectrum that minimizes the global estimation

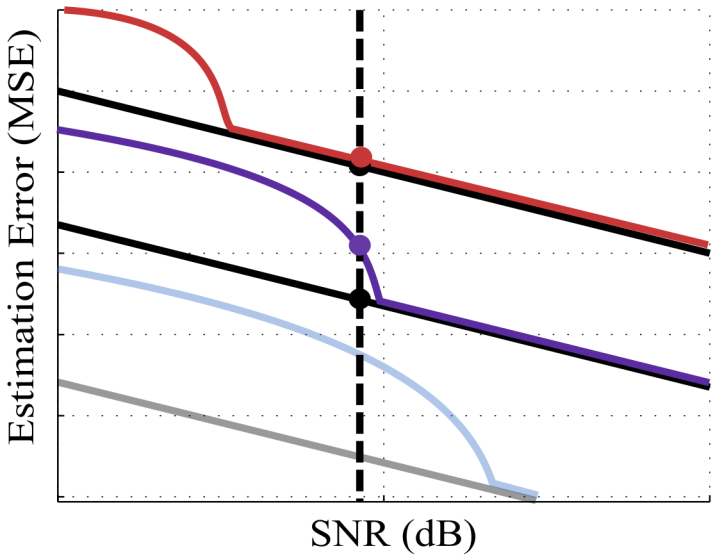

Figure 7.2: An example depicting the impact of the constraint given by Equation (7.6) on the feasible set for optimization. The dashed vertical line indicates the given SNR. The red, purple and blue solid curves indicate the estimator performance for different radar waveforms and the black solid lines indicate the CRLB for each radar waveform. The black dots indicate the CRLB values for various feasible radar waveforms at the given SNR. The red and purple dots indicate the actual estimation error variance (estimation performance) for various feasible radar waveforms at the given SNR. The grayed out curves indicate estimation performance for unfeasible radar waveforms at the given SNR. Minimizing the CRLB over the feasible set ensures that the optimal radar waveform will have the lowest estimation threshold point (or best estimation performance, taking both local and non-local estimation errors).

performance, we solve the following optimization problem:

$$\begin{aligned} \underset{\bar{p}}{\text{minimize}} \quad & \frac{1}{8\pi^2 B_{\text{rms}}(\bar{p})^2 T B(\text{SNR})}, \\ \text{subject to} \quad & p_i \in [0, 10] \ \forall i \\ & \frac{\sigma^2_{\text{est}}}{\sigma^2_{\text{CRLB}}} \leq \delta_{\text{constraint}} \\ & \mathbb{1}_A(\bar{p}) = 1 \qquad (\boldsymbol{C_2}) \end{aligned} \tag{7.7}$$

where $\bar{p} = (p_1, \ldots, p_N)$, and $p_1, \ldots, p_N$ are the coefficients of the polynomial phase for the unimodular waveform in Equation (7.1), and $B_{\text{rms}}(\bar{p})$ is given by Equation (2.9). The constraint $\boldsymbol{C_2}$ constrains the coefficients $\bar{p}$ such that the resulting spectrum of

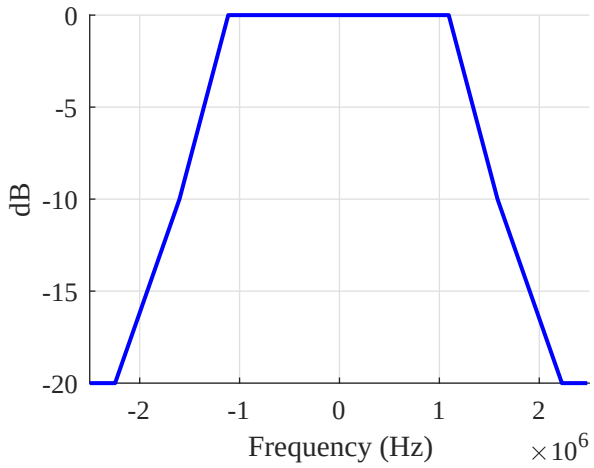

Figure 7.3: Spectral Leakage Mask used constrain the amount of energy in the radar spectrum leaking out at frequencies out of the system bandwidth range. The spectral leakage constraint is enforced by having the radar spectrum be below this thresholding spectral leakage mask.

the waveform stays below a certain masking threshold, which is represented by an indicator function, where A is the set of all phase coefficients that let the resulting masked spectrum stay below the masking threshold as shown in Figure 7.3.

Once the optimal radar waveform that maximizes the radar performance of a joint radar-communications system is designed, the continuous spectral WF algorithm described in Section 3.3 is employed to determine the spectral WF SIC data rate that maximizes the communications performance of a joint radar-communications system. This optimization process is called the minimum estimation error variance method. It should be noted that the optimization problem described in Equation (7.7) is a non-convex optimization problem.

7.2.2 Impact of Threshold Point Signal-to-Noise Ratio

As mentioned earlier in the chapter, we saw from References [4, 5] that the spectral shape of the radar waveform (the radar RMS bandwidth) impacts the performance of a joint radar-communications system. Shaping the radar spectrum imposes a trade-off both in terms of radar performance vs. communications performance and in terms

of improved estimation performance vs. an increased radar threshold SNR. In this subsection, we briefly discuss how the choice of the threshold SNR impacts both the shape of the radar waveform spectrum and the performance of the joint radar-communications system.

Selecting a low value for the threshold SNR implies that even for small radar SNR values, the probability of sidelobe confusion for the radar waveform autocorrelation function (which causes the estimator performance to deviate from the CRLB) is small. Radar waveforms with more energy at frequencies closer to center of the bandwidth allocation can have such autocorrelation functions. However, such a radar waveform has a smaller RMS bandwidth which degrades the overall estimation performance as seen in Equation (4.5). Furthermore, as we observe from Equation (3.4), radar waveforms with more spectral energy at the bandwidth center will reduce the noise spectral density, $N_{\text{int+n}}(f)$, due to minimal radar residual values ($N_{\text{radresi}}(f)$), thereby maximizing the data rate.

Conversely, selecting a larger value for the threshold point implies there is more ambiguity in the radar waveform autocorrelation function (higher sidelobes), which occurs for radar waveforms with more energy at frequencies closer to the edges of the bandwidth allocation. Such waveforms also have larger RMS bandwidth values and a better estimation performance. Finally, radar waveforms with more spectral energy at the bandwidth edges have larger $N_{\text{radresi}}(f)$ values and consequently, larger $N_{\text{int+n}}(f)$ values which degrade the communications data rate.

Thus, we see that selecting a low radar SNR threshold point increases the communications performance and decreases the radar performance but also results in a radar waveform with low sidelobes in the autocorrelation. Similarly, selecting a high threshold point increases the radar performance and decreases the communications performance but also results in a radar waveform with large autocorrelation sidelobes.

The objective is to select a threshold point that optimizes the spectral shape of the radar waveform such that the performance with respect to radar and communications is jointly maximized.

The results from the numerical study of the above optimization problem are discussed in Section 7.3.

7.3 Simulation Results

In this section, we present an example of the waveform design technique discussed in this paper, the minimum estimation error variance method, for an example parameter set. The parameters used in the example are shown in Table 7.1. We also study the effect of the order of the non-linear chirp phase on joint radar-communications performance.

7.3.1 Minimum Estimation Error Variance Method

We now discuss the numerical results from implementing the minimum estimation error variance method in Section 7.2.1. First, we highlight the impact of the threshold SNR value on the shape of the radar spectrum. We consider two threshold SNR values of -70dB and 50 dB and we choose $N = 5$ in Equation (7.1), i.e., $x(t) = e^{i\pi(\sum_{m=1}^{5} p_m t^{2m})}$. The minimum estimation error variance optimized radar waveform spectrum for this set of parameters is shown in Figure 7.4. From Figure 7.4, we see the optimal radar spectrum has more spectral energy at the edges of the bandwidth for high threshold SNR values and has more spectral energy closer to the center for low threshold SNR values, as we stated in Section 7.2.2.

We also study the impact of the threshold SNR (or radar SNR) on the system performance. For the purpose of this study, we choose $N = 5$.

For different values of SNR, we optimize the shape of the waveform, i.e., optimize

Table 7.1: Parameters used to generate examples of the minimum estimation error variance radar waveform design method.

Parameter	Value
Bandwidth (B)	5 MHz
Center Frequency	3 GHz
Effective Temperature (T_{temp})	1000 K
Communications Range	10 km
Communications Power (P_{com})	0.3 W
Communications Antenna Gain	0 dBi
Communications Receiver Side-lobe Gain	10 dBi
Radar Target Range	200 km
Radar Antenna Gain	30 dBi
Target Cross Section	10 m^2
Target Process Standard Deviation ($\sigma_{\tau,\text{proc}}$)	100 m
Time-Bandwidth Product (TB)	128
Radar Duty Factor (δ)	0.01
Threshold Point Constraint ($\delta_{\text{constraint}}$)	$1 + 0.01$

the coefficients $\bar{p} = (p_1, \ldots, p_5)$, to minimize the CRLB achieved with the waveform. We also impose the constraint $\sigma^2_{\text{est}}/\sigma^2_{\text{CRLB}} \leq \delta_{\text{constraint}}$, which ensures that for the given SNR, our feasible solution set include only waveforms whose threshold SNR is less than or equal to the given SNR (as discussed in Section 7.2.1). $\delta_{\text{constraint}}$ is tuned so that the ratio between the estimation error variance (which characterizes estimation performance in this paper) and the CRLB remains close to 1. For this simulation, we consider a $\delta_{\text{constraint}}$ value of $1 + \epsilon$, where ϵ introduces some flexibility to the constraint and typically has a value of 0.01. We solve the optimization problem

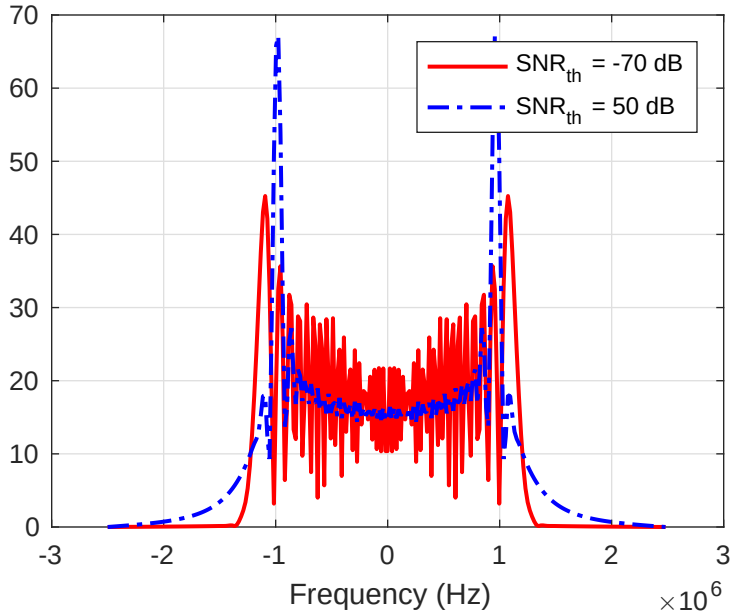

Figure 7.4: The minimum estimation error variance optimized radar waveform spectrum for different threshold SNR values. As expected, the radar waveform optimization was done for $N = 5$. We see the optimal radar spectrum has more spectral energy at the edges of the bandwidth for high threshold SNR values and has more spectral energy closer to the center for low threshold SNR values.

in Equation (7.7) using differential evolution (DE) [114]. [114] Figure 7.5 shows the RMS bandwidth values achieved with each optimized waveform for various values of threshold SNR. As expected, the optimal RMS bandwidth increases as we increase the threshold SNR. From Equation (4.5) and Section 7.2.2, we see that the optimal RMS bandwidth increasing as the threshold SNR increases will thereby reduce the CRLB as stated in Section 7.2.2.

Figure 7.6 shows the autocorrelation function achieved with each optimized waveform for various values of threshold SNR. For SNR values -50dB, -20dB and 20dB, we observed that the peak sidelobes in all three cases occur at $\pm 3\mu s$ and have values of -8dB, -5dB, and -3dB respectively. As expected, the peak sidelobe of the autocorrelation function increases as we increase the threshold SNR. As mentioned in Section 7.2.2, a higher threshold SNR implies the optimal waveform has more ambi-

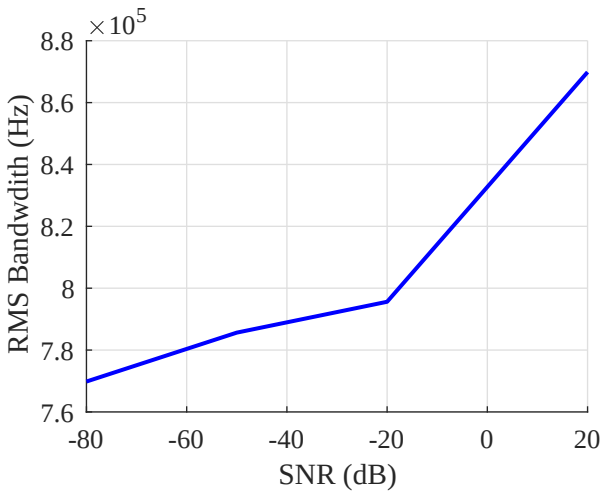

Figure 7.5: RMS bandwidth of the optimized radar waveform vs. SNR. As expected, the optimal RMS bandwidth increases as we increase the threshold SNR. From Equation (4.5), we see that the optimal RMS bandwidth increasing as the threshold SNR increases will thereby reduce the CRLB. As a result, we see that the estimation performance increases with SNR.

guity which translates into higher peak autocorrelation sidelobes.

Now, for each threshold SNR value we considered and the optimal waveform shape parameters p_1, p_2, p_3, p_4, p_5 we obtained above, we evaluate the radar estimation rate bound in Equation (4.2) and the spectral WF SIC data rate in Equation (3.7) corresponding to each of these waveforms. Figure 7.7 shows the plot of estimation rate and the data rate against the threshold SNR value. Clearly, according to the figure, the performance of the system improves with respect to the estimation rate as we increase the threshold SNR, which is expected as the minimum achievable CRLB decreases with threshold SNR, and the estimation rate increases with decreasing CRLB according to Equation (4.2) and Equation (4.6). However, we observe that the spectral WF SIC data rate reduces as the threshold SNR increases. This trend occurs because, as we stated in Section 7.2.2, as the threshold SNR increases, the noise spectral density, $N_{\text{int+n}}(f)$ achieves higher values due to larger radar residual values, which reduces the spectral WF SIC data rate.

We first investigate the relationship between the autocorrelation peak sidelobe

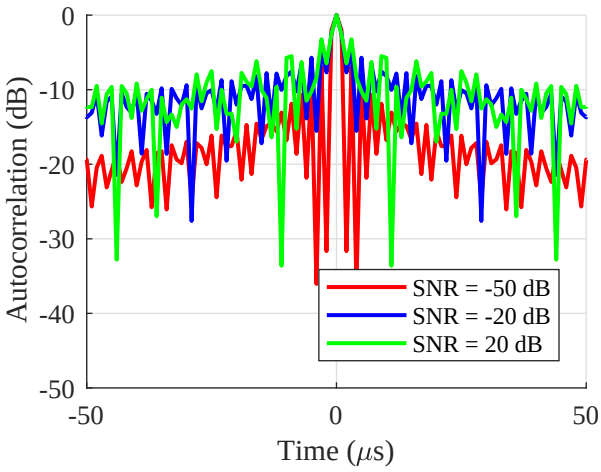

Figure 7.6: Autocorrelation function of the optimized radar waveform vs. SNR. As expected, the peak sidelobe of the autocorrelation function increases as we increase the threshold SNR. This trend is observed because a higher threshold SNR implies the optimal waveform has more ambiguity which translates into higher peak autocorrelation sidelobes.

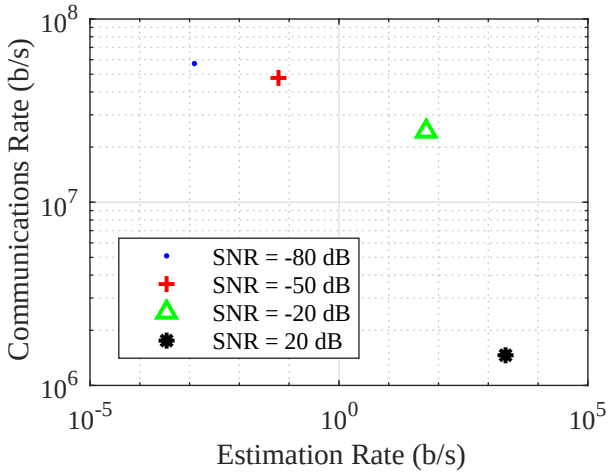

Figure 7.7: Estimation and data rates vs. threshold SNR. Clearly, we see the performance of the system improve with respect to the estimation rate and degrade with respect to the spectral WF SIC data rate as we increase the threshold SNR.

levels and N. Figure 7.8 shows the autocorrelation function for $N = 2$ and $N = 4$ at a threshold SNR value of 20dB. We clearly see that the autocorrelation peak sidelobes increase as N increases, which causes the estimation performance to drop overall as N increases.

As the shape of the waveform explicitly depends on the coefficients $p_1, \ldots, p_N$ in Equation (7.7), we now study the effect of the number of coefficients, N, on both

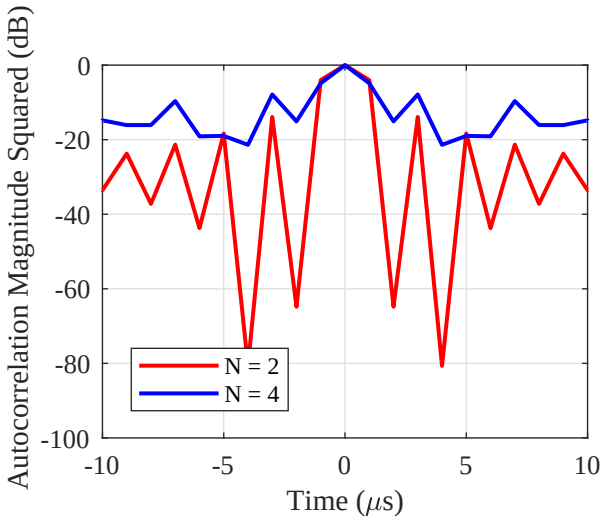

Figure 7.8: Autocorrelation function of the optimized radar waveform vs. N. We clearly see that the autocorrelation peak sidelobes increase as N increases, which causes the estimation performance to drop overall as N increases.

the estimation and the data rates. For this study, we choose a threshold SNR value of 50dB and vary N from 2 to 8. For each N and threshold SNR value, we solve Equation (7.7) and evaluate the estimation rate from Equation (4.2) and spectral WF SIC data rate from Equation (3.7). Figure 7.9 shows plots of these rates against N. From Figure 7.9, we see that as N increases, the estimation rate and the spectral WF SIC data rate decreases. This trend in the estimation rate is caused because increasing N means increasing the amount of energy at higher frequencies for the radar waveform spectrum. For a fixed threshold SNR value, while this increase in spectral energy at higher frequencies results in the B_{rms} value increasing, this also means that the ambiguity or peak autocorrelation sidelobes increase for the waveform (a trend we observed earlier). This increase in ambiguity results in an overall decrease in the estimation rate. This increase in the radar waveform's spectral content at higher frequencies means that the noise spectral density, $N_{\text{int+n}}(f)$, achieves higher values due to larger radar residual values, which reduces the spectral WF SIC data rate. We also notice that after $N = 6$, the estimation rate and spectral WF SIC data rate

saturate and do not decrease further. This trend occurs because we have used too many co-efficients and have over-fitted the spectrum.

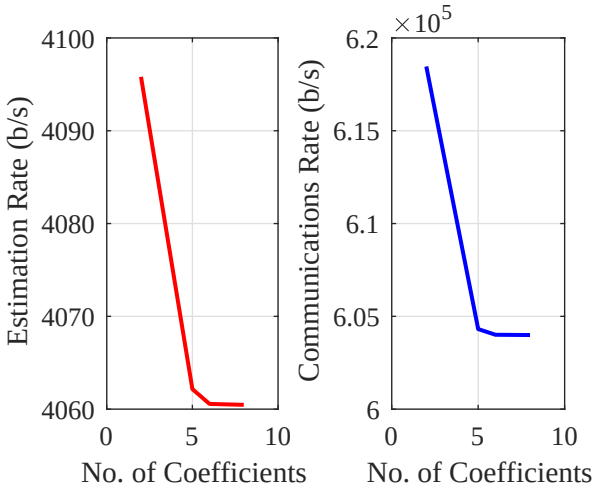

Figure 7.9: Estimation and data rates vs. N. We see that as N increases, the estimation rate and the spectral water-filling SIC data rate both decrease. This trend is caused because increasing N means increasing the amount of energy at higher frequencies for the radar waveform spectrum. While this results in the B_{rms} value increasing, this also means that the ambiguity or peak autocorrelation sidelobes increase for the waveform. This increase in ambiguity results in an overall decrease in the estimation rate. We also notice that after $N = 6$, the estimation rate and spectral WF SIC data rate start saturate and do not decrease further. This trend occurs because we have used too many co-efficients and have over-fitted the spectrum.

Finally, as we have mentioned earlier in Section 7.2.1, we would like to note that the optimization problem described in Equation (7.7) that the minimum estimation error variance method solves is a non-convex optimization problem. Given the non-trivial nature in solving non-convex optimization problems, additional investigation is required to better solve the non-convex optimization problem given in Equation (7.7).

Chapter 8

EXTENDING JOINT RADAR - COMMUNICATIONS PERFORMANCE BOUNDS TO INCLUDE MULTIPLE RADAR TARGETS, CLUTTER MITIGATION, PHASE NOISE, AND RADAR TARGET DETECTION

In this chapter, we develop several different extensions to the inner bounds on joint radar-communications system performance presented in Chapters 5 and 6. More specifically, we develop extensions to the performance bounds for target estimation for multiple targets, target estimation in the presence of clutter, target estimation with clutter mitigation in the presence of phase noise, and radar target detection. Examples of these performance bound extensions are then generated by evaluating them for a given set of parameters. We also highlight the effect phase noise has on clutter estimation and mitigation and how it effects joint system performance.

8.1 Extension of Performance Bounds for Multiple Radar Targets

In this section, the inner bounds on the performance of the joint radar-communications system developed in Section 5.1 are extended to include target parameter estimation for multiple independent targets that are far apart. The simulation scenario being considered in this section is described in Section 2.2.

8.1.1 Multiple Correlated, Closely Spaced Targets

For multiple targets that are closely spaced and have correlated range fluctuation process noise (tracking motion of the targets are correlated to some degree), deriving the radar estimation rate becomes much harder. In the Section 4.1, the estimation rate was easily constructed because we assumed that the CRLB for time delay estimation

and the range fluctuation process noise for a target was independent of the other targets, which meant that the mutual information between the radar target and the radar return was independent for each target and the total estimation rate was the sum of the individual mutual information over all targets.

However, for two targets that are closely spaced (even if they are resolvable), the CRLB for time delay estimation for one of those targets is dependent of the location of the other [115]. Additionally, if two targets are correlated (tracking motion of the targets are correlated), then they have dependent range fluctuation process noise. Hence, in scenarios where the targets are correlated and closely spaced, the mutual information between the radar target and the radar return are no longer independent for each target and the total estimation rate is not equal to the sum of the mutual information for each target. When targets are correlated and closely spaced, new methods have to be implemented to derive the total estimation rate, which are beyond the scope of this paper.

For multiple targets that are uncorrelated and far apart, the estimation rate can be easily computed and is given by Equation (4.4).

8.1.2 Inner Bounds on Joint Radar Communications System Performance

In this section, we present the previously derived inner bounds on the performance of the joint radar-communications system for multiple target parameter estimation. We consider N radar targets with the m^{th} target having delay τ_m and gain-propagation-cross-section product a_m. To simplify the discussion, we assume that all targets are far apart and that the range fluctuation process noise is independent for each target (radar tracking motion is independent for each target).

Isolated Sub-band Inner Bound

The bandwidth will be split between the two sub-bands according to some α such that,

$$B = B_{\text{rad}} + B_{\text{com}}\,,\; B_{\text{com}} = \alpha\, B\,,\; B_{\text{rad}} = (1-\alpha)\, B\,.$$

The corresponding communications rate (for the communications only sub-band) is given by

$$R_{\text{com}} \leq \alpha\, B \log_2\!\left(1 + \frac{\|b\|^2\, P_{\text{com}}}{k_B\, T_{\text{temp}}\, \alpha\, B}\right)\,. \tag{8.1}$$

and the corresponding radar estimation rate is given by

$$R_{\text{est}} \leq \frac{\delta}{2\,T} \sum_m \log_2\!\left(1 + \frac{2\sigma^2_{\tau_m,\text{proc}}\, \gamma^2\, (1-\alpha)^2 B^2\, T\, \|a_m\|^2\, P_{\text{rad}}}{k_B\, T_{\text{temp}}}\right)\,. \tag{8.2}$$

Communications Water-filling Bound

Given some bandwidth separation α,

$$B = B_{\text{com}} + B_{\text{mix}}\,,\; B_{\text{com}} = \alpha\, B\,,\; B_{\text{mix}} = (1-\alpha)\, B\,, \tag{8.3}$$

we apply the WF result derived in Section 5.1.3 and Reference [4]. The resulting communications rate bound in the communications-only sub-band is given by

$$R_{\text{CO}} \leq \alpha\, B \log_2\left(1 + \frac{\beta\, P_{\text{com}}\, b^2}{k_B\, T_{\text{temp}}\, \alpha\, B}\right)\,. \tag{8.4}$$

The mixed use communications rate inner bound is given by

$$R_{\text{MU}} \leq (1-\alpha)\, B\, \log_2\left(1 + \frac{b^2\, (1-\beta)\, P_{\text{com}}}{\sigma^2_{\text{int+n}}}\right), \tag{8.5}$$

where $\sigma^2_{\text{int+n}}$ is given by Equation (2.7). The corresponding radar estimation rate inner bound is then given by

$$R_{\text{est}} \leq \frac{\delta}{2\,T} \sum_{m=1}^{N} \log_2\!\left(1 + \frac{2\sigma^2_{\tau_m,\text{proc}} \gamma^2\, B^2_{\text{mix}}\, T\, \|a_m\|^2\, P_{\text{rad}}}{k_B\, T_{\text{temp}}}\right)\,. \tag{8.6}$$

Optimal Fisher Information Inner Bound

The bandwidth will be split between the two sub-bands according to some α such that,

$$B = B_{\text{rad}} + B_{\text{mix}}\,,\; B_{\text{rad}} = \alpha\, B\,,\; B_{\text{mix}} = (1-\alpha)\, B\,, \tag{8.7}$$

the Fisher information for this estimation problem for the m^{th} target, J_m, is given by

$$\begin{aligned} J_m = &\frac{8\pi^2 \left\|a_m\right\|^2 \alpha\, TB\, \rho_{\text{RO}}}{3k_B T_{\text{temp}} B} \left[\left(B_O - \frac{B}{2} + \alpha B\right)^3 - \left(B_O - \frac{B}{2}\right)^3\right] \\ &+ \frac{8\pi^2 \left\|a_m\right\|^2 (1-\alpha)\, TB\, \rho_{\text{MU}}}{3k_B T_{\text{temp}} B} \left[\left(B_O + \frac{B}{2}\right)^3 - \left(B_O - \frac{B}{2} + \alpha B\right)^3\right]. \end{aligned} \tag{8.8}$$

B_O, ρ_{RO} and ρ_{MU} are found in the manner described in Section 5.1.4. The resultant estimation rate bound for the radar system in both sub-bands is given by

$$R_{\text{est}} \leq \frac{\delta}{2\,T} \sum_{m=1}^{N} \log_2\!\left(1 + \sigma^2_{\text{proc}} J_m\right)\,, \tag{8.9}$$

where J_m is given by Equation (8.8) and related to the variance of the time-delay estimation by $\sigma^2_{\tau_{\text{m}},\text{est}} = J_m^{-1}$. The corresponding communications rate bound in the mixed use channel is

$$R_{\text{MU}} \leq (1-\alpha)\, B\, \log_2\!\left(1 + \frac{\left\|b\right\|^2 P_{\text{com}}}{\sigma^2_{\text{int+n}}}\right) \tag{8.10}$$

$$\sigma^2_{\text{int+n}} = \sum_{m=1}^{N} \left\|a_m\right\|^2 (1-\alpha) B\, \rho_{\text{MU}}\, \gamma^2\, (1-\alpha)^2 B^2 \sigma^2_{\text{proc}} + (1-\alpha) k_B\, T_{\text{temp}} B\,.$$

8.1.3 Examples

In Figure 8.1, we display an example of the inner bounds on performance. The values of parameter sets #1 - #5 used in the example are displayed in Table 8.1. Parameter sets #1 - #4 are used to generate the optimal Fisher information inner bounds shown in Figure 8.1a while parameter set #5 is used to generate the performance bounds shown in solid lines and parameter set #1 to generate the performance

bounds shown in dashed lines in Figure 8.1b. The parameters not mentioned in sets #2 - #5 have the same values as in set #1. Only one target is present in Figure 8.1a while there are three targets present in Figure 8.1b.

While deriving the optimal Fisher information bound, it was found that the distribution of radar power (or power spectral density) between the two sub-bands can only be optimized for $\alpha < 0.19$ and $\alpha > 0.81$. Outside this range of α, the radar power was found to be complex in nature, which was meaningless in terms of the radar system. In order to get an inner-bound on rate over all values of α a heuristic method is applied wherein the power in each sub-band has been set linearly for $\alpha < 0.19$ and $\alpha > 0.81$ such that the total power used by both sub-bands at α value is always the total radar power, P_{rad}.

In Figure 8.1a, the SIC bound is indicated by dashed lines and the optimal Fisher bound by solid lines for a particular parameter set. We see that the end points of the optimal Fisher bound are as expected. In the example, as the radar power, P_{rad}, is increased, as seen in parameter set #2, the optimal Fisher information bound shrinks (SIC vertex is lowered) and moves towards the right (radar estimation rate increases). Additionally, we see that as the communications power, P_{com}, is increased, as seen in parameter set #3, the optimal Fisher information bound increases in height (SIC vertex is raised). Finally, we see that as the time-bandwidth (TB) product, TB, is increased, as seen in parameter set #4, the optimal Fisher information bound moves towards the left (radar estimation rate decreases.)

In Figure 8.1b, the ISB is indicated by the brown line. The SIC bound is indicated by green. The WF bound is indicated by the blue line. The optimal Fisher information bound is indicated by the black line. From Figure 8.1b, we see that under the simple assumptions about the multiple radar targets, the total estimation rate, which is the sum of each individual target estimation rate, increases as the number

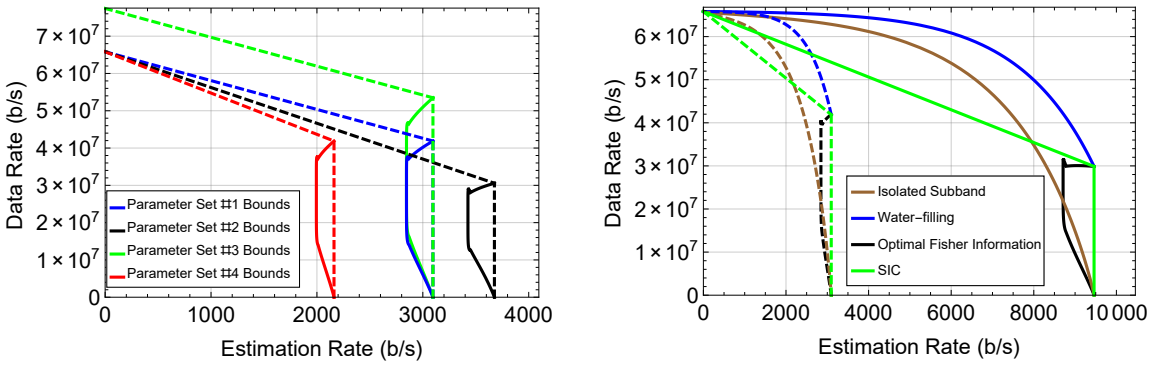

(a) Optimal Fisher Information Bounds for Parameter Sets #1-#4.

(b) Data Rate and Estimation Rate Bounds for 3 Targets

Figure 8.1: Data Rate and Estimation Rate Bounds for Parameters in Table 8.1

of targets increase which is what we expected.

8.2 Extension of Performance Bounds to Include Clutter

In this section, the inner bounds on the performance of the joint radar-communications system developed in Section 5.1 are extended to incorporate the effects of clutter with small intrinsic motion. We present a diagram of the scenario in which the joint radar-communications system is operating in Figure 8.2. The simulation scenario shown in Figure 8.2 is described in Section 2.2, with the addition of clutter scatterers to the environment.

8.2.1 Clutter Models

In this section, we will present the two models we will use to describe clutter and the techniques used to eliminate clutter under each model. We assume that all clutter scatterers are resolvable. We first look at clutter in each range cell (post-matched filtering for radar) and then calculate the total pre-matched filtering clutter return observed by the joint radar-communications system receiver. As mentioned earlier,

Table 8.1: Parameters used to generate example performance bounds for multiple radar targets in the 'basic multiple-access scenario.'

Parameter #1	**Value**
Bandwidth (B)	5 MHz
Center Frequency	3 GHz
Effective Temperature (T_{temp})	1000 K
Communications Range	10 km
Communications Power (P_{com})	100 W
Communications Antenna Gain	0 dBi
Communications Receiver Side-lobe Gain	10 dBi
Radar Target Range	100 km
Radar Antenna Gain	30 dBi
Radar Power (P_{rad})	100 kW
Target Cross Section	10 m^2
Target Process Std. Deviation ($\sigma_{\tau,\text{proc}}$)	100 m
Time-Bandwidth Product (TB)	100

Parameter #1	**Value**
Radar Duty Factor (δ)	0.01

Parameter #2	**Value**
Radar Power (P_{rad})	500 kW

Parameter #3	**Value**
Communications Power (P_{com})	500 W

Parameter #4	**Value**
Time-Bandwidth Product (TB)	200

Parameter #5	**Value**
Radar Target Range #2	80 km
Radar Target Range #3	120 km
Target Process Std. Deviation ($\sigma_{\tau,\text{proc}}$) #2	130 m
Target Process Std. Deviation ($\sigma_{\tau,\text{proc}}$) #3	90 m

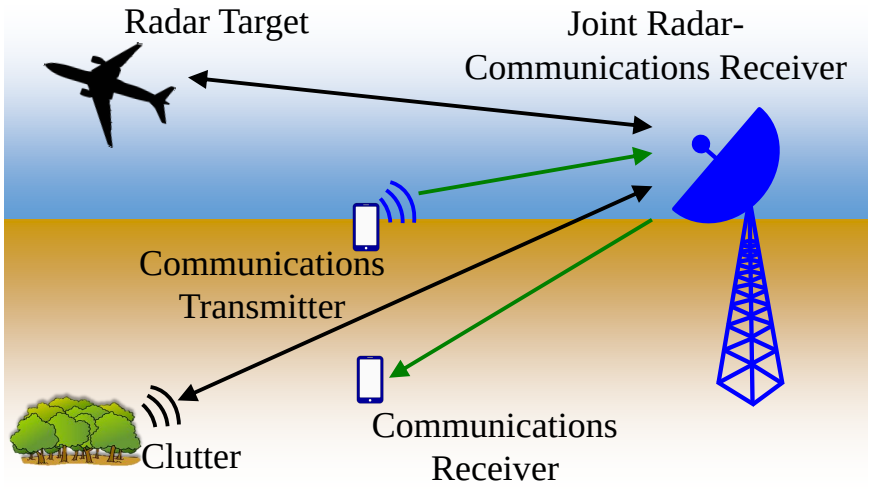

Figure 8.2: The joint radar-communications system simulation scenario with clutter and target scatterers. The joint radar-communications receiver can simultaneously perform radar target parameter estimation and decode a communications signal. By considering this idealized receiver in different scenarios, inner bounds on joint performance are derived.

the clutter elimination methods presented here are not standard clutter elimination techniques, but rather simplified methods employed so we can better study the effects of clutter on joint radar-communications system performance.

Static, Slowly Fluctuating Clutter

In this model, we assume the clutter is static but slowly fluctuating such that the radar return over N_p radar pulses is highly correlated (approximately constant). We assume that the clutter return is constant over the same N_p radar pulses for each scatterer, but there can be other models where the clutter return is constant for a different number of pulses for each scatterer. For L resolvable clutter scatterers, the radar return, $z(t)$, is given by

$$z(t) = \sqrt{P_{\text{rad}}} \sum_{m=1}^{L} a_{\text{m}}\, x(t - \tau_{\text{m}}) + n(t)\,. \tag{8.11}$$

With these assumptions, we perform matched filtering on the received signal and resolve each scatterer into a separate range cell. We perform maximum likelihood

estimation for the clutter return amplitude across each range cell, and use the estimate to eliminate the clutter return. Since the clutter return for each range cell is constant across a certain number of pulses, we can perform amplitude estimation over multiple pulses, moving the amplitude estimate closer to the true value. Eliminating clutter with this highly accurate estimate will leave behind only a tiny residual of clutter in each range cell. This residual can be interpreted as the minimum error between the true value of amplitude and its estimate and is given by a zero mean complex Gaussian [116], $n_{\text{resi}}(t)$, with variance given by the CRLB for amplitude estimation [100] which, for noise power $\sigma^2_{\text{noise}} = k_B\, T_{\text{temp}}\, B$, is given by,

$$\sigma^2_{\text{resi}} = \frac{k_B\, T_{\text{temp}}\, B}{n_s} = \frac{k_B\, T_{\text{temp}}\, B}{N_p TB}, \tag{8.12}$$

where n_s is the total number of independent samples in the period of integration.

Thus, after clutter elimination, each range cell will have a zero mean complex gaussian residue with variance given by Equation (8.12). Noting that matched filtering doesn't change the complex Gaussian nature of the clutter residual but adds a factor of $n_s = N_p\, TB$ to the variance, the radar return signal after clutter elimination is

$$z(t) = \sum_{m=1}^{L} \frac{1}{\sqrt{N_p\, TB}}\, n_{\text{resi}}(t) + \, n(t). \tag{8.13}$$

Thus, we see that $z(t) \sim \mathcal{CN}(0, \sigma^2_{\text{n+resi}})$, where $\sigma^2_{\text{n+resi}} = \sigma^2_{\text{noise}} + \frac{L\,\sigma^2_{\text{resi}}}{N_p\, TB}$.

Static Clutter with Intrinsic Clutter Motion

Similar to the previous model, we assume that the clutter is static over N_p radar pulses. However, in this model, we say that the clutter also has some small intrinsic motion (intrinsic clutter motion (ICM)) which causes the clutter returns to randomly fluctuate over each pulse. For each clutter scatterer, the ICM, which is not very large, induces a narrow Doppler spread, centered around zero Doppler, in the clutter power

spectrum. We model the clutter power spectrum as a very narrow Gaussian function with standard deviation σ_{f_D}, obtained empirically from real world data, centered around zero Doppler [117]. The Gaussian clutter spectrum for the m^{th} scatterer at range r is given by

$$C(f,r) = \frac{K_m\, P_{\text{rad}}}{r\,\sqrt{2\,\pi\,\sigma_{f_D}^2}}\,\exp\left(\frac{-f^2}{2\,\sigma_{f_D}^2}\right), \tag{8.14}$$

where K_m is a constant depending on parameters for the radar system and the m^{th} scatterer, derived from the radar range equation, such that $a_m = \frac{K_m}{r}$, where r is the corresponding range. Since the Doppler spread is very narrow, a three-tap model, with each tap located one standard deviation (σ_{f_D}) apart and centered at zero Doppler, to capture the Gaussian clutter power spectrum. Each tap in this configuration represents the average clutter power in the corresponding Doppler cell. The three-tap model for a Gaussian clutter spectrum for the m^{th} scatterer at range r is given by

$$\begin{aligned} C_{3-\text{Tap}}(f,r) = &\int_{\frac{-\sigma_{f_D}}{2}}^{\frac{\sigma_{f_D}}{2}} dfC(f,r)\,\delta(f) + \int_{\frac{-3\,\sigma_{f_D}}{2}}^{\frac{-\sigma_{f_D}}{2}} dfC(f,r)\,\delta(f+\sigma_{f_D}) \\ &+ \int_{\frac{\sigma_{f_D}}{2}}^{\frac{3\,\sigma_{f_D}}{2}} dfC(f,r)\,\delta(f-\sigma_{f_D})\,. \end{aligned} \tag{8.15}$$

Due to the fluctuations in clutter being random, we can model the distribution of the complex amplitude of the clutter return at each Doppler tap as zero mean complex Gaussian with variance given by the clutter power spectrum at each Doppler cell.

An example of the three tap model being used to represent a Gaussian clutter power spectrum is shown in Figure 8.3.

In order to eliminate clutter from the radar return signal, we perform simple Doppler processing. Once again, we note that the Doppler processing discussed in this section is not standard Doppler processing but a greatly simplified method implemented so we can better study the effects of clutter on system performance. The

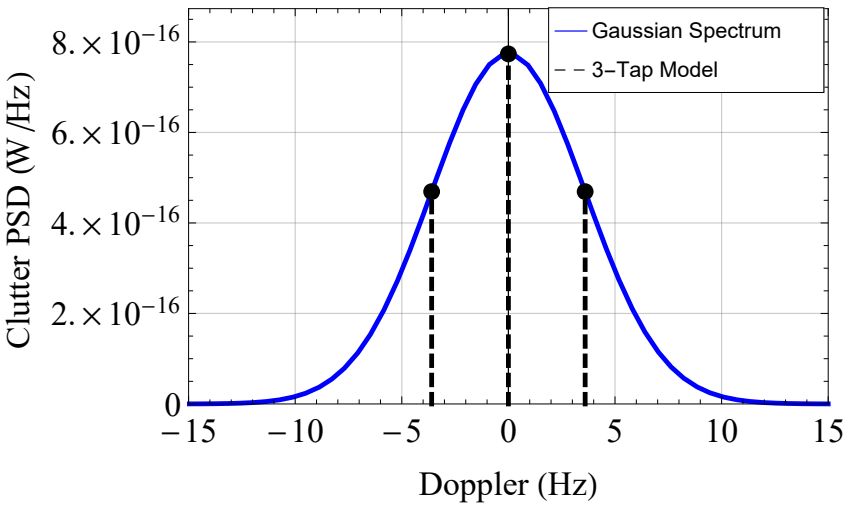

Figure 8.3: An example of the three-tap model being used to represent Gaussian clutter power spectrum. The narrow Gaussian clutter spectrum can be represented by placing three taps one standard deviation (σ_{f_D}) apart and centered at zero Doppler

time average of the radar return signal over N_p pulses (DFT at zero frequency) will give an estimate of the clutter spectrum at zero Doppler. Using this estimate, we eliminate the clutter response at zero Doppler for each clutter scatterer, with only a small residual remaining. Similar to the previous scenario, this residual will have a zero mean complex Gaussian distribution with variance given by Equation (8.12). Since this process only eliminates the clutter at the zero Doppler tap, the clutter at the non-zero Doppler taps caused by ICM still remain, resulting in a model mismatch.

Thus, after clutter elimination, each range cell with a clutter scatterer present will have a zero mean complex Gaussian residue with variance given by

$$\sigma^2_{\text{resi}} = \frac{k_B\, T_{\text{temp}}\, B}{N_p\, TB} + \sigma^2_{-1^{\text{th}}\text{DopplerTap}} + \sigma^2_{+1^{\text{th}}\text{DopplerTap}}. \tag{8.16}$$

As noted previously, since matched filtering only adds a factor of $n_s = N_p TB$ to the variance of the Gaussian residual, we see that, for L clutter scatterers, $z(t) \sim \mathcal{CN}(0, \sigma^2_{\text{n+resi}})$, where $\sigma^2_{\text{n+resi}} = \sigma^2_{\text{noise}} + \frac{L\,\sigma^2_{\text{resi}}}{N_p TB}$.

8.2.2 Received Signal with Predicted Radar Return Suppressed

We employ SIC, which was described in Section 2.3, at the joint radar-communications receiver.

We assume that the clutter elimination process discussed in Section 8.2.1 has taken place, and as a result the received signal will be corrupted with be the sum of thermal noise and clutter residual for L clutter scatterers, $n_{\text{n+resi}}(t)$, which is given by Equation (8.13). Thus, the pre-matched filtering clutter residual from all range cells, $L\,\frac{n_{\text{resi}}(t)}{\sqrt{N_p\,TB}}$, acts as interference from the communications receiver's perspective, when decoding the communications signal. On the other hand, it is assumed that post-matched filtering target detection is already done and estimation is performed only in range cells in which a target has been detected. Hence for radar estimation, the radar will only see the post-matched filtering clutter residue for a single range cell, $n_{\text{resi}}(t)$.

For N targets and L clutter scatterers, a communications receiver employing SIC will have an interference plus noise plus clutter residual variance given by [4]:

$$\sigma^2_{\text{int+n+resi}} = P_{\text{rad}} \left(\sum_{m=1}^{N} \|a_m\|^2 \,(2\pi)^2\, B^2_{\text{rms}}\, \sigma^2_{\tau_{\text{m}},\text{proc}} \right) + \sigma^2_{\text{noise}} + \frac{L\,\sigma^2_{\text{resi}}}{N_p\,TB}. \tag{8.17}$$

8.2.3 Radar Estimation Rate

The radar estimation information rate for time delay estimation is bounded explicitly as [4, 5]

$$\begin{aligned} R_{\text{est}} &\leq \sum_m \frac{\delta}{2T} \log_2\!\left(1 + \frac{\sigma^2_{\tau_{\text{m}},\text{proc}}}{\sigma^2_{\tau_{\text{m}},\text{est}}}\right) \\ &= \frac{1}{2} \sum_m B \log_2\!\left(1 + \frac{2\sigma^2_{\tau,\text{proc}}\,\gamma^2\,N_p\,B^2\,(TB)^2\,\|a_m\|^2\,P_{\text{rad}}}{TB\,k_B\,T_{\text{temp}}\,B + \sigma^2_{\text{resi}}}\right)^{\delta/(TB)}. \end{aligned} \tag{8.18}$$

8.2.4 Inner Bounds on Joint Radar-Communications System Performance

In this section, we derive inner bounds on the performance of the joint radar-communications system. We consider only a single radar target with delay τ and gain-propagation-cross-section product a and L resolvable clutter scatterers. We also assume that clutter elimination has taken place.

Successive Interference Cancellation Bound

When R_{com} is sufficiently low, the interference plus noise plus clutter residual from the communications receiver's perspective, $\sigma^2_{\text{int+n+resi}}$, is described by Equation (2.7), and the communications data rate will be,

$$R_{\text{com}} \leq B \, \log_2\left(1 + \frac{b^2 \, P_{com}}{\sigma^2_{\text{int+n+resi}}}\right) , \tag{8.19}$$

In this regime, the corresponding estimation rate bound R_{est} is given by Equation (8.18). The SIC inner bound is given by the convex hull between points given by Equations (5.4), (8.18) and (8.19).

Communications Water-filling Bound

Given some bandwidth separation α,

$$B = B_{\text{com}} + B_{\text{mix}} \, , \, B_{\text{com}} = \alpha \, B \, , \, B_{\text{mix}} = (1 - \alpha) \, B \, , \tag{8.20}$$

the resulting communications rate bound in the communications-only sub-band is given by

$$R_{\text{CO}} \leq \alpha \, B \log_2 \left(1 + \frac{\beta \, P_{\text{com}} \, b^2}{k_B \, T_{\text{temp}} \, \alpha \, B}\right) . \tag{8.21}$$

The mixed use communications rate inner bound is given by

$$R_{\text{MU}} \leq (1 - \alpha) \, B \, \log_2 \left(1 + \frac{b^2 \, (1 - \beta) \, P_{\text{com}}}{\sigma^2_{\text{int+n}}}\right) , \tag{8.22}$$

where $\sigma^2_{\text{int+n}}$ is given by Equation (8.17). The corresponding radar estimation rate inner bound is then given by

$$R_{\text{est}} \leq \frac{\delta}{2\,T} \log_2\left(1 + \frac{2\sigma^2_{proc}\gamma^2\, N_p\, B^4_{\text{mix}}\, T\, \|a\|^2 P_{\text{rad}}}{T B_{\text{mix}}\, k_B\, T_{\text{temp}} B_{\text{mix}} + \sigma^2_{\text{resi}}}\right) . \tag{8.23}$$

8.2.5 Examples

In Figure 8.4, we compare the inner bounds on performance in the presence of different types of clutter described in Section 8.2. The parameters used in the example are displayed in Table 8.2. It should be noted that the bounds presented in this section are not fundamental limits on performance, and much tighter bounds can be achieved by applying more effective methods of clutter elimination.

In Figure 8.4, the SIC bounds are represented by dashed lines and the WF bounds by solid lines. In Figure 8.4a, we compare the inner bounds of performance in the absence of clutter, shown in black, to the inner bounds on performance in the presence of clutter with large ICM, shown in red, and small ICM, shown in blue. In Figure 8.4b, we compare the inner bounds of performance in the presence of clutter with large ICM, shown in red, small ICM, shown in blue, and no ICM, shown in green.

As seen from Figures 8.4a and 8.4b, there is almost no change in performance in the presence clutter without ICM when compared to performance in the absence of clutter. This is expected since static, slowly-fluctuating clutter can easily be estimated accurately and eliminated, leaving behind a negligible amount of residual. However, the presence of clutter with ICM can impose a significant degradation on performance from both a communications and radar system's perspective. Whenever the communications and radar signals overlap, communications performance degrades significantly since the total clutter residual acts as interference from the communications receivers perspective. Furthermore, since radar estimation is done after target

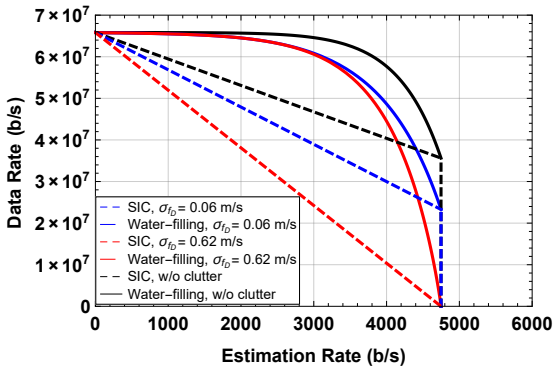

(a) Performance Bounds with Clutter Absent Vs. Performance Bounds with Clutter with Large and Small ICM Present

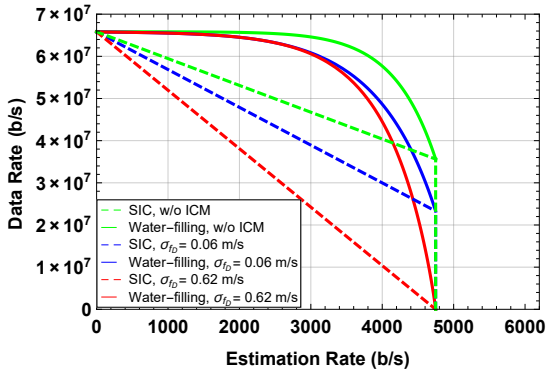

(b) Performance Bounds with Clutter with Small ICM Vs. Clutter with Large ICM Vs. Clutter with no ICM

Figure 8.4: Data Rate and Estimation Rate Bounds for Parameters in Table 8.2

detection, the clutter residual from only the current range cell effects estimation performance and as a result, radar performance degrades by a smaller amount when compared to communications performance. Additionally, as seen from Table 8.2, the radar target is far away, causing the clutter residual present in the target range cell to be negligible. Hence, the radar performance undergoes almost no degradation. However, radar performance would degrade significantly for closer radar targets. Finally, we see that clutter with large ICM will cause more degradation in performance when compared to the effect of clutter with small ICM on performance.

8.3 Extension of Performance Bounds to Account for Phase Noise Effects

In this section, the inner bounds on the performance of the joint radar-communications system developed in Section 5.1 are extended to incorporate the effects of phase noise while performing clutter mitigation. We consider the same simulation scenario shown in Figure 8.2 that was used in the previous section, Section 8.2.

The model used to characterize the clutter in this section is described in Section 8.2.1.

Table 8.2: Parameters used to generate example performance bounds for a single radar target in the presence of clutter for the 'basic multiple-access scenario.'

Parameter	Value
Bandwidth (B)	5 MHz
Center Frequency	3 GHz
Effective Temperature (T_{temp})	1000 K
Communications Range	10 km
Communications Power (P_{com})	100 W
Communications Antenna Gain	0 dBi
Communications Receiver Sidelobe Gain	10 dBi
Radar Target Range	80 km
Radar Antenna Gain	30 dBi
Radar Power (P_{rad})	100 kW
Target Cross Section	10 m^2
Target Process Std. Deviation ($\sigma_{\tau,\text{proc}}$)	100 m
Time-Bandwidth Product (TB)	100
Radar duty factor (δ)	0.01
Number of Clutter Scatterers	50
Total Pulses Integrated	40
Doppler Spread Std. Deviation (Small ICM)	1.2 Hz
Doppler Spread Std. Deviation (Large ICM)	12.4 Hz
Clutter Cross Section	100 m^2

8.3.1 Piecewise Linear Phase Noise Model

We can account for the effects of phase noise once the phase noise power spectral density at the carrier frequency is known. In this report, we assume that the local oscillator used by the joint radar-communications receiver (which is also a radar transmitter) is a quartz oscillator with a natural frequency of 10 MHz. Up-conversion to a higher carrier frequency will increase the phase noise spectrum by a constant up-conversion factor K_{conv}, given by the square of the ratio of the higher carrier frequency to the oscillator's natural frequency [118]. The phase noise model used in this paper will incorporate the effects of such an up-conversion. We assume that the phase noise power spectral density ($S(f)$) can be modeled as a linear piecewise function. The piece-wise linear phase noise spectrum $S(f)$ can be characterized by the following parametric model [118]

$$S(f) = K_{\text{conv}} \sum_{i=-3}^{0} b_i \, f^i \,, \tag{8.24}$$

where K_{conv} is the up-conversion factor and, b_i, the phase noise slope coefficients, are obtained from data sheets for real quartz oscillators.

For this paper, we consider the Agilent 10811 quartz oscillator and obtain phase noise slope coefficients as seen in Table 8.3. The oscillator will have a phase noise power spectral density at its natural frequency as shown in Figure 8.5 [118]. After up-conversion to a higher carrier frequency, the oscillator will have a phase noise power spectral density as shown in Figure 8.6. We also consider a carrier frequency of 3 GHz, which results in a up-conversion factor $K_{\text{conv}} = 300^2$.

Range Decorrelation Effects on Phase Noise

When looking at the radar return spectrum, the presence of phase noise causes a scatterer's frequency response to spread. However, this spreading is also range dependent.

Table 8.3: The slope coefficient values employed for the phase noise model.

f, Hz	S(f), dBc/Hz
b_0	-162
b_{-1}	-137
b_{-2}	-131
b_{-3}	-103

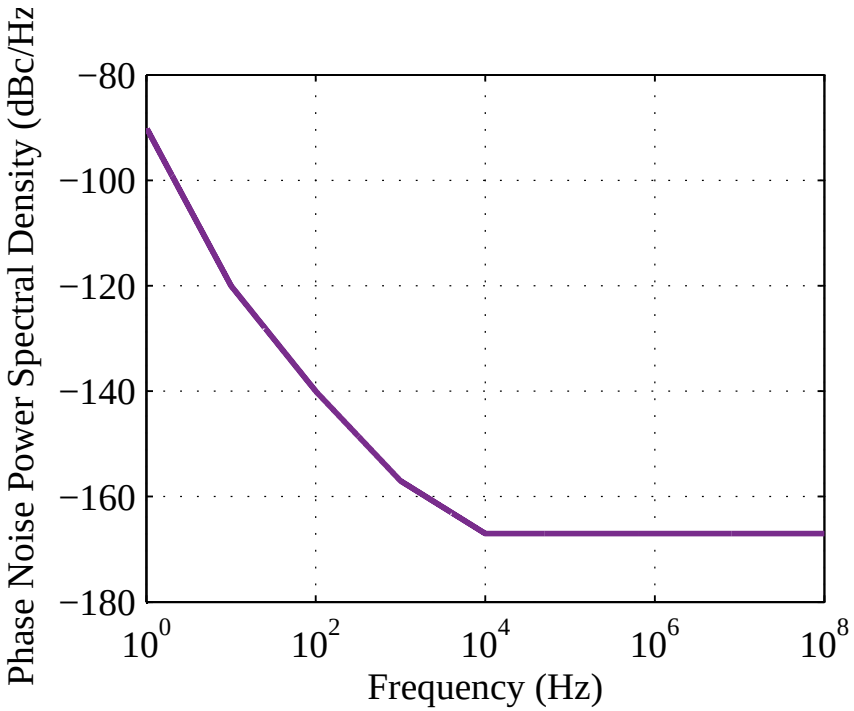

Figure 8.5: A plot of the linear piecewise phase noise power spectral density at the oscillator's natural frequency. This up-conversion will cause the phase noise spectrum to increase by the up-conversion factor.

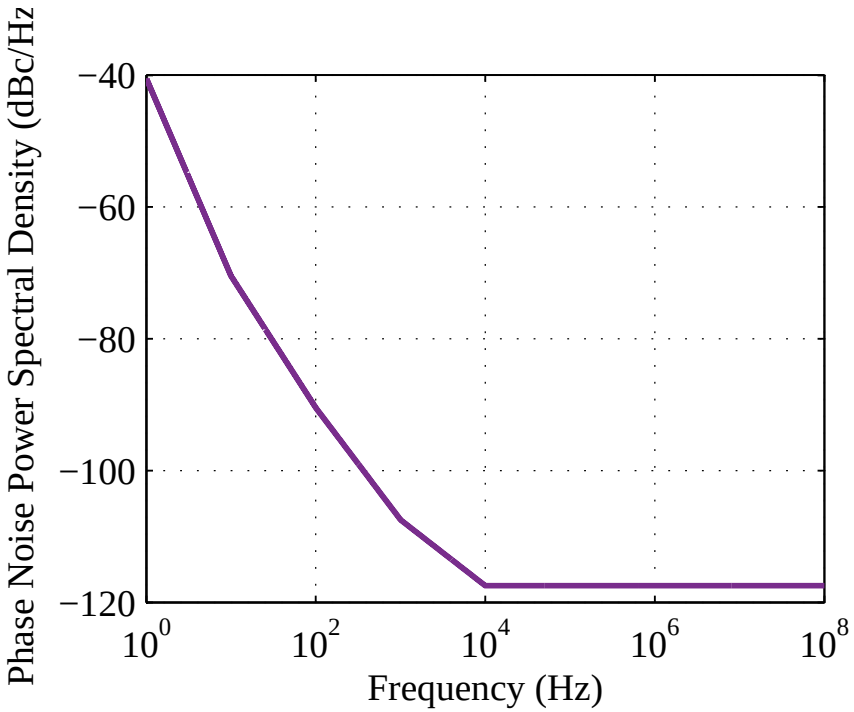

Figure 8.6: A plot of the linear piecewise phase noise power spectral density after up-conversion to a higher carrier frequency. This linear piecewise power spectral density is constructed by obtaining phase noise slope coefficients b_i from a real oscillator and then applying the phase noise model given by Equation (8.24).

The contribution of phase noise on a scatterer response depends on a filtering effect known as range decorrelation. The closer a scatterer is, the less phase noise impacts the scatterer's return. This range dependency is because the effects of phase noise arises due to the decorrelation in the received signal and local oscillator's phase. This difference in phase depends on the time delay (or range) between the transmitted and received signals. The shorter the time delay (or range), the smaller the decorrelation between phases. In other words, the longer the time delay (range) between transmitted and received signals, the longer the phase of the local oscillator drifts, causing a larger amount of phase noise.

The effects of range decorrelation on phase noise can be modeled as a filter, and

the phase noise spectrum is modeled as

$$S_{\text{PN+range}}(f, r) = S(f)\, 4\, \sin^2\left(2\,\pi\, r\, \frac{f}{c}\right), \tag{8.25}$$

where the range decorrelation filter component is $4\sin^2 2\pi r\frac{f}{c}$ for a scatterer at range r.

Finally, the total clutter spectrum with phase noise and range decorrelation for the m^{th} scatterer at range r is given by

$$S_{\text{clutter+PN+range}}(f, r) = C_{3-\text{Tap}}(f, r) + C_{3-\text{Tap}}(f, r) * S_{\text{PN+range}}(f, r)\,. \tag{8.26}$$

8.3.2 Clutter Mitigation with Phase Noise Processing

In this section, we briefly describe the clutter mitigation and phase noise techniques used by the joint radar-communications receiver. Once clutter mitigation and phase noise processing have occurred, the clutter cancellation residual power $\sigma^2_{\text{residual}}$ is computed by integrating the clutter spectrum in the presence of phase noise. The processing chain for clutter cancellation is similar to the one described in [105]. A block diagram representation of the entire clutter cancellation processing chain is shown in Figure 8.7.

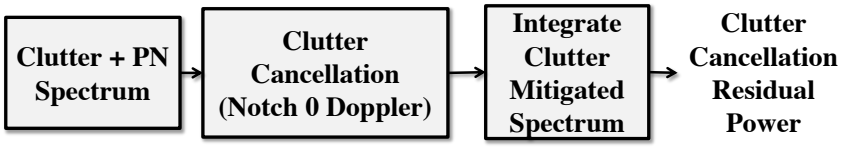

Figure 8.7: Block diagram representation of computation of clutter cancellation residual in the presence of phase noise. Simple clutter cancellation techniques are employed (notching 0 Doppler) and the residual power is calculated by integrating the resulting clutter spectrum.

As stated earlier, we assume that target detection has already occurred. Thus, clutter only affects radar estimation performance if there is clutter present in the same range cell as the target of interest. However, the communications system sees

the clutter response for all the scatterers. Thus, the communications system can be adversely affected by clutter and as a result, clutter mitigation has to be done before any communications signal decoding. We will only consider there to be a single clutter scatterer located in the same range cell as the target of interest. Doppler filtering is used to suppress the clutter return.

Clutter processing is done over N_p radar pulses of coherent integration. Thus, the communications system has to wait until N_p radar returns arrive at the receiver. Since we are integrating over multiple pulses, the radar return spectrum will have narrow pulse repetition frequency (PRF) sidelobes which occur at every multiple of the PRF. However, these sidelobes generally are located far away from the main lobe and thus will not affect radar performance. Additionally, even though the communications system will see these narrow sidelobes, they occur at known frequency intervals and the effects of it can easily be mitigated through pre-coding. Thus, these PRF sidelobes can be ignored.

We assume our clutter mitigation filter is the length of the returned waveform without pulse compression, and is a narrow notch filter equivalent to a frequency domain window where unit gain is present in all bins except DC. Therefore, the resulting notch filter perfectly cancels clutter if there is no ICM and no phase noise. When either or both of these conditions exist, a residual remains. We integrate the clutter spectrum after clutter mitigation is done to obtain the residual power $\sigma^2_{\text{residual}}$, and treat it as an additional noise power term that degrades radar performance. In addition, as we will see, this degrades the communications user who now has additional residual signal power left over after SIC is complete. We assume the resulting residual is an additional Gaussian noise term, independent of the thermal noise contribution. A block diagram of the joint radar-communications system in this scenario is shown in Figure 8.8.

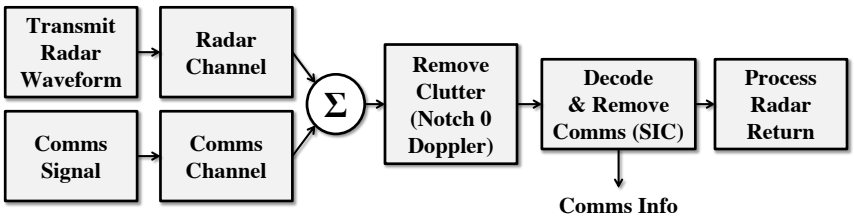

Figure 8.8: Joint radar-communications system block diagram for clutter cancellation in the presence of phase noise. Since the communications system can be adversely affected by clutter, clutter mitigation has to be done before any communications signal decoding. Additionally, the clutter cancellation residual further degrades the channel, adversely impacting both the communications and radar performances.

8.3.3 Examples

In Figures 8.9 to 8.11, we display examples of the effects of clutter and phase noise on the inner bounds on performance and the relationship between phase noise and scatterer range. The parameters used in the examples are displayed in Table 8.2. In Figure 8.9, we look at the estimation rate as a function of range for a cluttered return with and without phase noise. In this case, no ICM is present in the clutter, as ICM dominates phase noise effects for spectral spreading. Interestingly, the most impactful ranges are the closest to the radar, effectively less than 2 km in this example. While range decorrelates the phase noise and makes clutter cancellation difficult, the power of the clutter drops rapidly. As a result, the phase noise contribution becomes negligible compared to thermal noise at the radar receiver. Near to the radar, while we have more correlation assisting with clutter cancellation, the clutter is much more powerful.

To see the effect of the clutter with ICM (using previously mentioned model) and phase noise on the joint multiple-access system, we look at the joint radar-communications outer and inner bounds in Figure 8.10. Immediately, one striking difference from previous work is that the WF solution is occasionally bested by the CIR time share inner bound. In prior work where clutter was ignored [4, 5, 8, 103],

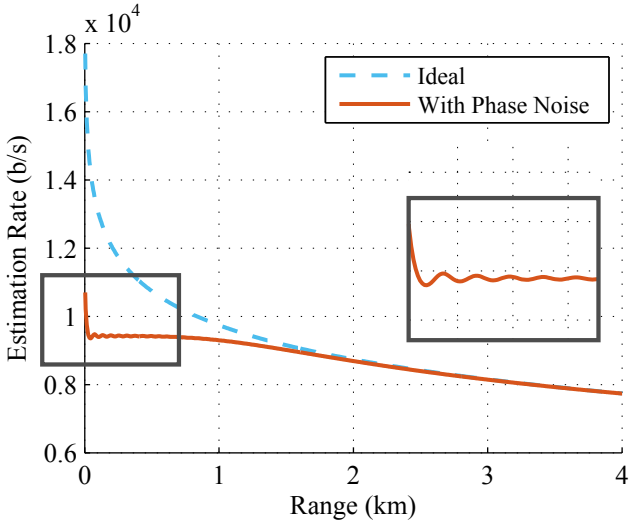

Figure 8.9: Estimation rate in the presence of clutter (no ICM) and phase noise as a function of range. Close in, the clutter power is overwhelming, despite improved phase correlation. Out far, though decorrelated, the clutter power has dropped such that the residual power is overcome by thermal noise. The inset plot shows detail of the estimation rate with phase noise near 0 km.

this was never the case. The ISB has similar behavior. When the two converge, the WF algorithm is deciding not to use the degraded radar channel, as it is not optimal use of the communications power.

To see the effects of clutter with ICM (using previously mentioned model) in general more clearly, we compare the ideal inner and outer bounds to the ones just discussed. This is shown in Figure 8.11. The estimation rate is halved in the ideal case. Note the communications user without any radar interference is unaffected, so the outer bound on the y-axis is unchanged. However, all communications bands with radar returns, such as those employing SIC, are affected by the residual clutter noise.

8.3.4 Effect of Phase Noise on Clutter Estimation and Mitigation

In this section we investigate the effect phase noise has on clutter estimation and mitigation and also show that by combining observations and results obtained from

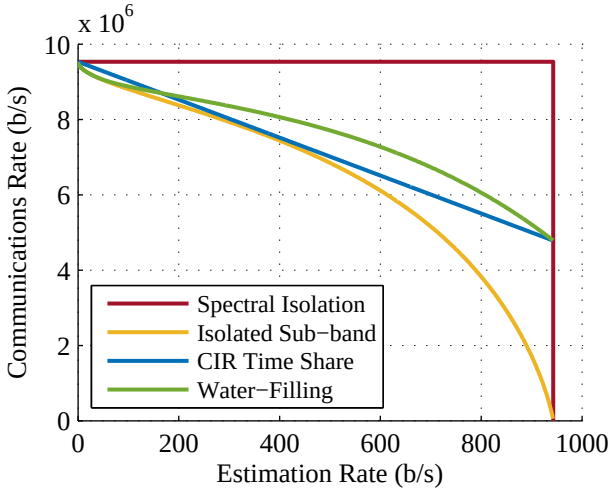

Figure 8.10: Multi-access bounds for radar and communication in the presence of clutter with ICM using previously mentioned model. Shown are outer bounds in red, indicating interference free operation, and a series of inner bounds described previously. The ISB is shown in yellow, while the CIR time share line is given in blue. Finally, the WF bound is shown in green.

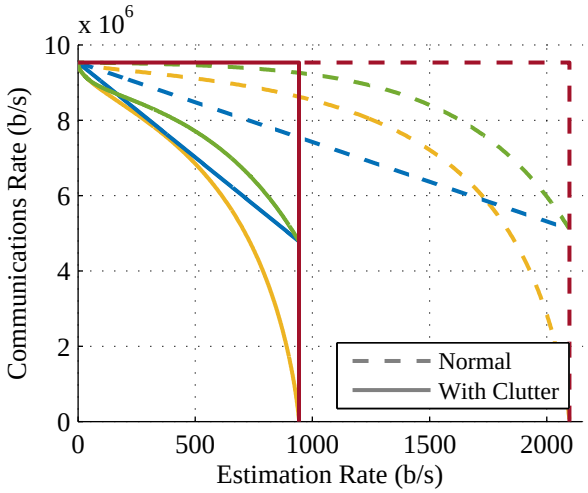

Figure 8.11: Multi-access bound for radar and communication, compared for with and without clutter with ICM using previously mentioned model. The colored lines are the same as in the previous plot, with the legend omitted for clarity. Instead, a dashed line indicates ideal operation if no clutter is present, while the corresponding same colored solid line indicates the cluttered system. The red lines are the interference free outer bounds. The ISB is shown in yellow, while the CIR time share line is given in blue. Finally, the WF bound is shown in green.

both Sections 8.2 and 8.3, the effects of phase noise can be clearly highlighted.

In Section 8.3, we considered the estimation rate as a function of range for a cluttered return with and without phase noise for a single target. Clutter here was considered to have no ICM such as the clutter model described in Section 8.2.1. From Figure 8.9, we saw that the estimation rate for a cluttered return in the presence of phase noise was adversely affected only at closer ranges (approximately less that 2 km in the example described). Essentially, this means that as range of the radar target increases, the effect of phase noise on the estimation rate decreases and the estimation rates for both scenarios converge. Additionally, from Figure 8.11, we also see that the estimation rate in the presence of clutter (with ICM) and phase noise does not match the ideal case estimation rate (without clutter or phase noise), by almost a factor of 2 in this case. It is easy to erroneously attribute this disparity in performance to the presence of clutter, especially in light of the observations made from Figure 8.9. By looking at results from Section 8.2, we can see how it is in fact phase noise that is responsible for the degradation in performance.

From Figure 8.4, we see that in the presence of clutter (either with or with out ICM) and no phase noise, the estimation rate undergoes a negligible performance degradation. In fact, the estimation rate remains the same for clutter with out ICM. It becomes clear now that the performance degradation seen in Figure 8.11 was due to the presence of phase noise. In Section 8.2, we used a optimal form of clutter estimation and mitigation through which the clutter residual was minimized. This resulted in the estimation rate barely being affected by the presence of clutter. However, when phase noise is present, the clutter returns cannot be estimated accurately and hence, sub-optimal clutter mitigation techniques must be used. This results in larger clutter residuals which cause the adverse effect on performance seen in Figure 8.11.

8.4 Extension of Performance Bounds for Radar Target Detection

In this section, we extend the previously derived joint radar-communications performance bounds to include radar detection. We consider a scenario in which a communications user operates while an in-band radar user searches for a potentially nonexistent target. We assume that clutter is present, and that the clutter scatterers are static over some N_p radar pulses and have no ICM. The clutter can be estimated in the absence of a radar target during the first coherent processing interval (CPI) (N_p pulses). These estimates can then be used to mitigate clutter in the next CPI, in which a target may or may not be present. This estimation and mitigation of clutter is performed via one-dimensional (1D) coherent change detection [119], which assumes that the clutter estimates from the previous CPI is a good estimate for clutter in the current CPI.

We consider a simulation scenario and joint radar-communications receiver similar to the one described in Section 2.2. The inner bounds on performance are found by considering this ideal receiver in different scenarios and deriving performance bounds on radar and communications systems respectively. The simulation scenario considered in this paper is depicted in Figure 8.12.

8.4.1 Clutter Model and Mitigation

The clutter model and associated processing techniques used here were first discussed in Section 8.2.1 [9]. We assume that there are multiple resolvable clutter scatterers. We first look at clutter in each range cell (post-matched filtering for radar) and then calculate the total pre-matched filtering clutter return observed by the joint radar-communications system receiver. The residual clutter power remaining after clutter mitigation is assumed to be Gaussian and is treated as an additional additive

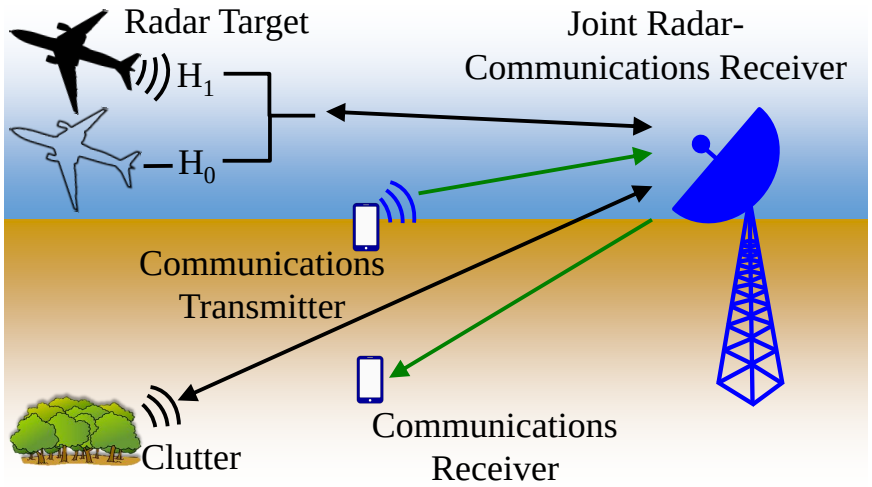

Figure 8.12: Top level diagram of joint radar-communications detection problem description. Environment contains radar clutter, an in-band communications user and, possibly a radar target. The joint radar-communications receiver is capable of simultaneous target detection and communications decoding. A target is illuminated along with clutter in the alternative hypothesis. If this is true, the reflected energy arrives at the joint radar-communications receiver. Otherwise, only clutter energy is seen at the joint radar-communications receiver. A communications signal is input to the system through the antenna sidelobe. The superposition of the radar signal and the communications signal is perturbed by thermal receiver noise and clutter.

noise term.

We assume that each clutter scatterer is static (with no ICM) over some N_p radar pulses such that the radar return over this time period is highly correlated (approximately constant). With these assumptions, we resolve the scatterers into appropriate range cells and perform maximum likelihood amplitude estimation for clutter returns from the first CPI. These range and amplitude estimates of clutter are used to mitigate the clutter return in the next CPI.

As seen in Section 8.2.1, the clutter residual in each range cell has power given Equation (8.12). This minimum error (residual) is a zero mean complex Gaussian, $n_{\text{resi}}(t)$, with variance given by Equation (8.12). The radar return signal after clutter mitigation for L clutter scatterers is given by Equation (8.13). Thus, $z(t) \sim \mathcal{CN}(0, \sigma^2_{\text{n+resi}})$, where $\sigma^2_{\text{n+resi}} = \sigma^2_{\text{noise}} + \frac{L\sigma^2_{\text{resi}}}{N_p TB}$.

Performing clutter mitigation in this manner requires that the clutter estimates obtained from the previous CPI remain good estimates for the current CPI, which is an optimistic assumption. If less accurate clutter estimates are used, the resulting clutter residual is larger and the system performance is further degraded.

The estimation and mitigation of clutter can performed using 1D coherent change detection [119], which ascertains when the estimation and mitigation CPIs begin and end. Clutter is then mitigated by subtracting the total power of the first CPI from the second.

8.4.2 Importance of Clutter

Inclusion of clutter is necessary because of a subtlety in the problem formulation. Because both systems share the same spectrum allocation, each system pushes for more spectral access. For a communications system, an increase in spectral access directly improves performance by increasing the data rate. For a radar system, increased spectral access improves radar estimation but not radar detection. For example, a radar waveform with an impulse-like spectrum can perform target detection, but has poor ranging resolution and degrades time-delay estimation performance (which traditionally succeeds radar detection).

The introduction of clutter couples radar detection performance with spectral allocation. By increasing spectral allocation for the radar system, ranging resolution is improved, resulting in smaller range cells. As a result of smaller range cells, the number of scatterers in the target range cell reduces, thereby reducing the clutter residual power after mitigation and improving radar detection performance.

8.4.3 Communications Message Decoding and Mitigation

In this section, we also discuss how the joint radar-communications system is able to simultaneously decode a communications message and perform target estimation. At the receiver, we employ a communications signal mitigation technique which is similar to SIC employed in Section 2.3 [4]. The algorithm used in this paper decodes the communications message from the composite received signal at a lower rate to ensure that communications signal decoding and radar detection can be done co-operatively. We assume that the radar interference can be modeled as a Gaussian random variable. Thus, the radar interference essentially raises the noise floor from a communications receiver's perspective. At a much lower data rate, the communications message can be decoded and removed from the received signal. Radar target estimation can then be done without any communications interference.

Prior works employing SIC [4, 5, 9] assumed that target detection and acquisition (for tracking) had already taken place and used the target tracking information to perform radar mitigation prior to communications decoding. As a result, the same SIC mitigation technique can not be employed here. Additionally, treating radar interference as noise is not a realistic assumption and results in sub-optimal communications performance. However, we argue that once a target has been detected, SIC can be used to improve communications performance.

By employing the mitigation technique described above at the receiver, the received signal is corrupted by thermal noise as well as returns from all L clutter scatterers, which has an adverse effect on communications performance. Hence, we have to perform clutter mitigation first. In doing so, communications performance is affected by the total clutter residual as well. However, for radar detection performance, since matched filtering is already done and the environment has been resolved into range

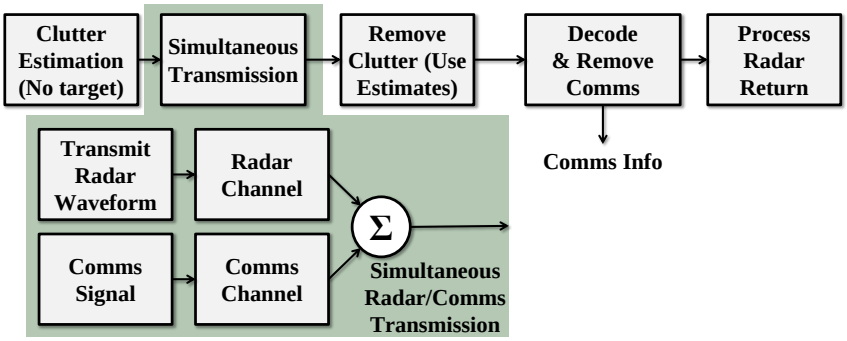

Figure 8.13: Joint radar-communications system block diagram showcasing clutter mitigation and simultaneous communications signal decoding and target detection. Since the communications system can be adversely affected by clutter, clutter mitigation has to be done before any communications signal decoding. Additionally, the clutter cancellation residual further degrades the channel, adversely impacting both the communications and radar performances.

cells, the radar will only see clutter residue from the current range cell in which target detection is being performed. A block diagram of the joint radar-communications system in this scenario is shown in Figure 8.13. Given the following received signal for N targets and L clutter scatterers,

$$\tilde{z}_{\text{com}}(t) = \sqrt{P_{\text{com}}}\, b\, r(t) + \sqrt{P_{\text{rad}}} \sum_{m=1}^{N} a_m x(t-\tau_m) + \sum_{m=1}^{L} \frac{1}{\sqrt{N_p T B}}\, n_{\text{resi}}(t) + n(t)\,, \tag{8.27}$$

the interference plus noise plus clutter residual variance from the communications receiver's perspective is given by Equation (8.17) [5, 9].

8.4.4 Receiver Operating Characteristic Curves for Radar Detection

In this section, we show how radar detection performance is measured and derive false alarm and detection probabilities for the joint radar-communications system. The receiver operating characteristic (ROC) curves for radar detection in a joint radar-communications system are derived for the aforementioned scenario. Since SIC is employed at the receiver, the received signal, $z(t)$, contains only the radar return

and thermal noise. We perform matched filtering and measure the total energy in each range cell for each CPI. Assuming H_0 is the null hypothesis,

$$\begin{aligned} H_0 :\ & z(t) = n_{\text{resi}}(t) + n(t) \\ H_1 :\ & z(t) = a\,\sqrt{N_p T B P_{\text{rad}}}\,x(t-\tau) + n_{\text{resi}}(t) + n(t)\,, \end{aligned} \tag{8.28}$$

where $\sqrt{N_p\,TB}$ is present due to the coherent integration factor from matched filtering. Equation (8.28) implies that the radar return energy from a range cell is drawn from either a complex central chi-squared distribution of one degree under H_0 ($P_{\|z(t)\|^2|H_0}(q) = P^{\mathbb{C}}_{\chi^2}(q\,, N_p\,, \sigma^2_{\text{noise}} + \frac{\sigma^2_{\text{resi}}}{N_p\,TB})$) or a complex non-central chi-squared distribution of one degree under H_1 ($P_{\|z(t)\|^2|H_1}(q) = P^{\mathbb{C}}_{\chi^2_{\text{nc}}}(q\,, \sigma^2_{\text{noise}} + \frac{\sigma^2_{\text{resi}}}{N_p\,TB}\,, N_p\,TB\,a^2\,P_{\text{rad}})$) [100, 105].

Hence, at detection threshold η, the resulting false-alarm probability is given by [100]

$$P_{\text{FA}} = 1 - \frac{1}{\Gamma(N_p)}\gamma\left(N_p, \frac{\eta}{\sigma^2_{\text{noise}} + \frac{\sigma^2_{\text{resi}}}{N_p\,TB}}\right)\,, \tag{8.29}$$

and the detection probability is given by [100]

$$P_{\text{D}} = Q_{N_p}\left(\sqrt{\frac{2\,N_p\,TB\,a^2\,P_{\text{rad}}}{\sigma^2_{\text{noise}} + \frac{\sigma^2_{\text{resi}}}{N_p\,TB}}}\,, \sqrt{\frac{2\,\eta}{\sigma^2_{\text{noise}} + \frac{\sigma^2_{\text{resi}}}{N_p\,TB}}}\right)\,. \tag{8.30}$$

8.4.5 Examples

In this section, through Figures 8.14 and 8.15, we present example performance bounds by evaluating the WF bound defined in Section 5.1.3 and the results of Section 8.4.4 for a set of example parameters. The parameter set used in this section is displayed in Table 8.4.

The evaluated communications WF bound on performance is shown in Figure 8.14 for different values of number of radar pulses integrated (N_p). The communications

Table 8.4: Parameters used to generate example performance bounds for radar detection of a single radar target in the presence of clutter for the 'basic multiple-access scenario.'

Parameter	**Value**
Bandwidth (B)	5 MHz
Center Frequency	3 GHz
Effective Temperature (T_{temp})	1000 K
Communications Range	10 km
Communications Power (P_{com})	100 W
Communications Antenna Gain	0 dBi
Communications Receiver Sidelobe Gain	10 dBi
Radar Target Range	80 km
Radar Antenna Gain	30 dBi
Radar Power (P_{rad})	1000 W
Target Cross Section	10 m^2
Time-Bandwidth Product (TB)	100
Number of Clutter Scatterers	10000
Total Pulses Integrated	10, 5, 1

performance, measured by data rate, and the detection performance, measured by area under the ROC curves, are compared against each other as the bandwidth splitting parameter α is swept from 0 to 1. For values of α closer to 1, more bandwidth is allocated for communications only, resulting in improved communications performance and lower radar detection performance. When α is 1, the radar does not have any spectral allocation and cannot illuminate the environment, resulting in the detector making random guesses for target detection. This is highlighted by an area under the ROC curve of 0.5, which is characteristic of a random guess detector, when α is

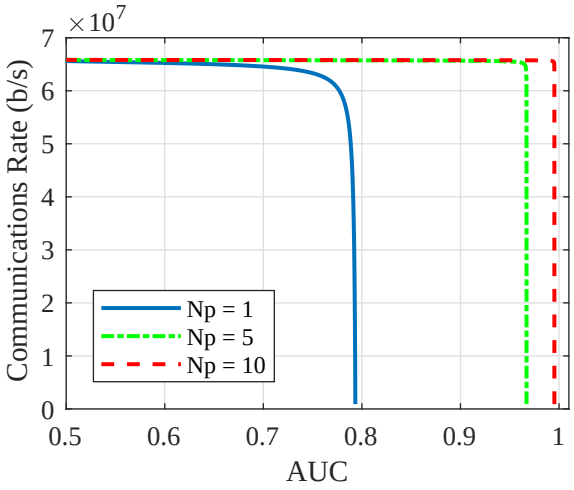

Figure 8.14: The evaluated communications WF bound on performance vs. area under the ROC curve. The figure shows the communications data rate and detection area under the ROC curves as α, the bandwidth splitting parameter, is swept from 0 to 1. We see that as α increases, more bandwidth is assigned to communications only, hence communications performance increases and radar performance decreases. The opposite effect on bandwidth happens as α approaches 0 and as a result radar performance increases and communications performance decreases, reaching the SIC communications rate at $\alpha = 0$.

1. Similarly, for values of α closer to 0, more bandwidth is allocated for mixed use, resulting in improved detection performance and communications performance approaching the SIC communications rate. Additionally, target detection performance also depends on the number of integrated radar pulses, N_p. An increase in N_p results in improved target detection performance, characterized by an area under the ROC curve closer to 1, as seen in Figure 8.14. The sample evaluation presented in this section uses a simplistic model for clutter. Under more complicated clutter models, the clutter residual is larger and adversely affects communications performance. As shown in Reference [9], introducing a small amount of ICM has a significant negative impact on communications performance.

In Figure 8.15, we more closely evaluate the relationship between detection performance and spectral allocation assigned for mixed use (i.e. spectrum allocated for radar). In this figure, detection performance is captured via ROC curves. As ex-

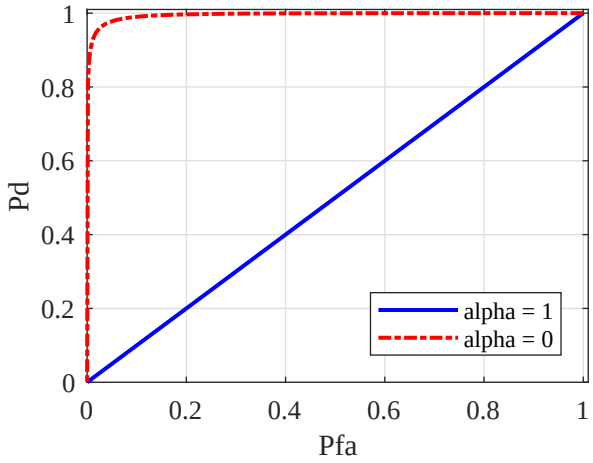

Figure 8.15: Detection performance for different values of α and $Np = 10$. Detection performance here is highlighted through ROC curves for different values of α. As expected, we see that detection performance improves as α moves from 1 to 0. When α is 1, the radar cannot illuminate the environment and the detector has to make random guesses for target detection, resulting in a ROC curve given by a straight line, which is characteristic of a random guess detector.

pected, the detection performance improves as α moves from 1 to 0. When α is 1, the radar cannot illuminate the environment and the detector has to make random guesses for target detection, resulting in a ROC curve given by a straight line, which is characteristic of a random guess detector.

Chapter 9

SUMMARY

In this dissertation, we first describe the problem of radar-communications coexistence and the challenges for finding a solution and achieving RF convergence. We perform a survey of previously proposed solutions and considering the joint radar-communications problem as a joint information problem, we present a novel approach to constructing future solutions. We derive the estimation rate, an information metric for estimation performance symmetric to the communications rate, and provide a more intuitive understanding of the estimation rate. We also develop an extension to the estimation rate that takes into account non-local estimation errors as well. We develop multiple solutions to cooperative radar and communications coexistence for a simple multi-access scenario, which can be applied to more complicated scenarios. Using the estimation rate and the communications data rate, we then develop several cooperative signaling schemes that are used to develop inner bounds on joint performance. We also note how the information measured by the estimation and communications rate in bits for each system can have different values or priority, depending on the importance of each system. Two methods for choosing an optimal operating point for a joint radar-communications system are also presented. We also present a new radar waveform design method for a joint radar-communications system in which the radar waveform spectrum and communications power spectral distribution are optimized to maximize joint performance. The performance of this radar waveform design algorithm is also studied. Finally, we develop extensions to the previously derived performance bounds for target estimation for multiple targets, target estimation in the presence of clutter, target estimation with clutter mitigation

in the presence of phase noise, and radar target detection.

REFERENCES

[1] H. Griffiths, L. Cohen, S. Watts, E. Mokole, C. Baker, M. Wicks, and S. Blunt, "Radar spectrum engineering and management: Technical and regulatory issues," *Proceedings of the IEEE*, vol. 103, no. 1, pp. 85–102, January 2015.

[2] B. Paul, A. R. Chiriyath, and D. W. Bliss, "Survey of RF communications and sensing convergence research," *IEEE Access*, vol. 5, no. 1, pp. 252–270, December 2016.

[3] J. Chapin. Shared spectrum access for radar and communications (SSPARC). [Online]. Available: http://www.darpa.mil/program/shared-spectrum-access-for-radar-and-communications

[4] D. W. Bliss, "Cooperative radar and communications signaling: The estimation and information theory odd couple," in *IEEE Radar Conference*, May 2014, pp. 50–55.

[5] A. R. Chiriyath, B. Paul, G. M. Jacyna, and D. W. Bliss, "Inner bounds on performance of radar and communications co-existence," *IEEE Transactions on Signal Processing*, vol. 64, no. 2, pp. 464–474, January 2016.

[6] A. R. Chiriyath, B. Paul, and D. W. Bliss, "Radar-communications convergence: coexistence, cooperation, and co-design," *IEEE Transactions on Cognitive Communications and Networking*, vol. 3, no. 1, pp. 1–12, February 2017.

[7] A. R. Chiriyath, S. Ragi, H. D. Mittelmann, and D. W. Bliss, "Radar waveform optimization for cooperative radar-communications receiver," *Submitted to IEEE Transactions on Aerospace and Electronic Systems*, 2018.

[8] A. R. Chiriyath and D. W. Bliss, "Joint radar-communications performance bounds: Data versus estimation information rates," in *2015 IEEE Military Communications Conference, MILCOM*, October 2015, pp. 1491–1496.

[9] ——, "Effect of clutter on joint radar-communications system performance inner bounds," in *2015 49th Asilomar Conference on Signals, Systems and Computers*, November 2015, pp. 1379–1383.

[10] A. R. Chiriyath, B. Paul, and D. W. Bliss, "Joint radar-communications information bounds with clutter: The phase noise menace," in *IEEE Radar Conference*, May 2016, pp. 690–695.

[11] ——, "Simultaneous radar detection and communications performance with clutter mitigation," in *IEEE Radar Conference*, May 2017, pp. 279–284.

[12] P. M. Woodward, *Probability and Information Theory, with Applications to Radar*. Dedham, Massachusetts: Artech House, 1953.

[13] P. Woodward, "Information theory and the design of radar receivers," *Proceedings of the IRE*, vol. 39, no. 12, pp. 1521–1524, December 1951.

[14] M. R. Bell, "Information theory and radar waveform design," *IEEE Transactions on Information Theory*, vol. 39, no. 5, pp. 1578–1597, September 1993.

[15] J. R. Guerci, R. M. Guerci, A. Lackpour, and D. Moskowitz, "Joint design and operation of shared spectrum access for radar and communications," in *IEEE Radar Conference*, May 2015, pp. 761–766.

[16] C. Shannon, "A mathematical theory of communication," *Bell System Technical Journal*, vol. 27, pp. 379–423, 623–656, July, October 1948.

[17] C. Kreucher, A. O. Hero, and K. Kastella, "A comparison of task driven and information driven sensor management for target tracking," in *Proceedings of the 44th IEEE Conference on Decision and Control*, Dec 2005, pp. 4004–4009.

[18] C. Kreucher, K. Kastella, and A. O. Hero, "A Bayesian method for integrated multitarget tracking and sensor management," in *Sixth International Conference of Information Fusion, 2003. Proceedings of the*, vol. 1, July 2003, pp. 704–711.

[19] A. Turlapaty and Y. Jin, "A joint design of transmit waveforms for radar and communications systems in coexistence," in *IEEE Radar Conference*. IEEE, May 2014, pp. 315–319.

[20] D. Guo, S. Shamai, and S. Verdú, *The Interplay Between Information and Estimation Measures*, ser. Foundations and Trends in Signal Processing. Hanover, MA: now Publishers Inc, 2012, vol. 6, no. 4.

[21] R. A. Romero and N. A. Goodman, "Cognitive radar network: Cooperative adaptive beamsteering for integrated search-and-track application," *IEEE Transactions on Aerospace and Electronic Systems*, vol. 49, no. 2, pp. 915–931, April 2013.

[22] C. D. Richmond, P. Basu, R. E. Learned, J. Vian, A. Worthen, and M. Lockard, "Performance bounds on cooperative radar and communication systems operation," in *IEEE Radar Conference*, May 2016, pp. 1–6.

[23] M. Bica, K.-W. Huang, V. Koivunen, and U. Mitra, "Mutual information based radar waveform design for joint radar and cellular communication systems," in *IEEE International Conference on Acoustics, Speech and Signal Processing (ICASSP)*, March 2016, pp. 3671–3675.

[24] C. Sturm and W. Wiesbeck, "Waveform design and signal processing aspects for fusion of wireless communications and radar sensing," *Proceedings of the IEEE*, vol. 99, no. 7, pp. 1236–1259, July 2011.

[25] C. Sturm, T. Zwick, and W. Wiesbeck, "An OFDM system concept for joint radar and communications operations," in *IEEE 69th Vehicular Technology Conference*, April 2009, pp. 1–5.

[26] K.-W. Huang, M. Bica, U. Mitra, and V. Koivunen, "Radar waveform design in spectrum sharing environment: coexistence and cognition," in *IEEE Radar Conference*. IEEE, May 2015, pp. 1698–1704.

[27] A. Turlapaty, Y. Jin, and Y. Xu, "Range and velocity estimation of radar targets by weighted OFDM modulation," in *IEEE Radar Conference*, May 2014, pp. 1358–1362.

[28] T. Guo and R. Qiu, "OFDM waveform design compromising spectral nulling, side-lobe suppression and range resolution," in *IEEE Radar Conference*, May 2014, pp. 1424–1429.

[29] G. Lellouch, A. Mishra, and M. Inggs, "Impact of the Doppler modulation on the range and Doppler processing in OFDM radar," in *IEEE Radar Conference*, May 2014, pp. 803–808.

[30] B. J. Donnet and I. D. Longstaff, "Combining MIMO radar with OFDM communications," in *3rd European Radar Conference (EuRAD)*, September 2006, pp. 37–40.

[31] S. Gogineni, M. Rangaswamy, and A. Nehorai, "Multi-modal OFDM waveform design," in *2013 IEEE Radar Conference*, April 2013, pp. 1–5.

[32] D. Garmatyuk, K. Kauffman, J. Schuerger, and S. Spalding, "Wideband OFDM system for radar and communications," in *IEEE Radar Conference*, May 2009, pp. 1–6.

[33] S. C. Thompson and J. P. Stralka, "Constant envelope OFDM for power-efficient radar and data communications," in *International Waveform Diversity and Design Conference*, February 2009, pp. 291–295.

[34] D. Garmatyuk, Y. J. Morton, and X. Mao, "On co-existence of in-band UWB-OFDM and GPS signals: Tracking performance analysis," in *2008 IEEE/ION Position, Location and Navigation Symposium*, May 2008, pp. 196–202.

[35] X. Shaojian, C. Bing, and Z. Ping, "Radar-communication integration based on DSSS techniques," in *8th International Conference on Signal Processing*, vol. 4, November 2006, pp. 1–4.

[36] Y. Xie, R. Tao, and T. Wang, "Method of waveform design for radar and communication integrated system based on CSS," in *First International Conference on Instrumentation, Measurement, Computer, Communication and Control*, October 2011, pp. 737–739.

[37] M. Roberton and E. R. Brown, "Integrated radar and communications based on chirped spread-spectrum techniques," in *2003 IEEE MTT-S International Microwave Symposium Digest*, vol. 1, June 2003, pp. 611–614.

[38] P. Mahalanobis, "On the generalised distance in statistics," *Proceedings of the National Institute of Sciences of India*, vol. 2, no. 1, pp. 49–55, Apr. 1936.

[39] J. R. Krier, M. C. Norko, J. T. Reed, R. J. Baxley, A. D. Lanterman, X. Ma, and J. R. Barry, "Performance bounds for an OFDM-based joint radar and communications system," in *2015 IEEE Military Communications Conference, MILCOM*, October 2015, pp. 511–516.

[40] A. Khawar, A. Abdel-Hadi, and T. C. Clancy, "MIMO radar waveform design for coexistence with cellular systems," in *IEEE International Symposium on Dynamic Spectrum Access Networks (DYSPAN)*, April 2014, pp. 20–26.

[41] Y. L. Sit and T. Zwick, "MIMO OFDM radar with communication and interference cancellation features," in *IEEE Radar Conference*, May 2014, pp. 265–268.

[42] B. Li, A. P. Petropulu, and W. Trappe, "Optimum co-design for spectrum sharing between matrix completion based MIMO radars and a MIMO communication system," *IEEE Transactions on Signal Processing*, vol. 64, no. 17, pp. 4562–4575, May 2016.

[43] Y. Zhang, Q. Li, L. Huang, and J. Song, "Waveform design for joint radar-communication system with multi-user based on MIMO radar," in *2017 IEEE Radar Conference (RadarConf)*, May 2017, pp. 0415–0418.

[44] A. Aubry, V. Carotenuto, A. De Maio, A. Farina, and L. Pallotta, "Optimization theory-based radar waveform design for spectrally dense environments," *IEEE Aerospace and Electronic Systems Magazine*, vol. 31, no. 12, pp. 14–25, December 2016.

[45] Y. Huang, M. Piezzo, V. Carotenuto, and A. De Maio, "Radar waveform design under similarity, bandwidth priority, and spectral coexistence constraints," in *2017 IEEE Radar Conference (RadarConf)*, May 2017, pp. 1142–1147.

[46] A. Aubry, V. Carotenuto, and A. De Maio, "Radar waveform design with multiple spectral compatibility constraints," in *2016 IEEE Radar Conference (RadarConf)*, May 2016, pp. 1–6.

[47] H. Shajaiah, A. Khawar, A. Abdel-Hadi, and T. C. Clancy, "Resource allocation with carrier aggregation in LTE advanced cellular system sharing spectrum with S-band radar," in *IEEE International Symposium on Dynamic Spectrum Access Networks (DYSPAN)*, April 2014, pp. 34–37.

[48] J. R. Guerci and R. M. Guerci, "RAST: Radar as a subscriber technology for wireless spectrum cohabitation," in *IEEE Radar Conference*, May 2014, pp. 1130–1134.

[49] A. Aubry, A. De Maio, M. Piezzo, and A. Farina, "Radar waveform design in a spectrally crowded environment via nonconvex quadratic optimization," vol. 50, no. 2, pp. 1138–1152, April 2014.

[50] H. Deng and B. Himed, "Interference mitigation processing for spectrum-sharing between radar and wireless communications systems," *IEEE Transactions on Aerospace and Electronic Systems*, vol. 49, no. 3, pp. 1911–1919, July 2013.

[51] A. Babaei, W. H. Tranter, and T. Bose, "A practical precoding approach for radar-communications spectrum sharing," in *2013 8th International Conference on Cognitive Radio Oriented Wireless Networks (CROWNCOM)*, July 2013, pp. 13–18.

[52] S. U. Pillai, H. S. Oh, D. C. Youla, and J. R. Guerci, "Optimal transmit-receiver design in the presence of signal-dependent interference and channel noise," *IEEE Transactions on Information Theory*, vol. 46, no. 2, pp. 577–584, March 2000.

[53] D. A. Garren, M. K. Osborn, A. C. Odom, J. S. Goldstein, S. U. Pillai, and J. R. Guerci, "Enhanced target detection and identification via optimised radar transmission pulse shape," *IEEE Proceedings on Radar, Sonar and Navigation*, vol. 148, no. 3, pp. 130–138, June 2001.

[54] S. Sodagari, A. Khawar, T. C. Clancy, and R. McGwier, "A projection based approach for radar and telecommunication systems coexistence," in *IEEE Global Communications Conference (GLOBECOM)*, Decemeber 2012, pp. 5010–5014.

[55] S. C. Surender, R. M. Narayanan, and C. R. Das, "Performance analysis of communications & radar coexistence in a covert UWB OSA system," in *IEEE Global Telecommunications Conference (GLOBECOM)*, December 2010, pp. 1–5.

[56] A. Khawar, A. Abdel-Hadi, and T. C. Clancy, "Spectrum sharing between S-band radar and LTE cellular system: A spatial approach," in *IEEE International Symposium on Dynamic Spectrum Access Networks (DYSPAN)*, April 2014, pp. 7–14.

[57] L. Wang, J. McGeehan, C. Williams, and A. Doufexi, "Application of cooperative sensing in radar-communications coexistence," *IET Communications*, vol. 2, no. 6, pp. 856–868, July 2008.

[58] S. S. Bhat, R. M. Narayanan, and M. Rangaswamy, "Bandwidth sharing and scheduling for multimodal radar with communications and tracking," in *IEEE 7th Sensor Array and Multichannel Signal Processing Workshop (SAM)*, June 2012, pp. 233–236.

[59] M. P. Fitz, T. R. Halford, I. Hossain, and S. W. Enserink, "Towards simultaneous radar and spectral sensing," in *IEEE International Symposium on Dynamic Spectrum Access Networks (DYSPAN)*, April 2014, pp. 15–19.

[60] R. Saruthirathanaworakun, J. M. Peha, and L. M. Correia, "Opportunistic primary-secondary spectrum sharing with a rotating radar," in *International Conference on Computing, Networking and Communications (ICNC)*, January 2012, pp. 1025–1030.

[61] H. Wang, J. Johnson, C. Baker, L. Ye, and C. Zhang, "On spectrum sharing between communications and air traffic control radar systems," in *IEEE Radar Conference*. IEEE, May 2015, pp. 1545–1551.

[62] A. Lackpour, A. Rosenwinkel, J. R. Guerci, A. Mody, and D. Ryan, "Design and analysis of an information exchange-based radar/communications spectrum sharing system (RCS3)," in *IEEE Radar Conference*, May 2016, pp. 1–6.

[63] G. N. Saddik, R. S. Singh, and E. R. Brown, "Ultra-wideband multifunctional communications/radar system," *IEEE Transactions on Microwave Theory and Techniques*, vol. 55, no. 7, pp. 1431–1437, July 2007.

[64] R. Saruthirathanaworakun, J. M. Peha, and L. M. Correia, "Opportunistic sharing between rotating radar and cellular," *IEEE Journal on Selected Areas in Communications*, vol. 30, no. 10, pp. 1900–1910, November 2012.

[65] F. Paisana, J. P. Miranda, N. Marchetti, and L. A. DaSilva, "Database-aided sensing for radar bands," in *IEEE International Symposium on Dynamic Spectrum Access Networks (DYSPAN)*, April 2014, pp. 1–6.

[66] T. Grettenberg, "Signal selection in communication and radar systems," vol. 9, no. 4, pp. 265–275, October 1963.

[67] A. Hassanien, M. G. Amin, Y. D. Zhang, and F. Ahmad, "A dual function radar-communications system using sidelobe control and waveform diversity," in *2015 IEEE Radar Conference*, May 2015, pp. 1260–1263.

[68] A. Hassanien, M. G. Amin, Y. D. Zhang, F. Ahmad, and B. Himed, "Non-coherent PSK-based dual-function radar-communication systems," in *IEEE Radar Conference*, May 2016, pp. 1–6.

[69] S. D. Blunt, P. Yatham, and J. Stiles, "Intrapulse radar-embedded communications," *IEEE Transactions on Aerospace and Electronic Systems*, vol. 46, no. 3, pp. 1185–1200, July 2010.

[70] M. Scharrenbroich and M. Zatman, "Joint radar-communications resource management," in *IEEE Radar Conference*, May 2016, pp. 1–6.

[71] Y. Nijsure, Y. Chen, C. Yuen, and Y. H. Chew, "Location-aware spectrum and power allocation in joint cognitive communication-radar networks," in *Sixth International ICST Conference on Cognitive Radio Oriented Wireless Networks and Communications (CROWNCOM)*, June 2011, pp. 171–175.

[72] A. Aubry, A. De Maio, M. Piezzo, M. M. Naghsh, M. Soltanalian, and P. Stoica, "Cognitive radar waveform design for spectral coexistence in signal-dependent interference," in *IEEE Radar Conference*, May 2014, pp. 474–478.

[73] K.-W. Huang, M. Bică, U. Mitra, and V. Koivunen, "Radar waveform design in spectrum sharing environment: Coexistence and cognition," in *2015 IEEE Radar Conference*, May 2015, pp. 1698–1703.

[74] J. Jakabosky, B. Ravenscroft, S. D. Blunt, and A. Martone, "Gapped spectrum shaping for tandem-hopped radar/communications and cognitive sensing," in *IEEE Radar Conference*, May 2016, pp. 1–6.

[75] P. Stinco, M. Greco, F. Gini, and B. Himed, "Channel parameters estimation for cognitive radar systems," in *2014 4th International Workshop on Cognitive Information Processing (CIP)*, May 2014, pp. 1–6.

[76] J. M. Chapin and W. H. Lehr, "Cognitive radios for dynamic spectrum access - the path to market success for dynamic spectrum access technology," *IEEE Communications Magazine*, vol. 45, no. 5, pp. 96–103, May 2007.

[77] W. Zhang, S. Vedantam, and U. Mitra, "Joint transmission and state estimation: A constrained channel coding approach," *IEEE Transactions on Information Theory*, vol. 57, no. 10, pp. 7084–7095, October 2011.

[78] A. Pezeshki, A. R. Calderbank, W. Moran, and S. D. Howard, "Doppler resilient Golay complementary waveforms," *IEEE Transactions on Information Theory*, vol. 54, no. 9, pp. 4254–4266, September 2008.

[79] S. Tsugawa, "Energy ITS: Another application of vehicular communications," *IEEE Communications Magazine*, vol. 48, no. 11, pp. 120–126, November 2010.

[80] V. Orlando, "The Mode S beacon radar system," *Lincoln Laboratory Journal*, vol. 2, no. 3, pp. 345–362, 1989.

[81] M. Strohmeier, M. Schäfer, V. Lenders, and I. Martinovic, "Realities and challenges of nextgen air traffic management: The case of ADS-B," *IEEE Communications Magazine*, vol. 52, no. 5, pp. 111–118, May 2014.

[82] C. Gu, Z. Peng, and C. Li, "High-precision motion detection using low-complexity Doppler radar with digital post-distortion technique," *IEEE Transactions on Microwave Theory and Techniques*, vol. PP, no. 99, pp. 1–11, 2016.

[83] J. Lipsky. (2015, May) Google gestures at 60 GHz. [Online]. Available: http://www.eetimes.com/document.asp?doc_id=1326726

[84] A. Herschfelt and D. Bliss, "Multi-static space-time-frequency multiple access channel simulation and results," in *IEEE Radar Conference*, May 2017, pp. 975–980.

[85] ——, "Joint radar-communications waveform multiple access and synthetic aperture radar receiver," in *51st Asilomar Conference on Signals, Systems and Computers*, November 2017.

[86] H. Yu, H. Lee, R. M. Gutierrez, A. Herschfelt, and D. W. Bliss, "WISCA SDR network," in *Milcom 2017*, Baltimore, USA, Oct. 2017.

[87] R. M. Gutierrez, A. Herschfelt, H. Yu, and D. W. Bliss, "Joint radar-communications system implementation using software defined radios: Feasibility and results," to appear in *Proc. 51st Asilomar Conference on Signals, Systems, and Computers*, 2017.

[88] Z. Liu and I. Elhanany, "RL-MAC: A QoS-aware reinforcement learning based MAC protocol for wireless sensor networks," in *2006 IEEE International Conference on Networking, Sensing and Control*, April 2006, pp. 768–773.

[89] H. A. A. Al-Rawi, K.-L. A. Yau, H. Mohamad, N. Ramli, and W. Hashim, "Reinforcement learning for routing in cognitive radio ad hoc networks," *The Scientific World Journal*, vol. 2014, pp. 1–22, July 2014.

[90] S. Arunthavanathan, S. Kandeepan, and R. J. Evans, "A Markov decision process-based opportunistic spectral access," *IEEE Wireless Communications Letters*, vol. 5, no. 5, pp. 544–547, October 2016.

[91] P. Nurmi, "Reinforcement learning for routing in ad hoc networks," in *2007 5th International Symposium on Modeling and Optimization in Mobile, Ad Hoc and Wireless Networks and Workshops*, April 2007, pp. 1–8.

[92] Y.-H. Chang, T. Ho, and L. P. Kaelbling, "Mobilized ad-hoc networks: a reinforcement learning approach," in *International Conference on Autonomic Computing, 2004. Proceedings.*, May 2004, pp. 240–247.

[93] A. Ghaffari, "Real-time routing algorithm for mobile ad hoc networks using reinforcement learning and heuristic algorithms," *Wireless Networks*, vol. 23, no. 3, pp. 703–714, 2017.

[94] R. Razavi, S. Klein, and H. Claussen, "Self-optimization of capacity and coverage in LTE networks using a fuzzy reinforcement learning approach," in *21st Annual IEEE International Symposium on Personal, Indoor and Mobile Radio Communications*, September 2010, pp. 1865–1870.

[95] N. Mastronarde and M. van der Schaar, "Fast reinforcement learning for energy-efficient wireless communication," *IEEE Transactions on Signal Processing*, vol. 59, no. 12, pp. 6262–6266, December 2011.

[96] T. X. Brown, "Low power wireless communication via reinforcement learning," in *Advances in Neural Information Processing Systems*, November 2000, pp. 893–899.

[97] F. Zhou, D. Zhou, and G. Yu, "Target tracking in interference environments reinforcement learning and design for cognitive radar soft processing," in *2008 Congress on Image and Signal Processing*, vol. 4, May 2008, pp. 73–77.

[98] F. Smits, A. Huizing, W. van Rossum, and P. Hiemstra, "A cognitive radar network: Architecture and application to multiplatform radar management," in *2008 European Radar Conference*, October 2008, pp. 312–315.

[99] T. M. Cover and J. A. Thomas, *Elements of Information Theory*, 2nd ed. Hoboken, New Jersey: John Wiley & Sons, 2006.

[100] D. W. Bliss and S. Govindasamy, *Adaptive Wireless Communications: MIMO Channels and Networks*. New York, New York: Cambridge University Press, 2013.

[101] M. de Berg, C. Otfried, M. van Kreveld, and M. Overmars, *Computational Geometry: Algorithms and Applications, 3rd Edition*. Springer, 2008.

[102] R. G. Gallager, *Information Theory and Reliable Communication*, 2nd ed. Hoboken, New Jersey: John Wiley & Sons, 1968.

[103] B. Paul and D. W. Bliss, "Extending joint radar-communications bounds for FMCW radar with Doppler estimation," in *IEEE Radar Conference*, May 2015, pp. 89–94.

[104] ——, "Estimation information bounds using the I-MMSE formula and Gaussian mixture models," in *2016 50th Annual Conference on Information Sciences and Systems (CISS)*, March 2016, pp. 292–297.

[105] M. A. Richards, *Principles of Modern Radar: Basic Principles*, J. A. Sheer and W. A. Holm, Eds. Raleigh, North Carolina: SciTech Publishing, 2010.

[106] B. Paul and D. W. Bliss, "Constant information radar for dynamic shared spectrum access," in *2015 49th Asilomar Conference on Signals, Systems and Computers*, November 2015, pp. 1374–1378.

[107] H. Van Trees, *Detection, Estimation, and Modulation Theory: Part 1*, 1st ed. Hoboken, New Jersey: John Wiley & Sons, 2004.

[108] C. D. Richmond, "Mean-squared error and threshold SNR prediction of maximum-likelihood signal parameter estimation with estimated colored noise covariances," *IEEE Transactions on Information Theory*, vol. 52, no. 5, pp. 2146–2164, May 2006.

[109] A. Chiriyath, "Joint radar-communications performance bounds: Data versus estimation information rates," *M.S. Thesis, Dept. of Electrical, Computer and Energy Engineering, Arizona State University*, Jul. 2014.

[110] H. L. Van Trees, *Detection, Estimation, and Modulation Theory: Radar-Sonar Signal Processing and Gaussian Signals in Noise*. Malabar, Florida: Krieger Publishing Company, July 1992.

[111] B. Paul, A. R. Chiriyath, and D. W. Bliss, "Joint communications and radar performance bounds under continuous waveform optimization: The waveform awakens," in *IEEE Radar Conference*, May 2016, pp. 865–870.

[112] M. A. Richards, *Fundamentals of Radar Signal Processing*, 2nd ed. Raleigh, North Carolina: McGraw-Hill Professional, 2013.

[113] S. M. Kay, *Fundamentals of Statistical Signal Processing: Estimation Theory*, 1st ed. Upper Saddle River, NJ, USA: Prentice-Hall, Inc., 1993.

[114] S. Das and P. N. Suganthan, "Differential evolution: A survey of the state-of-the-art," *IEEE Transactions on Evolutionary Computation*, vol. 15, no. 1, pp. 4–31, February 2011.

[115] P. Stoica and A. Nehorai, "Performance study of conditional and unconditional direction-of-arrival estimation," *IEEE Transactions on Acoustics, Speech and Signal Processing*, vol. 38, no. 10, pp. 1783–1795, Oct. 1990.

[116] S. M. Kay, *Fundamentals of Statistical Signal Processing: Estimation Theory.* Upper Saddle River, NJ: Prentice Hall, 1993.

[117] M. I. Skolnik, *Introduction to Radar Systems.* McGraw-Hill, 2002.

[118] E. Rubiola, *Phase Noise and Frequency Stability in Oscillators*, 1st ed. New York, New York: Cambridge University Press, 2010.

[119] W. L. Melvin, *Principles of Modern Radar: Advanced Techniques*, J. A. Sheer, Ed. Raleigh, North Carolina: SciTech Publishing, 2012.

APPENDIX A

LIST OF ACRONYMS

APPENDIX A

List of Acronyms

1D one-dimensional

AWGN additive white Gaussian noise

BER bit error rate

CIR constant information radar

CPI coherent processing interval

CRLB Cramér-Rao lower bound

DARPA The Defense Advanced Research Projects Agency

DE differential evolution

FIM Fisher information matrix

ISB isolated sub-band

INR interference-to-noise ratio

ICM intrinsic clutter motion

LFM linear frequency modulation

LTE Long-Term Evolution

MAC multiple access channel

MIMO Multiple-input multiple-output

MMSE minimum mean-squared error

OFDM orthogonal frequency-division multiplexing

PAPR peak-to-average power ratio

PRF pulse repetition frequency

PRI pulse repetition interval

PSP principle of stationary phase

RMS root mean square

RF electromagnetic radio frequency

ROC receiver operating characteristic

SIC successive interference cancellation

SISO single-input single-output

SNR signal-to-noise ratio

TB time-bandwidth

WF water-filling

APPENDIX B

DERIVATION OF REDUCED FISHER INFORMATION FOR TIME-DELAY ESTIMATION

APPENDIX B

Derivation of Reduced Fisher Information for Time-Delay Estimation

In this appendix, we first derive the Fisher information cross terms for joint amplitude and time-delay estimation and find the value of the free parameter B_O that sets these cross-terms to 0. We then show that by setting the cross-terms to 0, the reduced Fisher information for time-delay estimation is the same as the Fisher information for time-delay estimation, given by Equation (5.23).

We consider the same scenario as described in Section 5.1.4. The total bandwidth is split into two sub-bands and the radar power (or power spectral density) is distributed between the two sub-bands. The bandwidth and radar power (power spectral densities) are split between the two sub-bands according to some α.

Now, consider a radar signal $x(t)$ with bandwidth B, whose frequency spectrum $X(f)$ is flat and centered around B_O. $x_{\mathrm{RO}}(t)$ and $x_{\mathrm{MU}}(t)$ are the spectrally orthogonal sub-band signals with bandwidths $\alpha\, B$ and $(1-\alpha)B$ respectively.

Thus, the joint receiver observes the following return signal

$$z(t) = a\, x(t-\tau) + b\,\sqrt{P_{\mathrm{com}}}\, r(t) + n(t)\,. \tag{B.1}$$

where $x(t-\tau) = \sqrt{P_{\mathrm{RO}}}\, x_{\mathrm{RO}}(t-\tau) + \sqrt{P_{\mathrm{MU}}}\, x_{\mathrm{MU}}(t-\tau)$, $r(t)$ is the communications signal that is present in the mixed use channel and $n(t)$ is circularly symmetric Gaussian noise with zero mean and variance $\sigma^2 = k_B\, T_{\mathrm{temp}}\, B$.

Let $\boldsymbol{\theta} = \left[\begin{smallmatrix}\tau\\ a\end{smallmatrix}\right]$ be the parameters to be estimated. From Equation (B.1), we see that $z(t) \sim \mathcal{CN}(a\, x(t-\tau) + b\,\sqrt{P_{\mathrm{com}}}\, r(t), \sigma^2)$ and has the following score function,

$s(\boldsymbol{\theta}; z(t))$ is given by

$$\begin{aligned} s(\boldsymbol{\theta}; z(t)) &= \nabla_{\boldsymbol{\theta}} \{\log p(z(t); \boldsymbol{\theta})\} \\ &= \begin{pmatrix} \frac{a\, n^*(t)\, x'(t-\tau)}{\sigma^2} + c.c. \\ \\ \frac{n^*(t)\, x(t-\tau)}{\sigma^2} + c.c. \end{pmatrix}, \end{aligned} \tag{B.2}$$

where c.c. stands for the complex conjugate term and $x'(t-\tau) = \frac{\partial}{\partial \tau} x(t-\tau)$. Now, the FIM for this estimation problem, $\mathbf{J}$, is given by

$$\begin{aligned} \mathbf{J} &= \langle s(\boldsymbol{\theta}; z(t)) s^{\dagger}(\boldsymbol{\theta}; z(t)) \rangle \\ &= \left\langle \begin{pmatrix} \frac{a\, n^*(t)\, x'(t-\tau)}{\sigma^2} + c.c. \\ \\ \frac{n^*(t)\, x(t-\tau)}{\sigma^2} + c.c. \end{pmatrix} \begin{pmatrix} \frac{a^*\, [x(t-\tau)]^*\, n(t)}{\sigma^2} + c.c.^* & \frac{x^*(t-\tau) n(t)}{\sigma^2} + c.c.^* \end{pmatrix} \right\rangle \\ &= \begin{pmatrix} J_{\tau,\tau} & J_{\tau,\mathrm{a}} \\ J_{\mathrm{a},\tau} & J_{\mathrm{a,a}} \end{pmatrix}. \end{aligned} \tag{B.3}$$

We now simplify the cross terms of the FIM. Starting with $J_{\tau,\mathrm{a}}$, we see that on simplification,

$$J_{\tau,\mathrm{a}} = \frac{a\, \langle x'(t-\tau) x^*(t-\tau)] \rangle}{\sigma^2} + \frac{a^*\, \langle [x'(t-\tau)]^* x(t-\tau) \rangle}{\sigma^2}. \tag{B.4}$$

By multiplying the terms out, converting to frequency domain and applying Parseval's Theorem and the time-shift and differentiation properties of the Fourier Transform, for spectrally flat $X(f)$ (or $X_{\mathrm{RO}}(f)$ and $X_{\mathrm{MU}}(f)$), we get

$$J_{\tau,\mathrm{a}} = \frac{(i\, a - i\, a^*)}{\sigma^2} \int_{B_O - \frac{B}{2}}^{B_O + \frac{B}{2}} \mathrm{d}f (2\pi f)\, X(f)\, X^*(f). \tag{B.5}$$

Applying the definition of $x(t)$ and simplifying, we get

$$\begin{aligned} J_{\tau,\mathrm{a}} &= \frac{(i\,a - i\,a^*)}{\sigma^2}\left[\pi\,\alpha\,TB\,\rho_{\mathrm{RO}} f^2\big|_{B_O-\frac{B}{2}}^{B_O-\frac{B}{2}+\alpha B} + \pi\,(1-\alpha)\,TB\,\rho_{\mathrm{MU}} f^2\big|_{B_O-\frac{B}{2}+\alpha B}^{B_O+\frac{B}{2}}\right] \\ &= \frac{(i\,a - i\,a^*)\;\pi\,\alpha\,TB\,\rho_{\mathrm{RO}}}{\sigma^2}\left[\left(B_O - \frac{B}{2} + \alpha B\right)^2 - \left(B_O - \frac{B}{2}\right)^2\right] \\ &\quad + \frac{(i\,a - i\,a^*)\;\pi\,(1-\alpha)\,TB\,\rho_{\mathrm{MU}}}{\sigma^2}\left[\left(B_O + \frac{B}{2}\right)^2 - \left(B_O - \frac{B}{2} + \alpha B\right)^2\right], \end{aligned} \tag{B.6}$$

Similarly, using the same properties as mentioned above, on simplifying the other cross term in the FIM we see that

$$J_{\mathrm{a},\tau} = J_{\tau,\mathrm{a}}\,.$$

In order to find the value of B_O that sets the FIM cross-terms $J_{\mathrm{a},\tau}$ and $J_{\tau,\mathrm{a}}$ to 0, we set $J_{\mathrm{a},\tau} = J_{\tau,\mathrm{a}} = 0$ and solve for B_O. The resultant value for B_O is

$$B_O = \frac{\alpha\,B\,(1-\alpha)[\rho_{\mathrm{MU}}(\alpha-1) + \rho_{\mathrm{RO}}\alpha]}{2(\rho_{\mathrm{MU}}(\alpha-1)^2 + \rho_{\mathrm{RO}}\alpha^2)}\,. \tag{B.7}$$

This means that the Fisher information cross terms are be 0 whenever the value of B_O is given by Equation (B.7). In this case, the reduced Fisher Information [100] for time-delay estimation is

$$\begin{aligned} J_{\tau,\tau}^{(R)} &= \left(J_{\tau,\tau} - J_{\tau,\mathrm{a}}\,J_{\mathrm{a,a}}^{-1}\,J_{\mathrm{a},\tau}\right) \\ &= (J_{\tau,\tau} - 0) \\ &= J_{\tau,\tau}\,. \end{aligned} \tag{B.8}$$